

<sub>1</sub> Chapter 1

<sub>2</sub> Introduction (Flavio,Christos) [5 pages]

<sup>1</sup> Chapter 2

<sup>2</sup> Scientific and technical motivations  
<sup>3</sup> (Jarek, Thomas)[10 pages]

<sup>1</sup> Chapter 3

<sup>2</sup> ProtoDUNE detector overview  
<sup>3</sup> (Flavio,Christos,Thomas)[15 pages]

# <sup>1</sup> Chapter 4

## <sup>2</sup> Detector components (Tim, Jim)[5-10 p. <sup>3</sup> per sub-system = 60 - 120 p.]

### <sup>4</sup> 4.1 Anode Plane Assemblies

<sup>5</sup> The current baseline for the protoDUNE single-phase TPC is a double-sided structure consisting  
<sup>6</sup> of wires that wrap in a helical pattern around the length of the APA frame. All wires eventually  
<sup>7</sup> terminate on the short end of the APA frame, with electronic readout of all channels located on  
<sup>8</sup> only one end, thus enabling the APAs to be "tiled" into a plane within the cryostat.

#### <sup>9</sup> 4.1.1 Scope, requirements, design parameters (Mitch and Bo)

<sup>10</sup> Figure 4.1 depicts a protoDUNE APA. Each side of a double-sided APA consists of four layers of  
<sup>11</sup> anode wires, plus an additional mesh layer that serves to shield the anode planes from pickup from  
<sup>12</sup> the Photon Detection System and also from "ghost" tracks created when ionizing particles have a  
<sup>13</sup> trajectory that passes through the anode planes.

<sup>14</sup> Requirements - listing of basic physics requirements.

<sup>15</sup> Overall physical description - connection to requirements.

<sup>16</sup> • Size

<sup>17</sup> • Wire spacing

<sup>18</sup> • Plane spacing

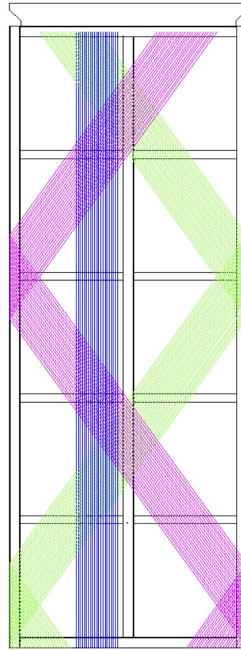


Figure 4.1: Sketch of a protoDUNE APA. Each APA features a Collection plane (blue wires) on both sides, as well as Induction planes (purple and green) that have wires continuously “wrapped” around the frame.

`fig:tpc_`

- <sup>1</sup> • Number of channels
- <sup>2</sup> • Angle and reason for chosen angle
- <sup>3</sup> • Wire placement accuracy
  - <sup>4</sup> – Wire Tension
  - <sup>5</sup> – Double anchor at each wire end
  - <sup>6</sup> – Need for intermediate support
    - <sup>7</sup> \* Sag prevention
    - <sup>8</sup> \* Break mitigation
- <sup>9</sup> • Bias, and description of plane purposes (grid, induction, collection)
- <sup>10</sup> • Voltage requirements for induction plane transparency.
- <sup>11</sup> • Frame distortion consequences - (Lee G. will update previous study)
- <sup>12</sup> • Trapped volume and bubbles

- 1     • Mesh, reasons for mesh
- 2     • Grounding - (based on input from EE and grounding/shielding group)
- 3     The APA layers are listed in Table 4.1, along with their operating voltages. The arrangement,  
4     from the outside-in, is G-U-V-X-M. The grid layer is present for pulse-shaping purposes, and is  
5     not connected for electronics readout.

Table 4.1: Layers within the APA, and baseline bias voltages. All five of these layers are present on both sides of the APA structure, with the Induction layers connected (“wrapped”) electrically across both sides.

Anode Plane	Bias Voltage
Grid (G)	-665 V
Induction (U)	-370 V
Induction (V)	0 V
Collection (X)	820 V
Mesh (M)	0 V

## 6 4.1.2 APA physical description, Meeting requirements, Fabrication

### 7 Wires (Lee)

- 8     • Physical description (composition, size, conductivity)
- 9     • Yield and break strength
- 10    • Target tension and limits to variation from target
- 11    • Thermal expansion coefficient
- 12      – Similar to stainless steel
- 13      – Small wires cool and warm faster than frame - tension ramifications

### 14 APA Frame (Lee)

- 15    • Physical shape and dimensions
- 16    • Welded vs. modular choice and reason for choosing modular
- 17    • Wire loads on frames and ability to withstand these loads

- 1     ● FEA
  - 2       – APA hanging from TPC support
  - 3       – APA simply supported at ends - laid flat
  - 4       – APA in interface frame - laid flat
  - 5       – APA in interface frame - landscape position
- 6     ● Reasons that buckling from wire loads is not a concern
  - 7       – Wires stay in plane of APA frame
  - 8       – Tension drops quickly with deflection - unlike buckling conditions
  - 9       – Tension on opposing side increases because of board offset, i.e. - huge counter moment
  - 10      develops with start of deflection
- 11    ● Handling of frame during winding and installation

## 12   **Wire and Wire Wrapping (Lee)**

- 13    ● Geometry - for reference
- 14    ● Wire start and end locations
- 15    ● Number of channels per plane and per APA - total number of wires and wire segments.
- 16    ● Side and foot boards - tooth geometry - molded tooth strips.
- 17    ● Solder and glue
  - 18       – Proposed methods
  - 19       – Tests on shorts and long term strength of glue/solder bonds
- 20    ● Mesh description and application equipment
- 21    ● Head electronics boards
- 22    ● Modular electronics concept
  - 23       – Reasons for

<sup>1</sup> – Implementation

<sup>2</sup> **Wire supports on inner frame members - combs (Lee)**

<sup>3</sup> • Reasons for

<sup>4</sup> • Geometry and appearance

<sup>5</sup> • Installation method

<sup>6</sup> • Tests results concerning wire wear from these supports

<sup>7</sup> **APA Interconnect Features (Lee)**

<sup>8</sup> **Integration with TPC (Dan/Jack)**

<sup>9</sup> **4.1.3 Wire-winding Machines (Dan)**

<sup>10</sup> **Wire wrapping concept**

<sup>11</sup> **Design requirements**

<sup>12</sup> **Implementation**

<sup>13</sup> • Interface frames

<sup>14</sup> • Fixed APA vs. rotating APA

<sup>15</sup> • Tensioning head passed around frame

<sup>16</sup> • Half a layer wrapped before moving APA supports

<sup>1</sup> Intermittent stop to solder

<sup>2</sup> Wire wrapping machinery

<sup>3</sup> Description/photos of machinery under construction and test

<sup>4</sup> Assembly sequence

#### <sup>5</sup> 4.1.4 QC Procedures

<sup>6</sup> Quality documents (Bob, Mike Z.)

<sup>7</sup> • Material certs

<sup>8</sup> • Incoming inspection

<sup>9</sup> • Assembly travelers

<sup>10</sup> Test plan

<sup>11</sup> • Wire tension

<sup>12</sup> Assembly procedure (Lee or Dan)

#### <sup>13</sup> 4.1.5 Installation process in TPC (already elsewhere?)

### <sup>14</sup> 4.2 Cathode Plane Assemblies

#### <sup>15</sup> 4.2.1 Scope, Requirements and Design Parameters

<sup>16</sup> The cathode plane is constructed from  $6 \times 3$  cathode plane assemblies (CPAs) to form the  $16\text{m} \times 6\text{m}$  area. It has a HV cup at the beam downstream side to interface with the HV feedthrough.  
<sup>18</sup> The top and bottom field cage modules are mechanically and electrically connected to the top and  
<sup>19</sup> bottom edges of the cathode plane. The cathode plane is suspended through insulating bars to  
<sup>20</sup> the CPA installation rail.

<sub>1</sub> **Requirements**

- <sub>2</sub> • Provide equipotential surfaces at -180kV nominal bias voltage
- <sub>3</sub> • Maintain a flatness better than 1cm when submerged in the liquid argon
- <sub>4</sub> • Use materials with comparable CTEs to that of stainless steel
- <sub>5</sub> • Limit the electric field exposed to LAr to under 30kV/cm
- <sub>6</sub> • Prevent damage to the TPC including its readout electronics In case of a HV discharge anywhere on the cathode
- <sub>7</sub>
- <sub>8</sub> • Provide constant bias voltage and current to all attached field cage resistor divider chains
- <sub>9</sub> • Support the full weight of the 4 connected top/bottom field cage modules and a person on the bottom CPA at installation
- <sub>10</sub>
- <sub>11</sub> • Accommodate cryostat roof movement between warm and LAr filled states
- <sub>12</sub> • Constructed in modular form that can be easily installed in the cryostat
- <sub>13</sub> • Accommodate PD calibration features
- <sub>14</sub> • Has no trapped volume

<sub>15</sub> **Design Parameters**

<sub>16</sub> Width, height, sheet thickness, frame thickness, module width...

<sub>17</sub> **4.2.2 The need for highly resistive cathode planes**

<sub>18</sub> Stored energy, charge injection to FEE, dominant ionization current density

<sub>19</sub> Summarize key points in DUNE docdb 1320.

### <sup>1</sup> 4.2.3 The Design of the Cathode

### <sup>2</sup> 4.2.4 Overview

- <sup>3</sup> Introduce the design concept: strong frame with thin resistive cathode surface; field shaping strips  
<sup>4</sup> cover the frame; HV bus hidden behind the field shaping strips; outer edges of the CPA frame  
<sup>5</sup> surrounded by the metal profiles used by the field cage.

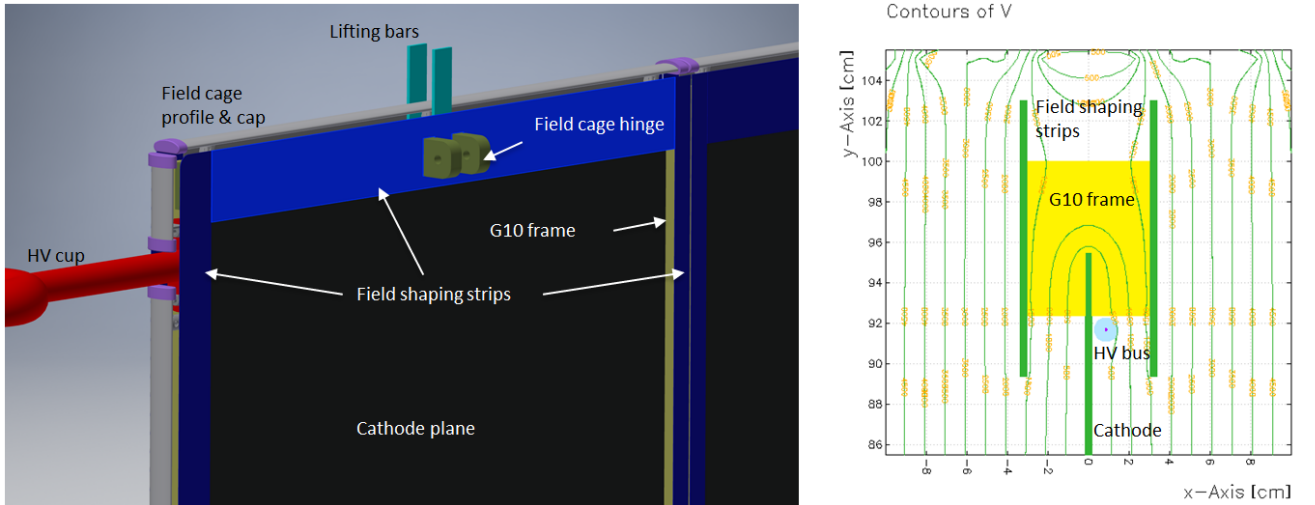


Figure 4.2: The resistive CPA concept. **Left:** A 3d model of a corner of the cathode showing major components **Right:** E field simulation of a portion of the cathode.

fig:cpa-

### <sup>6</sup> Resistive material

- <sup>7</sup> The main criteria for the selection of the resistive material to be used for the CPA panels include:
- <sup>8</sup> • Surface resistivity range.
  - <sup>9</sup> • Compatibility with cryogenic temperatures
  - <sup>10</sup> • Robustness to HV discharges, material ageing.
  - <sup>11</sup> • Radio-purity.
  - <sup>12</sup> • Availability on large area; achievable planarity
- <sup>13</sup> Several options have been evaluated.
- <sup>14</sup> • NORPLEX Micarta NP 315, phenolic laminate loaded with graphite: Intrinsic bulk resistivity in the required range (few  $M\Omega/cm$ ). Density comparable to LAr.
  - <sup>15</sup>

1     ● Screen printed resistive ink on G10/FR4 substrate ( 100 k $\Omega$ /square) printed with specific  
2       patterns to obtain required average surface resistivity

3     ● DuPont resistive Kapton film (25  $\mu\text{m}$  thickness, graphite loaded, available with resistivity in  
4       the 0.5 to 50 M $\Omega$ /square range) laminated on G10/FR4 substrate.

5     Also considered at earlier stage:

6       ● Zelec ESD powder mixed with polyurethane binder.

7       ● ESD surface conducting G10 from Current Composite.

8     Radiological tests performed at the LNGS low counting rate facility that G10/FR4 are preferable  
9       since MiCarta is more active by orders of magnitude for most relevant radioactive chains.

10    Screen printed ink and Kapton lamination on G10/FR4 are well established fabrication techniques  
11    available on panels as large as to 2.1x 1.2 m<sup>2</sup> (well matching the CPA panel required size). The  
12    screen print technique allows to choose precisely the average surface resistivity value, while Kapton  
13    exhibits a more uniform surface and resistivity.

14    Tests on large size panels have demonstrated that both options survive without deformation or  
15    delamination to repeated immersions in LAr. The resistivity increase at LAr temperature is  
16    bounded to less than a factor two for both cases. Electrical contacts are performed with specific  
17    silver paint paste highly stable at LAr temperature and resistant to mechanical scratches.

18    Tests on surface ageing when exposed to HV sparks indicate that Kapton is the preferred solution  
19    because:

20       ● in the resistive ink case, sparks tend to develop along direction of less resistivity, perpendicular  
21       to strip direction inducing a visible degradation of the material surface with some  
22       consistent ink evaporation and local measurable change in resistivity (Figure 4.3).

23       ● in the Kapton case instead, sparks are point-like inducing tiny localized carbonization on  
24       material surface at the spark position, but no change in average resistivity is recorded  
25       (Figure 4.4).

## 26    Support frame material properties

27    The main materials for the detector are stainless steel and what is called generically G10 material.  
28    G-10 is a thermosetting industrial fiber glass composite laminate consisting of a continuous filament  
29    glass cloth material with an epoxy resin binder. This product, first introduced in the 1950's,  
30    has characteristics of high strength, low moisture absorption, excellent electrical properties and  
31    chemical resistance. These properties are maintained not only at room temperature but also  
32    under humid or moist conditions. NEMA G10 was the designation given to Glass Epoxy sheet  
33    composite by the National Electrical Manufacture Association (NEMA) to specify a consistent

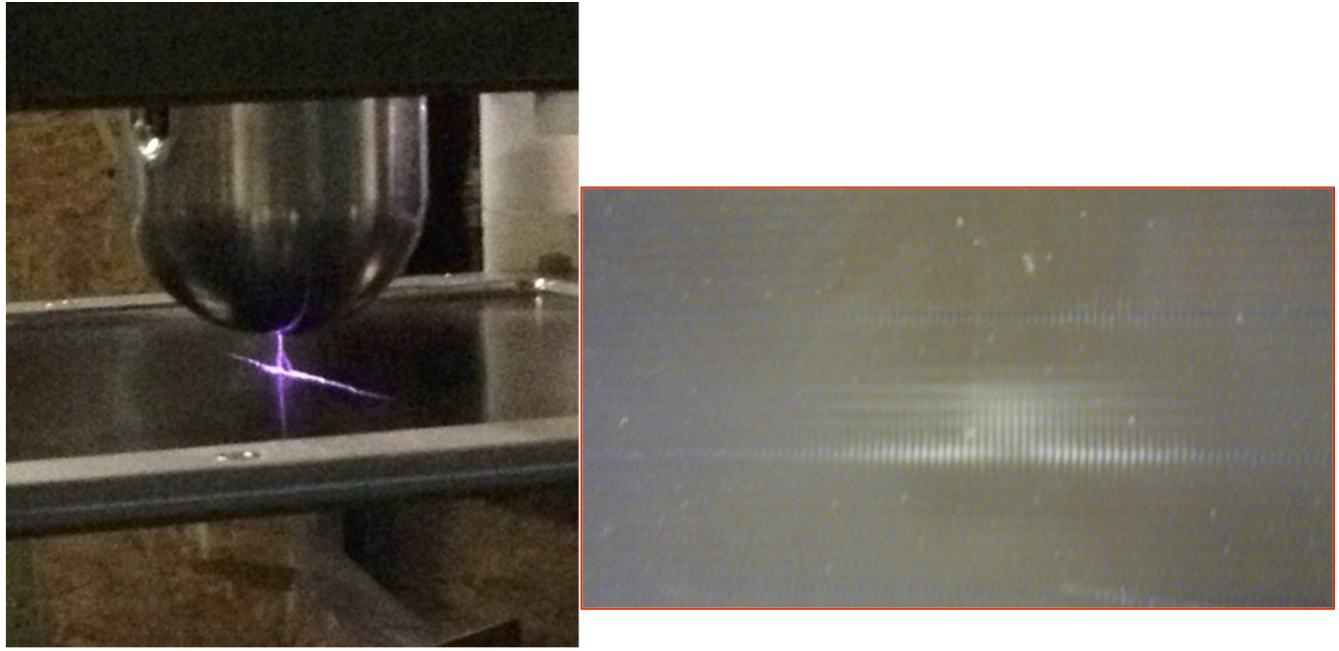


Figure 4.3: Resistive ink ageing from sparks. **Left:** spark propagation along preferred directions (lower resistivity), **Right:** Status after test: degradation with some material evaporation.

fig:cpa-

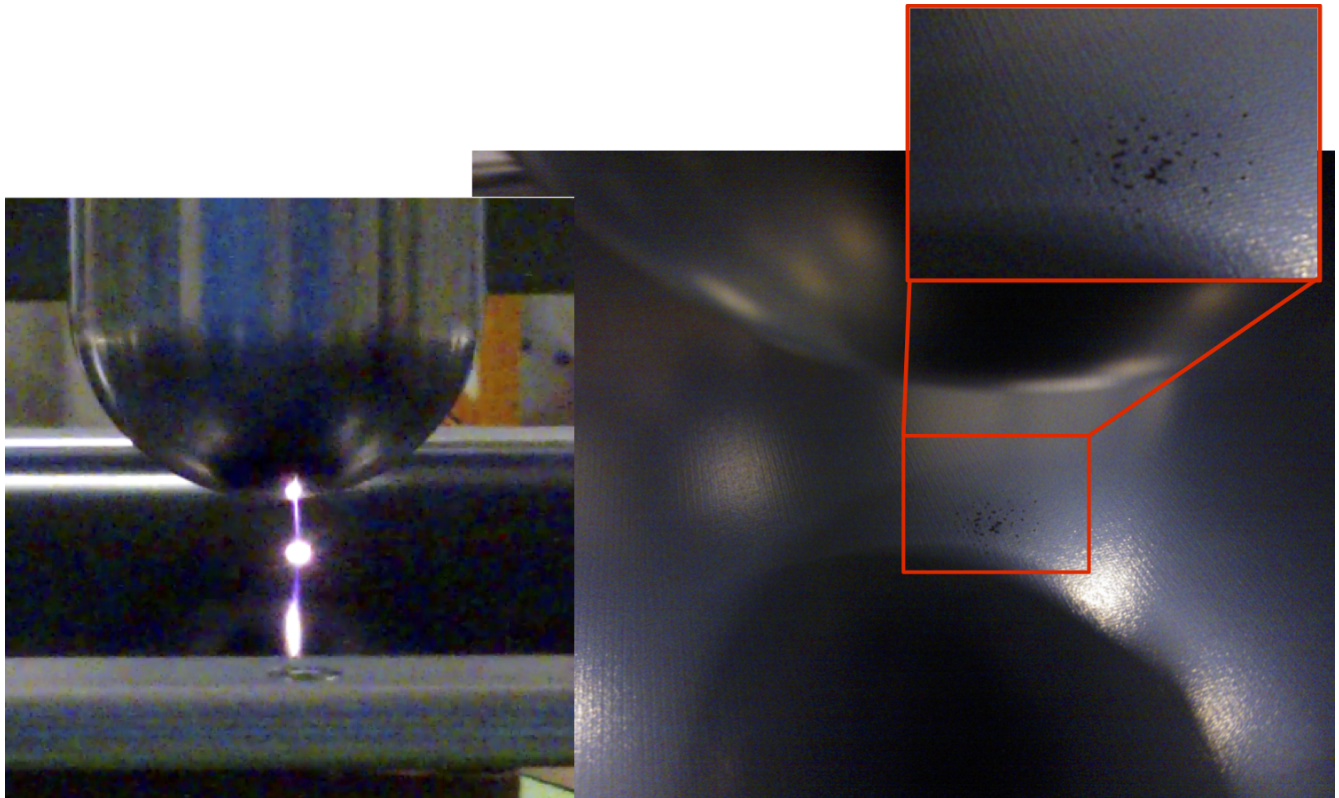


Figure 4.4: Resistive kapton ageing from sparks. **Left:** point-like sparks. **Right:** Localized carbonization on material surface, at the spark position.

fig:cpa-

- <sup>1</sup> product between manufactures.
- <sup>2</sup> G10 laminate sheet is made up with difunctional or trifunctional epoxy making up the bulk of heavy  
<sup>3</sup> sheet and then using finer glass cloth with high temperature resistant tetra-functional epoxy giving  
<sup>4</sup> a high performance outer finish.
- <sup>5</sup> FR4 is the brominated flame retardant version of G 10. The FR 4 material can usually be used  
<sup>6</sup> where G10 material is specified; however G10 Laminate should not be used where FR-4 is specified.  
<sup>7</sup> CERN requires that the material used be flame retardant but halogen free (and therefore bromine  
<sup>8</sup> free). FR4 meets the flame retardant requirement but not the halogen free requirement. Research  
<sup>9</sup> needs to be conducted into what type of G10/FR4 is available that meets CERNâŽs requirements.  
<sup>10</sup> Another variation of G10 fiberglass sheet is G10 CR laminate used in cryogenic applications.
- <sup>11</sup> Both G-10 and FR-4 are rated at 285 degree F continuous operating temperature. Because they  
<sup>12</sup> are thermosets, no melting will occur with these grades, however charring will be observed after  
<sup>13</sup> extended periods above this temperature rating. FR-4 has a UL flammability rating of 94 V-0.
- <sup>14</sup> A failure criteria needs to be defined for the G10 material because it is brittle and does not exhibit  
<sup>15</sup> ductile failure and a defined yield stress like stainless steel. Brittle materials typically rupture and  
<sup>16</sup> have a fractional reduction in area due to tensile strain of less than 0.05. For brittle materials it  
<sup>17</sup> is recommended that the modified Mohr Theory of Failure be used which states that the principle  
<sup>18</sup> tensile stresses be less than the ultimate stress of the material. See Shigley "Standard Handbook  
<sup>19</sup> of Machine Design," third edition. Stress concentrations are also a concern for brittle materials  
<sup>20</sup> and care should be taken to avoid sharp corners and other areas of stress concentrations. Shigley  
<sup>21</sup> also defines stress concentration factors which are multipliers for geometric areas where stresses  
<sup>22</sup> are higher and is a common method for evaluating high stress areas.

<sup>23</sup> The material properties used for calculations were:

#### G10:

Thermal expansion Coefficient	$9.6 \times 10^{-6}$ cm/cmK
Modulus of Elasticity	2,770ksi
Ultimate stress	32ksi

<sup>24</sup> Stainless Steel:

Thermal expansion Coefficient	$9.6 \times 10^{-6}$ cm/cmK
Modulus of Elasticity	30,000ksi
Yield stress	36ksi

<sup>25</sup> **Mechanical design and stress analysis**

<sup>26</sup>  Figures 4.5 and 4.6 show the basic geometry of the CPA. The CPA is composed of three modules  
<sup>27</sup> that are bolted and pinned together with tongue/groove joints to form the full CPA plane. Each  
<sup>28</sup> module consists of a framework in which the resistive panel is captured inside a groove. Each  
<sup>29</sup> module weights roughly 53 lbs. for a total weight of the CPA plane of 160 lbs.

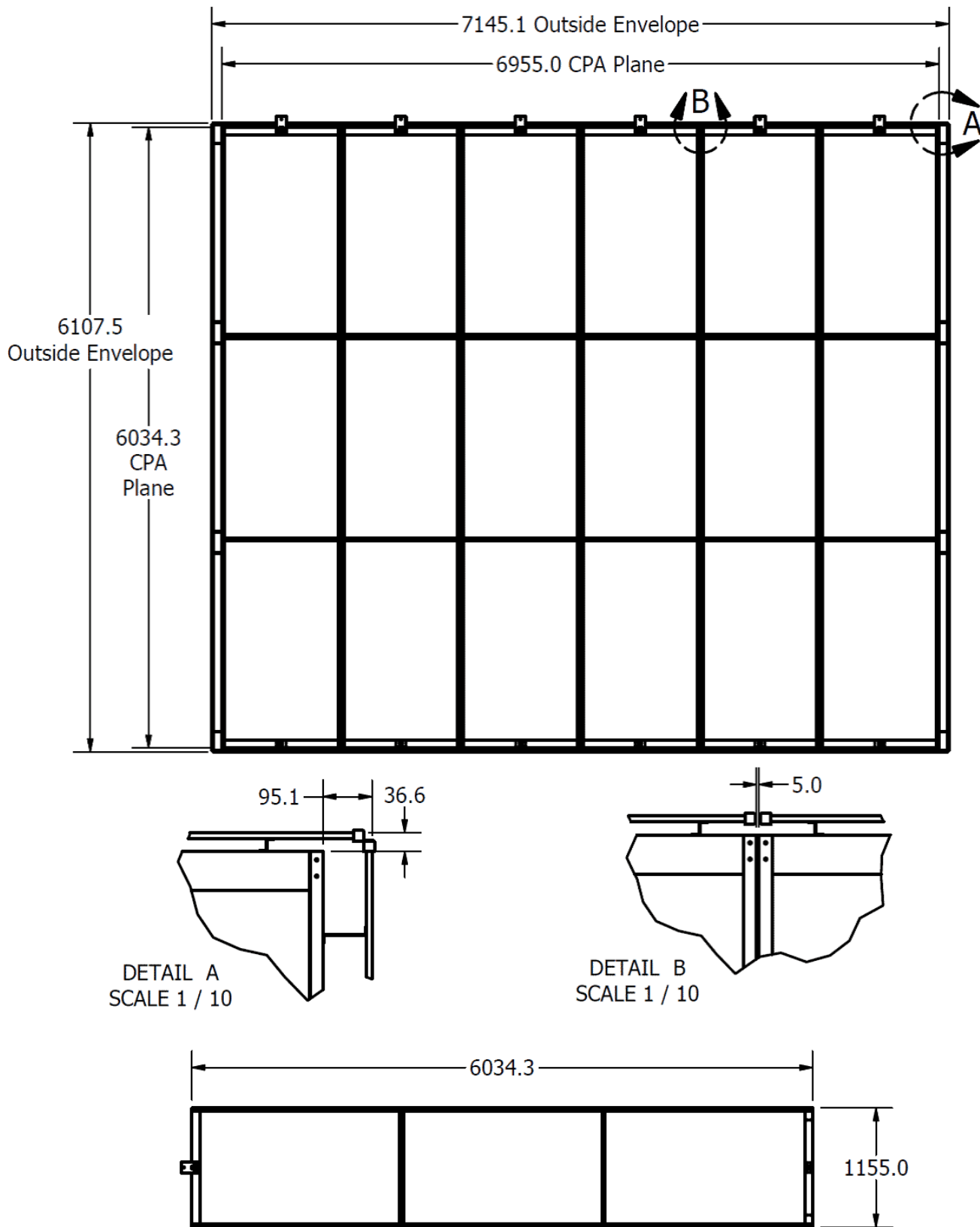


Figure 4.5: Basic geometry of the CPA array, close ups and a CPA column

fig:cpa-

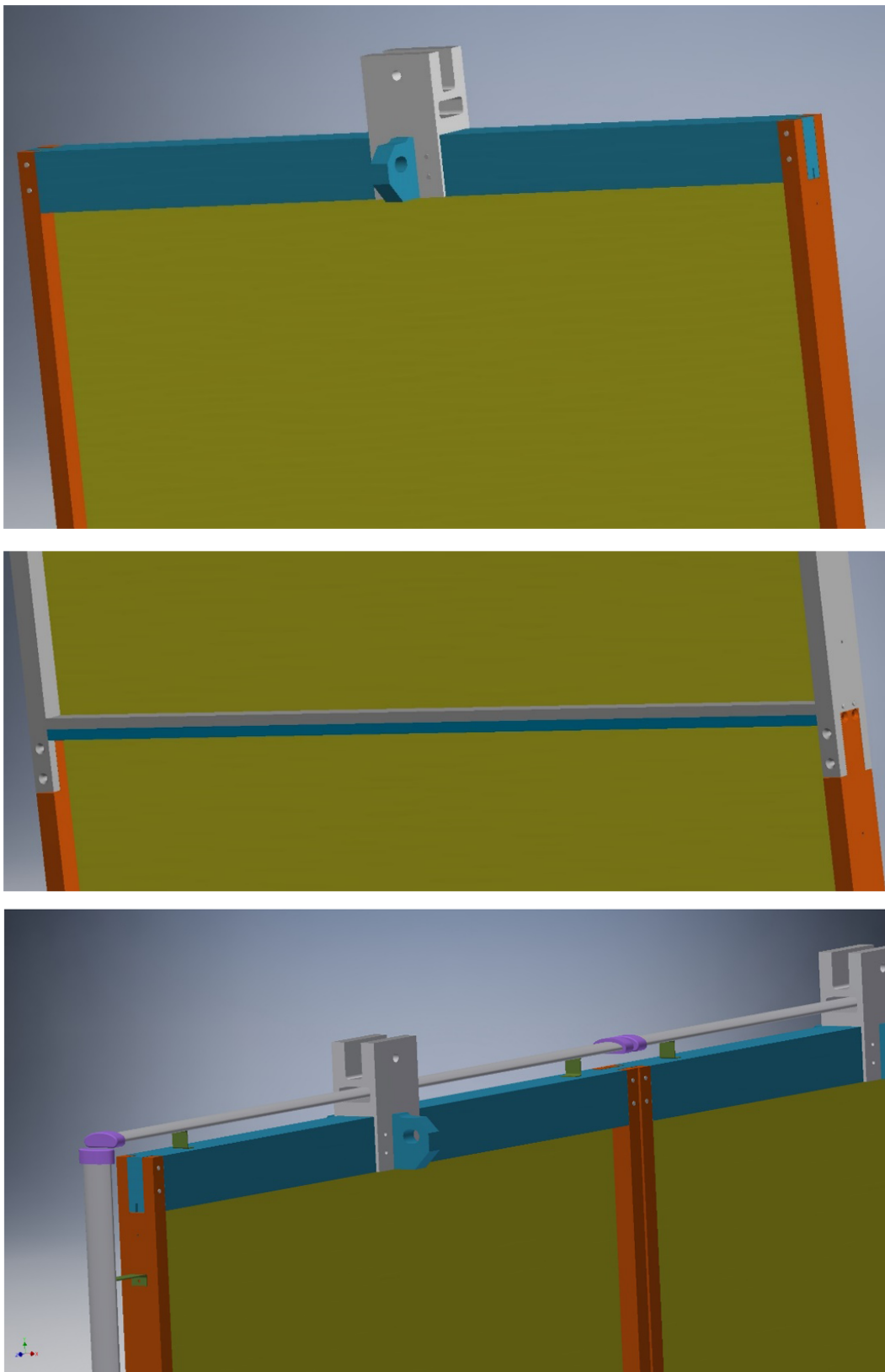
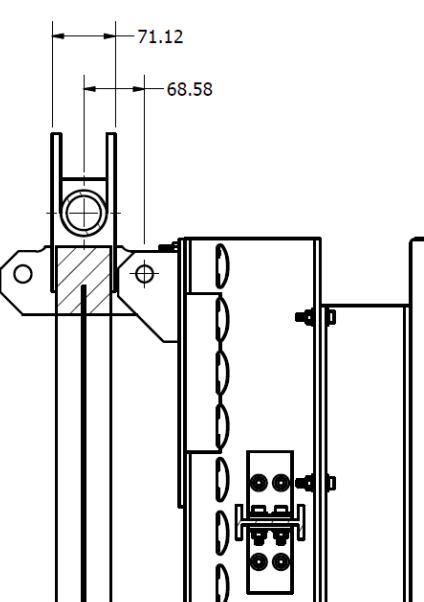
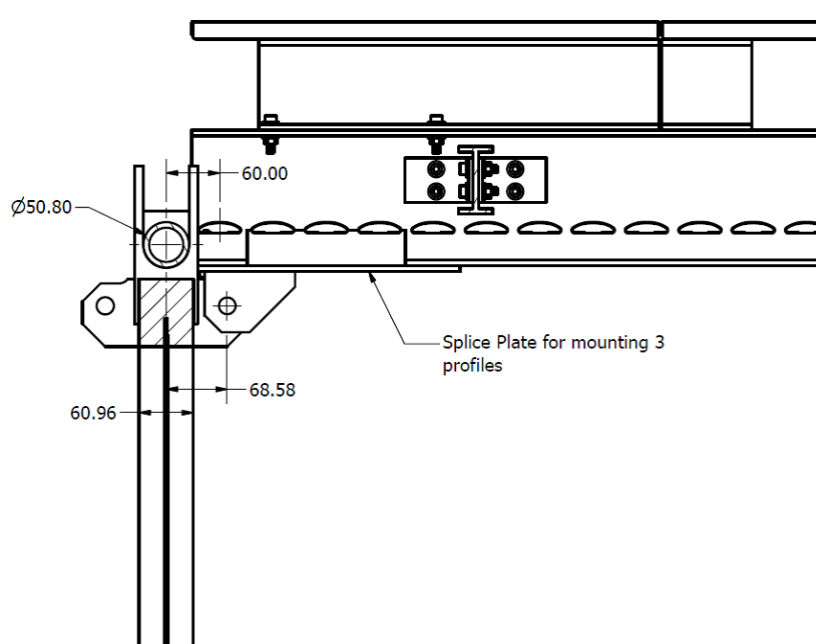


Figure 4.6: Views of various part of the CPAs

fig:cpa-

1 The resistive panel is 1/8" thick G10 and floats within the framework so that no external forces  
2 are applied to it. When hung vertically the weight of the resistive panel ( 30lbs per module) rests  
3 on the bottom cross bar of the module. The weight of the modules is transferred through the side  
4 bars of the frame and up to the top cross bar, see Figure 4.6a. The very top cross bar of the CPA  
5 plane has a block attached to it through which all of the load is transferred to the strap which  
6 attaches to the supporting stainless steel I-beam.

7   [fig:cpa-hinge1](#) [fig:cpa-view2](#)  
Figure 4.7 shows how the FC will be attached to the assembled CPA plane. The top and bottom  
cross bars will have elongated slots through which pins will be inserted to attach the hinged  
connection. The weight of the FC is applied to the center of each top and bottom bar.

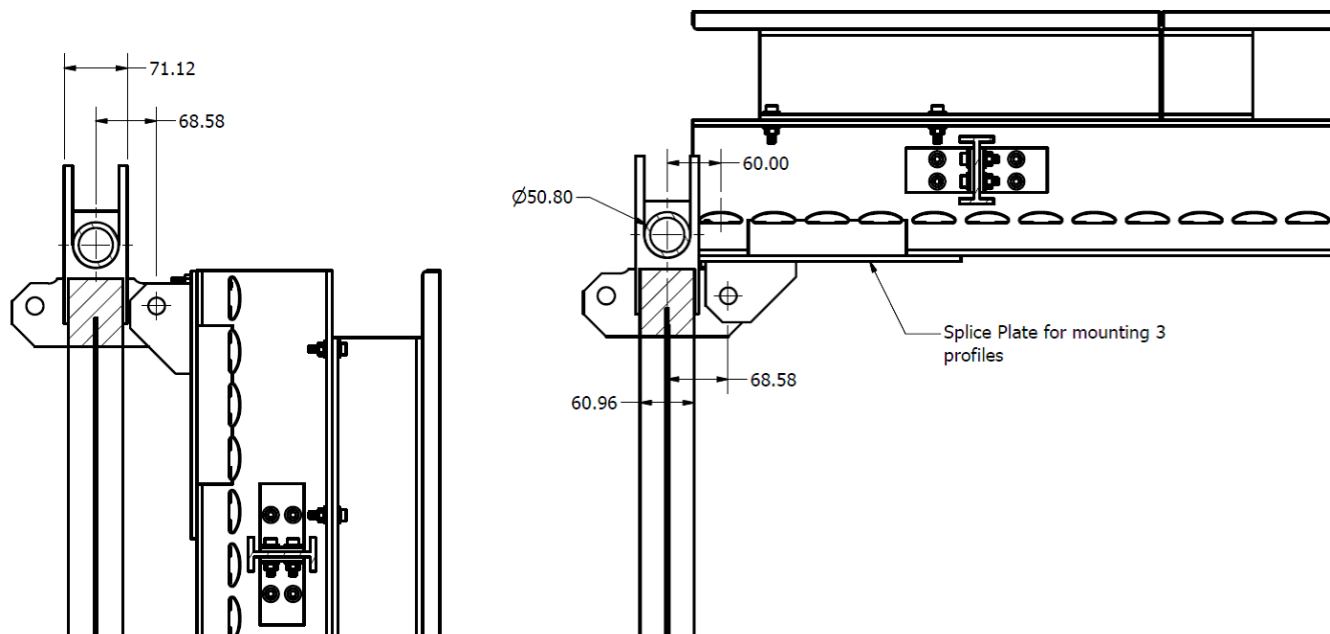
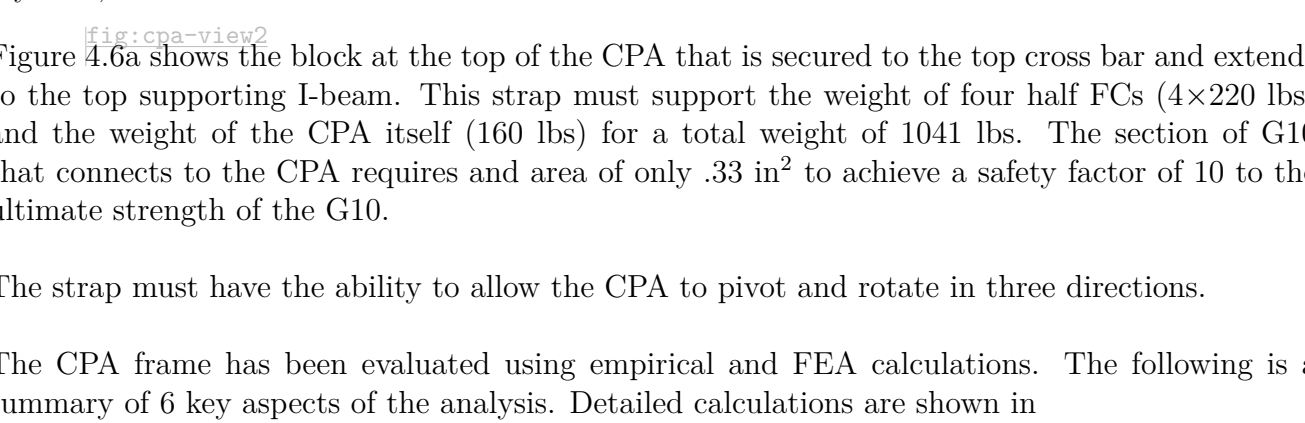


Figure 4.7: The top field cage modules are hung vertically with the CPAs when moved into the cryostat, then rotated to horizontal to attach to the APA

[fig:cpa-cpa](#)

10  [fig:cpa-view2](#)  
Figure 4.6a shows the block at the top of the CPA that is secured to the top cross bar and extends  
to the top supporting I-beam. This strap must support the weight of four half FCs ( $4 \times 220$  lbs)  
and the weight of the CPA itself (160 lbs) for a total weight of 1041 lbs. The section of G10  
that connects to the CPA requires an area of only .33 in<sup>2</sup> to achieve a safety factor of 10 to the  
ultimate strength of the G10.

15 The strap must have the ability to allow the CPA to pivot and rotate in three directions.

16 The CPA frame has been evaluated using empirical and FEA calculations. The following is a  
17 summary of 6 key aspects of the analysis. Detailed calculations are shown in

18 reference to Vic's writeup

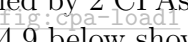
19 .

1 The highest stresses and deflections occur during assembly before the cryostat is filled with liquid.  
2 During installation the CPA must carry the full weight of the FC rather than sharing it with the  
3 APA and the buoyancy force which reduces the load from gravity is not present.  
  
4 In all of the analysis the resistive panels were not included. In the design of the CPA it is planned  
5 that the resistive panel will float within a frame and no load will be applied to it and therefore it  
6 does not contribute to the stiffness of the modules.

7 *A. Lifting the CPA During Installation*

8 During installation the three frames that make up a CPA module will be placed horizontally on  
9 the floor and connected together. The top of the module will then be secured to the crane and  
10 lifted; the bottom of the module will be pivoted on the floor. By lifting and transversing the hook  
11 attached to the top of the module the CPA will be lifted into the vertical position. The worst case  
12 loading occurs immediately after the crane begins to lift the top of the module when it is simply  
13 supported at the bottom and top. The stresses and deflections are small as see in Figure 4.8. The  
14 plane will sag a maximum of roughly 2" and the stresses are below 2,000psi which is far below the  
15 ultimate stress. 

16 *B. CPA Hanging with all FC Attached in Installation Position*

17 The current estimate for the FC weight is 440 lbs. This load is carried by 2 CPAs so each hinge on  
18 the CPA will supposed 220 lbs in the installation position. Figure 4.9 below shows the deflections  
19 and maximum stresses. The larges deflections are at the bottom cross bar of 0.07" and the stresses  
20 are less than 2,000psi which is far below the ultimate stress of G10. 

21 *C. CPA Hanging with all FC Attached in Deployed Position With Weight of Workers on FC*

22 The current estimate for the FC weight is 440 lbs. This load is carried by 2 CPAs and by the  
23 APAs so each hinge on the CPA will supposed 110 lbs in the installation position. In addition, in  
24 the worst case a 200 lbs worker could be standing directly over an I-beam on the FC directly next  
25 to a CPA. The top two hinges on the CPA will have 110 lbs applied. One of the bottom hinges  
26 will have a 110 lbs load also and the second bottom hinge will have 110 lbs of the FC plus the 200  
27 lbs of the worker applied. The largest deflection is 0.1" at the bottom cross bar and the stresses  
28 are less than 2200psi which is far below the ultimate stress of G10.

29 *D. Connection Stresses*

30 The weight of the CPA and the bottom FC is transferred through the side bars of the CPA frame.  
31 The connection between the side bars and the top cross bar therefore will experience the highest  
32 loads. A single 1/4" diameter G10 pin at the connection would have a shear stress of 7740psi  
33 which provides a safety factor of greater than 4. A second pin at each connection would increase  
34 the safety factor to 8.

35 *E. Deformation and Stress Due to Pressure from Circulating Liquid Argon*

36 Calculations done at FermiLab indicate that a uniform 2Pa pressure during cool down will be

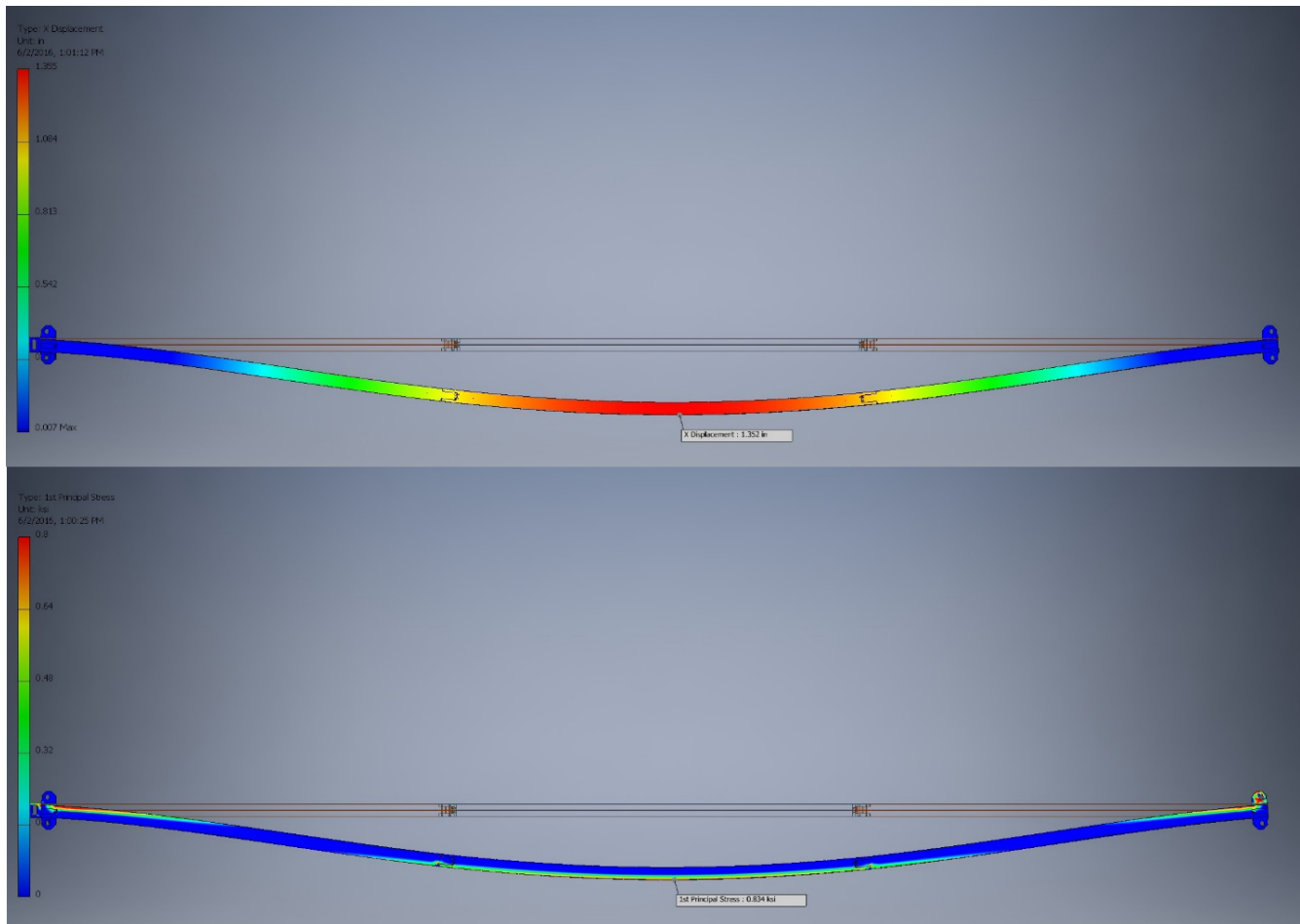


Figure 4.8: Stress and deflection of a connected 3 CPA stack in horizontal position supported at both ends

fig:cpa-

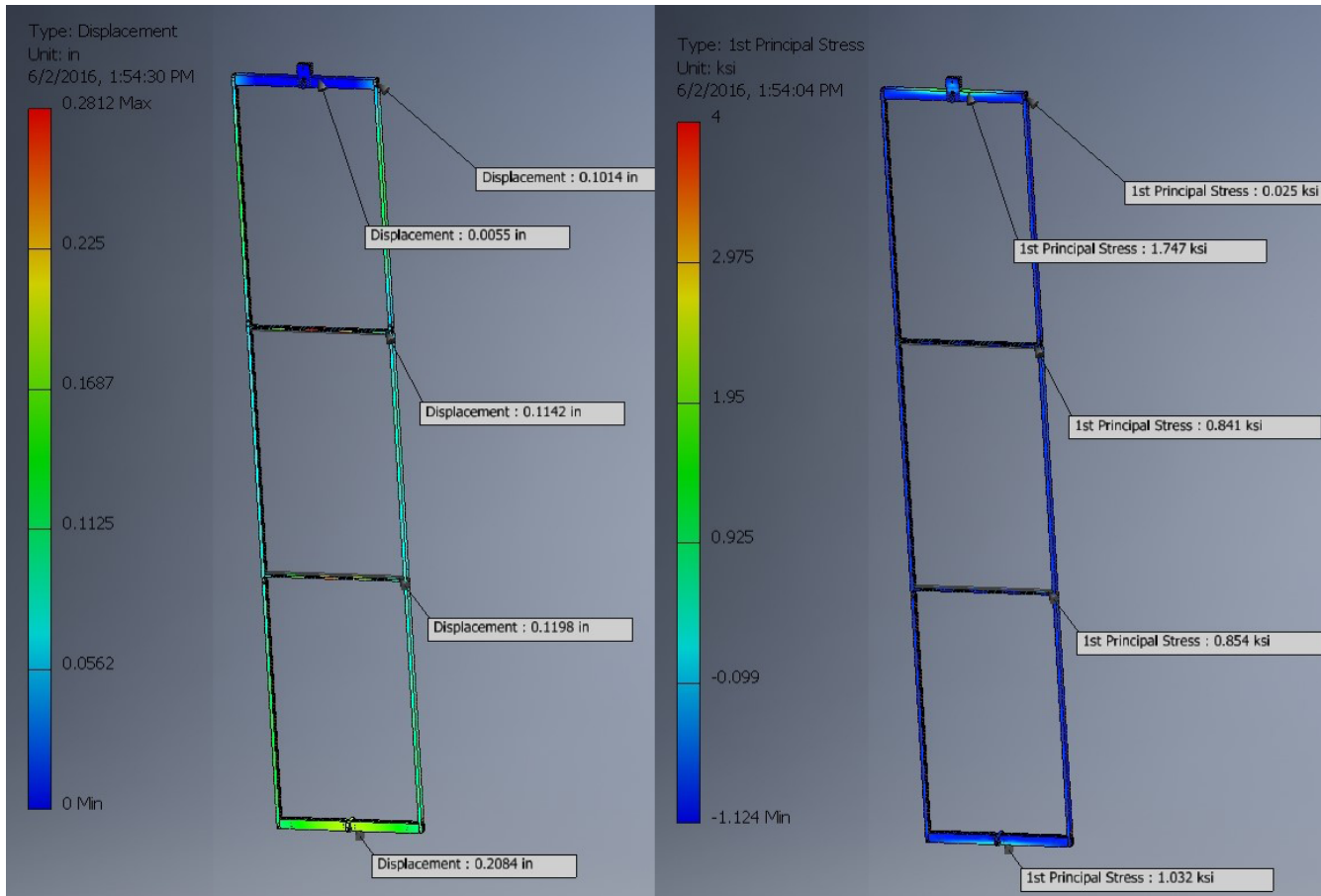


Figure 4.9: Stress and deflection of a connected 3 CPA stack suspended on the rail with 4 FC modules

fig:cpa-

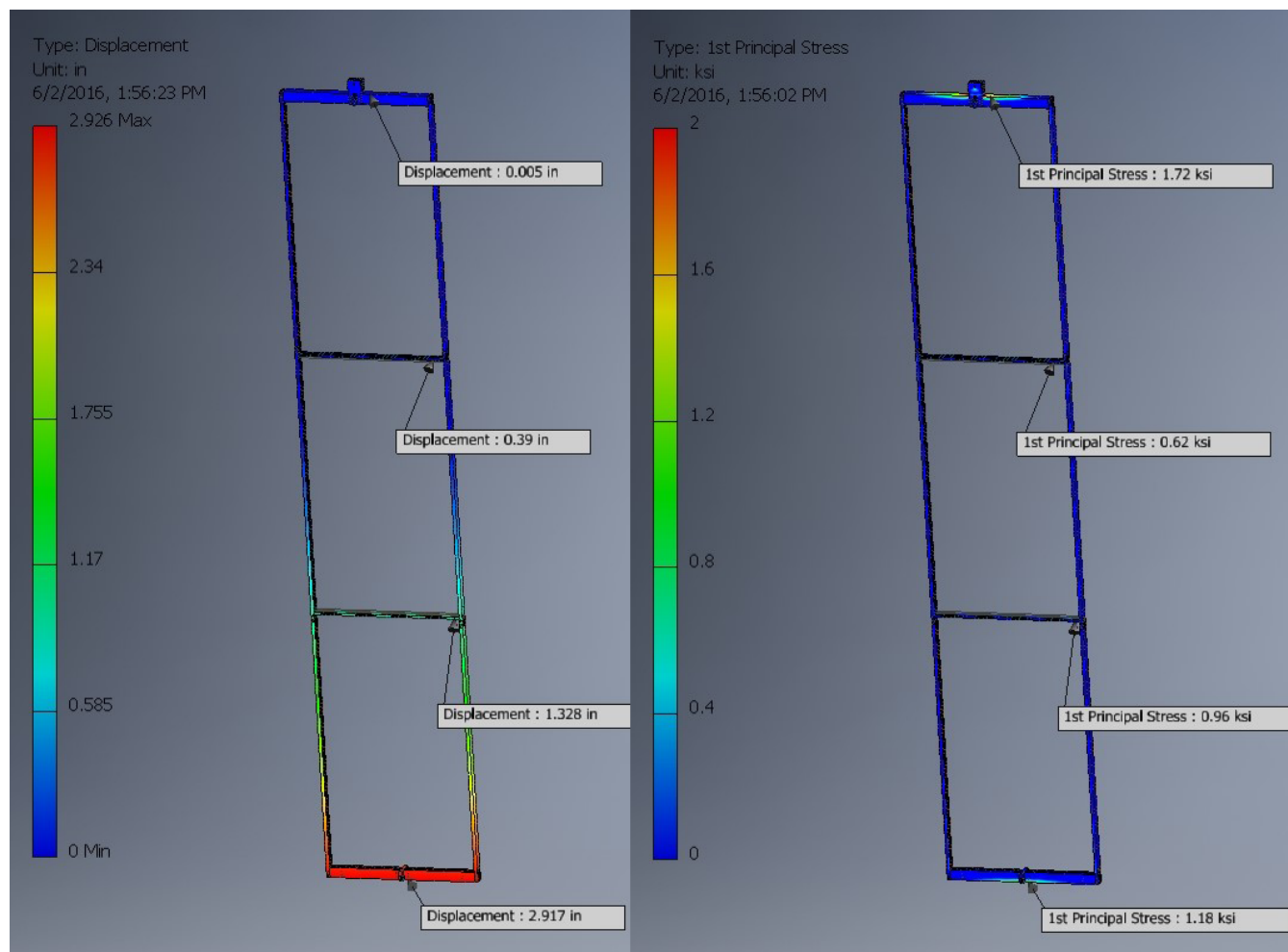


Figure 4.10: Stresses and Deflections of CPA with FC Deployed and 200 lb Worker Load

fig:cpa-

<sup>1</sup> applied to the resistive panels. Calculations show that this will result in 0.090" deflections of the  
<sup>2</sup> panel at its center. The CPA/FC/APA assembly will displace 8.8mm laterally as a result of the  
<sup>3</sup> next force from this pressure.

<sup>4</sup> *F. Thermal Considerations*

<sup>5</sup> When the CPA modules are cooled their width will shrink by 0.9mm. The supporting stainless  
<sup>6</sup> steel beam will shrink by 1.6mm over the width of the CPA. If the CPA supports are rigidly  
<sup>7</sup> attached to the supporting stainless steel beam then an interference of 1.6m-.9mm = .7mm will  
<sup>8</sup> occur. In order to prevent this interference an initial gap of 0.7mm between CPA's is required  
<sup>9</sup> which will insure that the CPAs are in contact after cool down.

<sup>10</sup> The steel beam between the CPA and APA will cool and shrink by 5.2mm. The joint between the  
<sup>11</sup> FC and the CPA must be able to accommodate this shrinkage.

<sup>12</sup> **The HV distribution bus and HV feedthrough receptacle**

<sup>13</sup> Should this be moved to the HV section?

<sup>14</sup> **The mechanical and electrical interconnect features between modules**

<sup>15</sup> There are a stack of 3 modules interconnected vertically to form the 6m height of the SP Proto-  
<sup>16</sup> DUNE cathode. The frames of these modules are bolted together using tongue and groove con-  
<sup>17</sup> nections at the ends, and the resistive cathode sheets, and the field shaping strips are connected  
<sup>18</sup> using a few metallic buttons to ensure redundant electrical contact between vertical modules.

<sup>19</sup> There are 6 columns of the 6m tall CPA modules in SP ProtoDUNE. Each column is suspended  
<sup>20</sup> to the CPA rail using a central lifting bar. Due to the roof movement between the warm and cold  
<sup>21</sup> phases of the cryostat, each column is expected to move 2mm relative to its neighbors. Several  
<sup>22</sup> pin and slot connections are implemented at the long edges of the CPA columns to ensure the  
<sup>23</sup> co-planarity of the modules and yet allow small vertical displacement. The HV bus interconnect  
<sup>24</sup> the resistive cathode surfaces across the columns to maintain a uniform voltage across the cathode  
<sup>25</sup> surface.

<sup>26</sup> **4.2.5 Assembly and Installation**

<sup>27</sup> Individual CPA panels will be assembled off site and shipped to CERN in the horizontal position.  
<sup>28</sup> Each panel weights roughly 53 lbs and therefore can be lifted out of the shipping crate by hand  
<sup>29</sup> and will not require and special fixtures.

<sup>30</sup> The three CPA modules that made up a CPA panel will be placed on the floor and screwed/pinned

- <sup>1</sup> together. The crane then will be attached to the top of the CPA and it will be lifted to the vertical  
<sup>2</sup> position.
- <sup>3</sup> The load transfer from the crane hook to the installation rail still needs to be determined.
- <sup>4</sup> Once two CPA planes are mounted they must be brought together within 1mm along their length.  
<sup>5</sup> (see thermal discussion in Section 7). There will be two pins located on the side of the first CPA  
<sup>6</sup> that will have to fit into a vertical slot on the side of the second CPA to lock them together in  
<sup>7</sup> plane.
- <sup>8</sup> The CPA plane may not hang vertically after being hung if the strap is not perfectly on center.  
<sup>9</sup> This can be corrected when the FC are mounted to a pair of CPA planes. The connection points  
<sup>10</sup> on the FC is fixed and therefore will tie the CPA's together and force them to hang vertically  
<sup>11</sup> because the assembly of the CPA planes and FC then becomes a two point support structure.
- <sup>12</sup> During assembly the FC will be hung from the CPA. In a worst case scenario the two FC will be  
<sup>13</sup> mounted on one side of the CPA first which will cause the CPA to rotate 2.9" due to the offset  
<sup>14</sup> loading.

## <sup>15</sup> 4.3 Field Cage

### <sup>16</sup> 4.3.1 Scope, Requirements and Design Parameters

<sup>17</sup> In the SP ProtoDUNE TPC, each pair of facing cathode and anode planes forms an electron-drift  
<sup>18</sup> region. A field cage must completely surround the four open sides of this region to provide the  
<sup>19</sup> necessary boundary conditions to ensure a uniform electric field within, unaffected by the presence  
<sup>20</sup> of the cryostat walls and other nearby conductive structures.

<sup>21</sup> The SP ProtoDUNE field cages are constructed from tiled field cage modules. Each module is build  
<sup>22</sup> with a number of parallel metal profiles interconnected by a resistive divider chain, and supported  
<sup>23</sup> by pultruded fiber glass beams (FRP) span between the CPA and the APA. The metal profiles  
<sup>24</sup> between modules are neither mechanically nor electrically connected. The electrical isolation  
<sup>25</sup> between the field cage modules minimizes the peak energy dump in case of a HV discharge.

- <sup>26</sup> • Provide the nominal drift field of 500V/cm
- <sup>27</sup> • Withstand -180kV near the cathode
- <sup>28</sup> • Define the drift distance between the APAs and CPAs to <1cm
- <sup>29</sup> • Limit the electric field exposed to LAr to under 30kV/cm
- <sup>30</sup> • Minimize the peak energy transfer in case of a HV discharge anywhere on the field cage, or

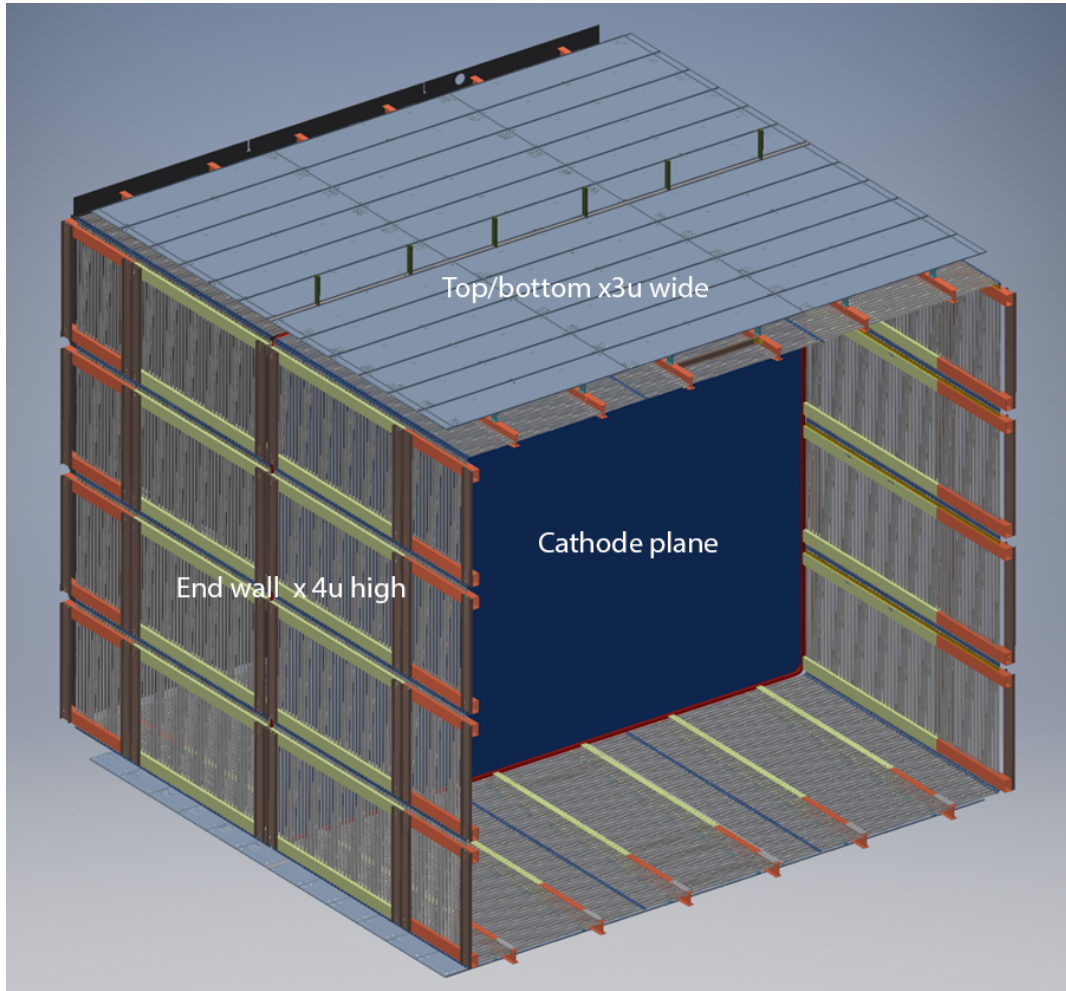


Figure 4.11: A view of the TPC field cage

fig:fc-

- 1           cathode
- 2       • Provide redundancy in the resistor divider
- 3       • The divider current must be » the ionization current in the TPC drift cell, yet less than the  
4           power supply current limit when all dividers are connected in parallel
- 5       • Constructed in modular form that can be easily installed in the cryostat
- 6       • Provide support for the beam plug
- 7       • Allow calibration laser beams to enter into the active volume
- 8       • The bottom field cage module must be able to support a person standing on its support  
9           beam
- 10      • Must be configurable to either 3.6m or 2.5m drift length inside the cryostat
- 11      • No trapped volume

### 12   **4.3.2 Electrical Design**

13   Given a large standoff distance between the field cage and the grounded cryostat wall, it is relatively  
14   easy to design a field cage that meet the 30kV/cm E field limit with 180kV bias. However, it  
15   becomes challenging if we want to reduce the clearance between field cage and ground to make  
16   more efficient use of liquid argon. To achieve this goal, one must look for electrode with a low  
17   profile, rounded edges, no trapped volumn, low cost. Several commercially available roll formed  
18   metal profiles were studied and appear to meet these requirements.

#### 19   **Electrostatic analysis**

20   One particular profile (Dahlstrom Roll Form # 1071) were found to have the lowest surface E field  
21   of about 12kV/cm when biased at 180kV with only a 20cm ground clearance (see Figure 4.12).  
fig:tc-profile1071

22   In order to maintain a modular design of the field cage, and minimize peak energy transfer in a  
23   discharge, we chose to construct the field cage with electrical isolation between neighboring modules  
24   such that if a discharge occurs on one field cage, the nearby electrodes from the neighboring  
25   modules will not arc over and causing a domino effect. This requires a high voltage insulation  
26   between profile ends of the order of 180kV. 5mm thick UHMW PE caps are placed over both ends  
27   of a profile to serve this purpose. This technique also limits the exposed electric field in LAr at  
28   the corner of the field cage, see Figure ??.

29   The center to center distance between the profiles is set to 6cm, and the inner surface of all profiles

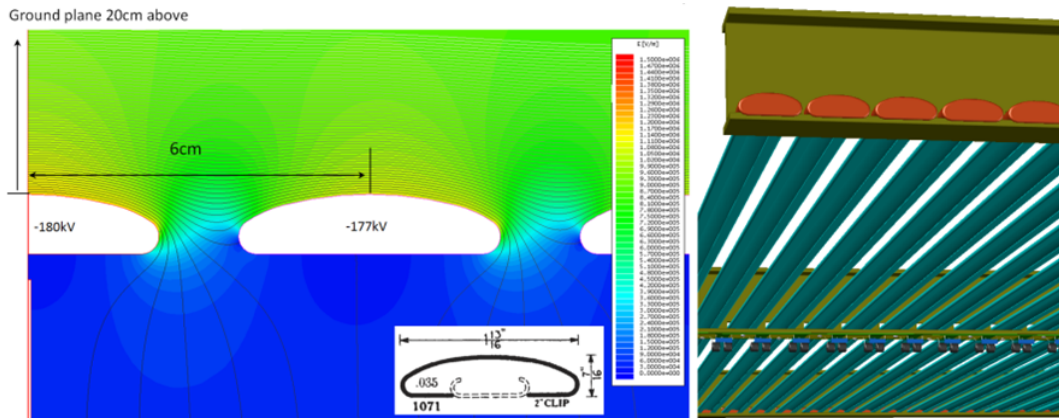


Figure 4.12: A 2D FEA of a configuration using profile 1071, and a conceptual design of the field cage module

fig:fc-p

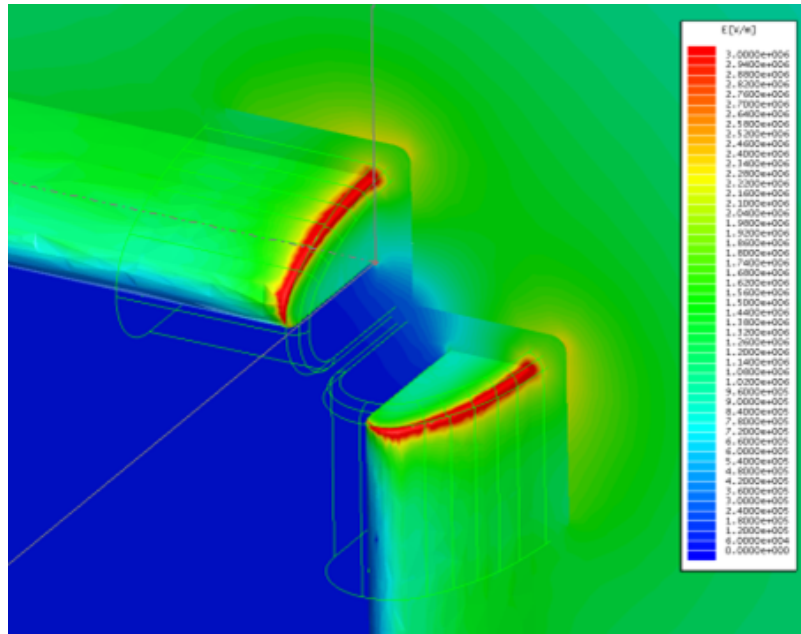


Figure 4.13: A 3D FEA of a field cage corner. The PE caps (in outline form) limit the exposed E field to

fig:fc\_p

1 on a field cage module is placed 5cm beyond the nearest surface of the TPC active volume (defined  
2 by the APA active aperture over the drift distance). The E field uniformity at the edge of the  
3 active volume is expected to be within  $\pm 2\%$  of the nominal value.

4 **Surge suppressor on field cage**

5 The resistors along the divider provide a linear DC voltage gradient. However, at shorter time  
6 scale ( $\ll 1\text{s}$ ), the electrical behavior of the divider is determined by the various capacitances on and  
7 between each electrode. This divider is no longer linear at this time scale.

8 A perfect capacitive divider requires the capacitance of each node to ground to be zero. In reality,  
9 there is always a finite capacitance from each node to ground. These capacitances resist change  
10 in the voltages on the nodes. In the event of a HV breakdown between the cathode to ground  
11 (cryostat), the cathode voltage quickly collapses to ground, but the first field cage electrode to  
12 ground capacitance keeps its voltage from changing instantaneously to follow the cathode voltage,  
13 resulting in a momentary larger voltage differential between the cathode and the first field cage  
14 electrode. This voltage differential can be a significant fraction of the cathode operating voltage,  
15 large enough to cause HV breakdown between the two electrodes, or worse yet, destroy the divider  
16 resistors between the two electrodes.

17 A natural solution to this problem is to significantly increase the capacitance between the nodes  
18 of this divider. This was the approach adopted in the 35ton field cage through the use of double  
19 sided printed circuit boards. However, the cost of the PCB version of the field cage at DUNE scale  
20 is very high. Adding discrete HV capacitors between divider taps is also expensive.

21 An alternative is to use surge suppressors in parallel with the divider resistors to divert the trans-  
22 sient current from the resistors. Extensive tests have been done by MicroBooNE (docdb 3242,  
23 arXiv:1406.5216v2) on the use of metal oxide varistors (MOV) and GDTs (gas discharge tubes) as  
24 a mean of limiting the over voltage condition in the event of a HV discharge in the TPC.

25 Both types will work for the purpose of restricting the voltage differential between field cage rings  
26 in LAr temperature: A GDT quickly shorts the terminals when the voltage differential exceeds a  
27 threshold; while a varistor changes its resistance to keep the voltage differential near the threshold  
28 voltage. The smooth transition and well defined clamping voltage of the varistors are preferred to  
29 the abrupt switching of the GDTs. The varistors could also function as redundant “resistors” in a  
30 divider chain in case a resistor is open circuit.

31 One readily available MOV family with high threshold voltage is the Panasonic ERZ-VXXD182.  
32 They have a threshold voltage around 1600V. Two of these in series could work with the current  
33 3kV differential between divider taps. However, we would not be able to raise the E field much  
34 above the nominal 500 V/cm with this configuration. To allow some headroom in operating field,  
35 3 such MOVs in series is needed.

<sup>1</sup> Resister tolerance and spec

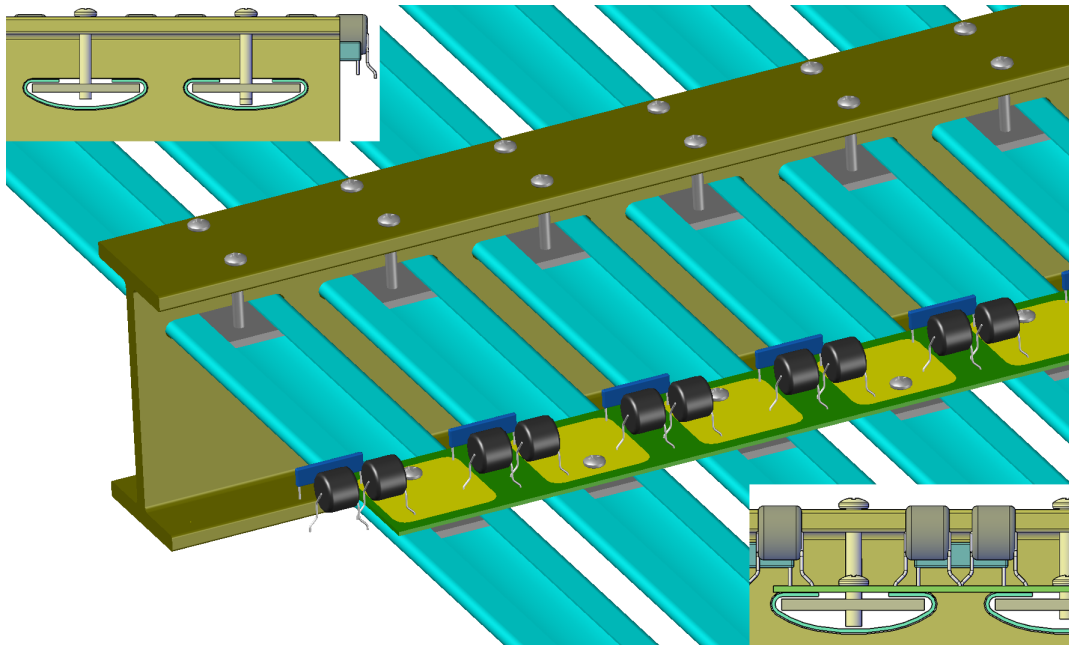


Figure 4.14: A view of a resistive divider

fig:fc-d

<sup>2</sup> Electrical Schematic

<sup>3</sup> **4.3.3 Validation tests of roll formed FC design**

<sup>4</sup> A dedicated test setup has been designed and constructed to validate the field cage concept in  
<sup>5</sup> purified LAr. It consists of a field cage (Figure 4.16), fitting into the ICARUS 50 liter cryostat  
<sup>6</sup> (1.1 m hight, 0.6 m diameter) available at CERN, and including:

- <sup>7</sup> • Roll-formed metal profiles with UHMW PE caps.
- <sup>8</sup> • Pultruded fiberglass I-beams form 4 mini panels.
- <sup>9</sup> • HV cable feed-through (equipped with corona monitor) allowing to apply up to 150 kV on  
<sup>10</sup> FC profiles.
- <sup>11</sup> • All profiles are at same potential to simplify HV connection
- <sup>12</sup> • ICARUS-like stainless steel ground planes placed 66mm away from FC profiles ( 1/3 of FD  
<sup>13</sup> bias voltage to reach same E field)
- <sup>14</sup> • Video cameras in Gas phase to monitor bubbles and sparks.

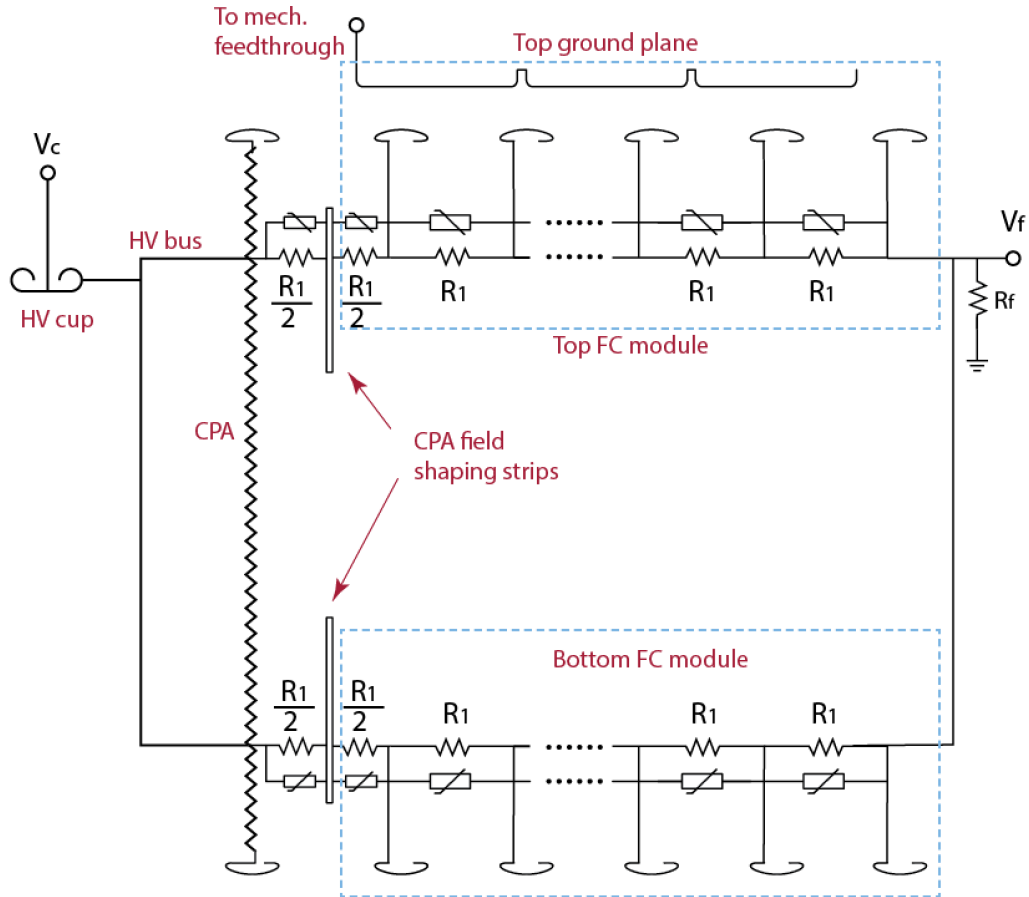


Figure 4.15: A schematic diagram of the CPA and a top/bottom field cage module pair

fig:fc-s

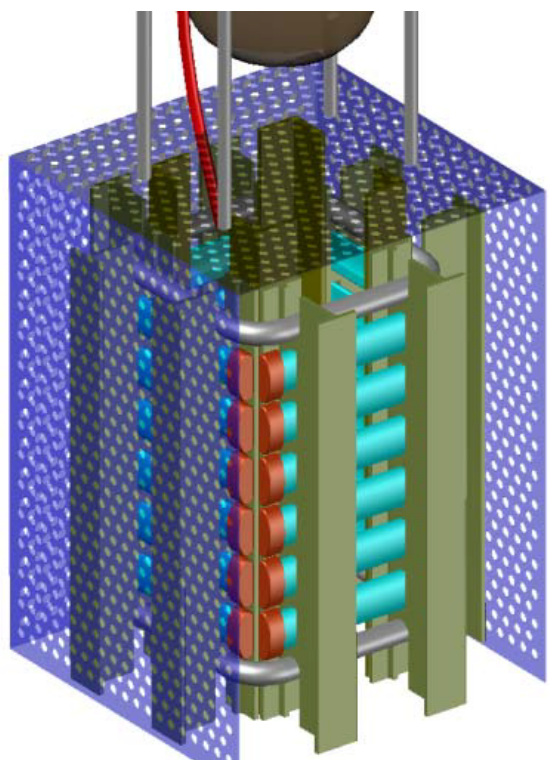


Figure 4.16: The field cage test setup. **Left:** schematic drawings of the cage showing the main elements: metal profiles, I-beams, ground planes. **Right:** Picture of the realized setup.

fig:fc-t

<sup>1</sup> Two choices of material (Aluminum, Stainless Steel) for the metal profiles have been tested. In  
<sup>2</sup> the Aluminum case, the surface finish has also been tested with scratches up to 100 um deep.

<sup>3</sup> The cage was operated both in commercial LAr and, connected to the ICARUS 50 liter recirculation  
<sup>4</sup> system, in LAr with purity better than 0.1 ppb O<sub>2</sub> equivalent. HV above 80 kV (corresponding  
<sup>5</sup> to an electric field about 20% higher than nominal) could be applied for several days, without  
<sup>6</sup> recording any discharge. Two additional regimes have been studied:

<sup>7</sup> • with the 50 liter vessel fully thermalized (no visible bubble formation along the detector) no  
<sup>8</sup> sparks ever recorded up to 100 kV.

<sup>9</sup> • HV instabilities arise in the 80-100 kV range if the LAr is not perfectly thermalized allowing  
<sup>10</sup> bubble formation from heat sources (HV feedthrough, ground connections): few random  
<sup>11</sup> sparks recorded, developing however around the HV cable and not between the field cage  
<sup>12</sup> and the ground plates

<sup>13</sup> All tested materials exhibited the same behaviour in the applied HV range.

<sup>14</sup> Nickel coating (up to 20 um) of aluminum profiles was also proposed to avoid oxidation of the  
<sup>15</sup> surface which could possibly be a source of HV instability. Its stability against thermal gradients  
<sup>16</sup> was positively tested. However HV tests showed no difference with respect to the uncoated version.

<sup>17</sup> A specific Breakdown Test has been performed to check dielectric rigidity of the UHMW PE end  
<sup>18</sup> caps in LAr, exposing few metal profiles equipped with PE end caps and connected the HV, to a  
<sup>19</sup> ground plane (Figure 4.17).

<sup>20</sup> Results demonstrated that the proposed end cap geometry and thickness can safely hold 150 kV.

#### <sup>21</sup> 4.3.4 Ground Plane Design

<sup>22</sup> In order to confine the electric field in the liquid argon region, it is foreseen to install a metallic  
<sup>23</sup> plane, put to ground, between the upper field cage module and the liquid-gas interface. The design  
<sup>24</sup> of such Ground Plane (GP) is inspired by the one from the ICARUS T600 detector, and it is meant  
<sup>25</sup> to limit the residual electric field in the liquid below the usual 30 kV/cm. value. The design details  
<sup>26</sup> of the planes were verified to comply with the requests on residual electric field with FEA. It is  
<sup>27</sup> noted that a similar GP could be added in front of all the other Field Cage (FC) modules, in order  
<sup>28</sup> to smooth the field in the LAr dead volume. However, so far it is foreseen to add an actual GP  
<sup>29</sup> only below the bottom FC, to further smooth the field in the region where pipings for the cryostat  
<sup>30</sup> filling are running. The distance between the cryostat walls and the end-wall field cage does not  
<sup>31</sup> require to insert a GP, instead.

<sup>32</sup> As mentioned, the GP design is inspired by the ICARUS T600 detector: in that case, 1 mm thick  
<sup>33</sup> Stainless Steel (SS) plates, punched with 10 mm holes, 15 mm pitch ( $\sim$  50% transparency), could  
<sup>34</sup> stand a potential differential of  $-150$  kV over 100 mm. In order to smooth the field, the edges of  
<sup>35</sup> the planes were rounded to  $\sim$  10 mm. The fraction of punched structure was selected to ensure



Figure 4.17: Setup to test dielectric rigidity of the UHMW PE end caps

fig:endc

<sup>1</sup> light-weight even with SS, and to allow fluid circulation above the planes.  
<sup>2</sup> In the ProtoDUNE configuration, the GP will be put at a distance of 200 mm from the FC profile,  
<sup>3</sup> with a structure of 6 mm holes, 10 mm pitch ( $\sim 25\%$  transparency): the lower fraction of pierced  
<sup>4</sup> surface is verified by simulations to maintain the field within the required values. The edges of  
<sup>5</sup> the plates, 20 mm high, are rounded at 5 mm, while the holes rounding radius, at production is  
<sup>6</sup> around 0.5 mm. The liquid level is expected to be at 40 mm above the GP bottom, i.e. 20 mm  
<sup>7</sup> above the edges. The radius of curvature for the holes is not a strict requirement. It depends on  
<sup>8</sup> the punching technique, and usually is at around 0.5 mm. The actual requirement is to have the  
<sup>9</sup> hole curvature on the inside (of the TPC) looking out.

<sup>10</sup> Two sets of pieces were initially produced in Europe:

- <sup>11</sup> • 8 pieces of dimension  $198 \times 571$  mm (weight  $< 1$  kg each) to be installed in the CERN field  
<sup>12</sup> cage prototype,
- <sup>13</sup> • 6 more pieces of  $525 \times 2318$  mm (weight around 8.5 kg each), which represent full scale  
<sup>14</sup> components for ProtoDUNE. The drawing of this second set of pieces, sent to US for test  
<sup>15</sup> assemblies, is shown in Figure 4.18. [Fig:gp\\_panels](#)

<sup>16</sup> The choice of electropolished Stainless Steel *AISI 304 L* over Aluminum derives from the experience  
<sup>17</sup> of the ICARUS detector, moreover:

- <sup>18</sup> • SS and G10 have very similar dilatation coefficients, while Aluminum does not. Choosing SS  
<sup>19</sup> ensures that all the *GP + G10* structure contracts consistently, without too large stresses  
<sup>20</sup> at the connections;
- <sup>21</sup> • SS is more ductile than Aluminum, which makes *easier* to machine the corners of the pieces.  
<sup>22</sup> Note that anyway some imperfections are present even in the SS case, and not all corners  
<sup>23</sup> will be perfectly identical.
- <sup>24</sup> • Though Aluminum would guarantee a factor 3 lighter GP, the overall weight of the SS pieces  
<sup>25</sup> remains contained (order of 550 kg).

#### <sup>26</sup> 4.3.5 Field Cage prototype at CERN

<sup>27</sup> The main description of the Field Cage Prototype built at CERN, and the tests performed on it,  
<sup>28</sup> is provided in section ... . In here simply the details concerning the GP are reminded. The smaller  
<sup>29</sup> pieces of GP were installed on the field cage prototype at CERN, to test the configuration. As  
<sup>30</sup> described elsewhere, the actual distance between the field cage profiles and the GP in this prototype  
<sup>31</sup> is of 60 mm, therefore a voltage of 60 kV minimum must be attained to verify the ProtoDUNE  
<sup>32</sup> field configuration. (Figure [Fig:fc\\_prot](#)) During multiple tests in LAr, both with open-air dewars and in  
<sup>33</sup> a clean liquid configuration, the structure always stood the 60 kV voltage, and it was in general  
<sup>34</sup> possible to reach the value of 80-100 kV, after which discharges would start. However discharges  
<sup>35</sup> were always localized on the HV cables, not involving the GP-FC structure.

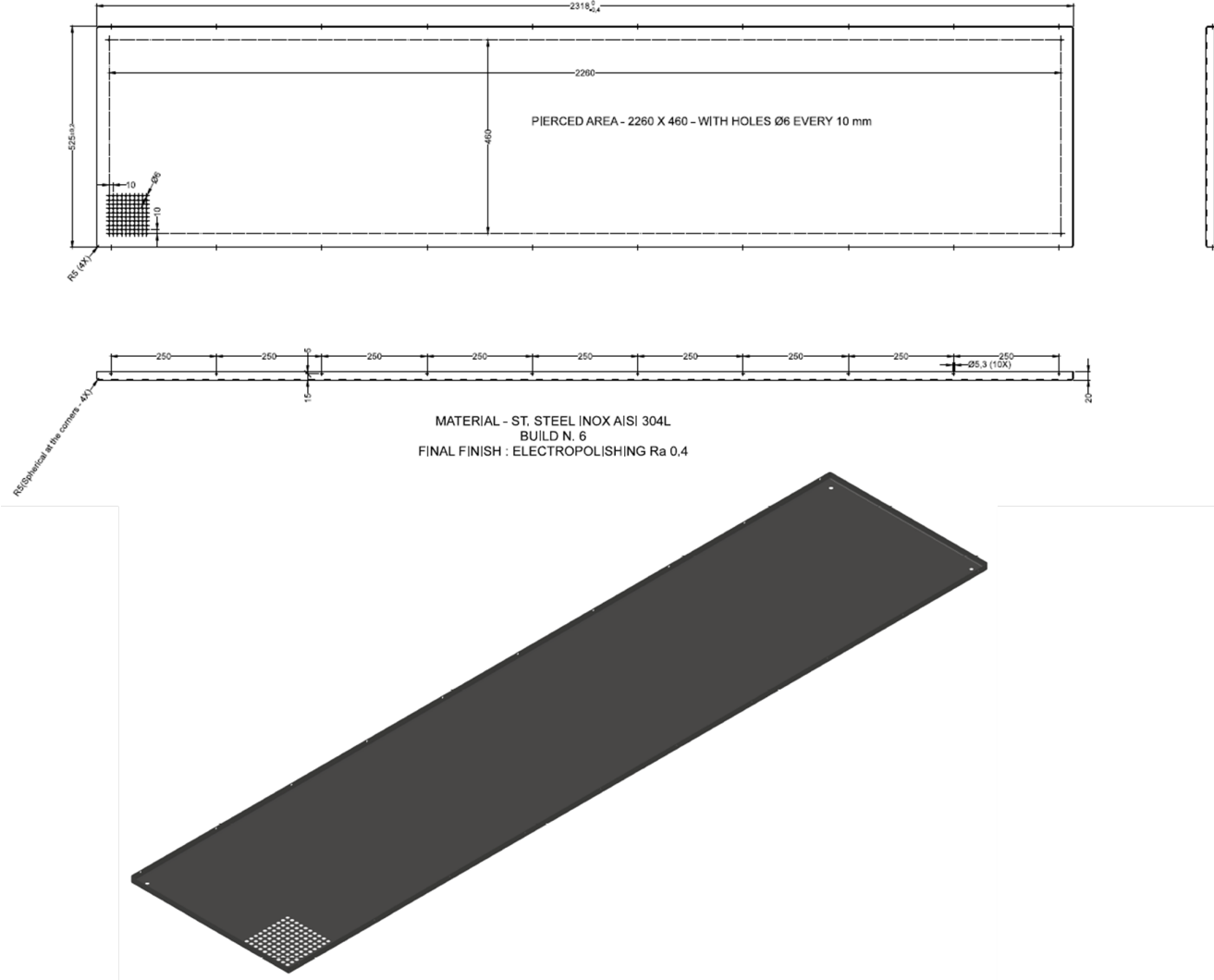


Figure 4.18: Top: Technical Drawing, by Claudio Montanari, of the Ground Plane panels for ProdoDUNE. Bottom: 3D model of one panel

fig:gp\_p

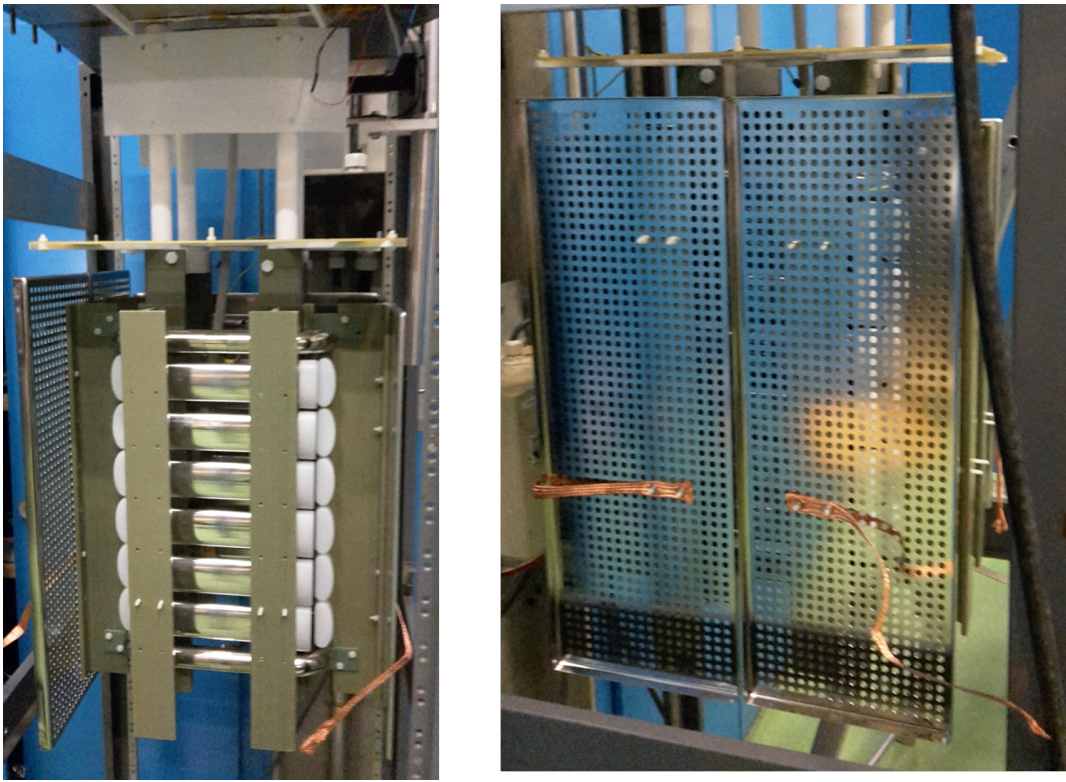


Figure 4.19: Details of the Field Cage Prototype at CERN, showing the installed GP panels.

`fig:fc_p`

#### **4.3.6 Field Cage and Ground Plane in ProtoDUNE**

The design details of the FC+GP modules for ProtoDUNE is described and shown in the next section. Here a 3D model of one fully assembled module is shown for understanding in Figure 4.20.

One module will be made of 6 pieces, put next to each other along the 2318 mm direction: this dimension is made to match the APA and FC module widths. The planes are connected to the FC beam with further G10 pieces that are used also to connect two neighboring GP panels.

The electrical continuity between consecutive panels can be performed with metallic screws (with holes on the planes edges) or with looser connections, like copper strips, that better adapt to the shrinking of the structure during cool-down. Copper strips were successfully employed on the CERN FC prototype. As for most detector systems, the GP should be referenced to the detector ground, set at cryostat top.

The GP modules will be installed on the corresponding FC modules in the clean room outside the cryostat, to facilitate the connections. The description of how the top/bottom FC modules are assembled and connected to the CPA before insertion in the cryostat is provided in section ... .

Further GP panels need to be attached to the top FC module:

- smaller panels will have to be connected on the modules on one side of the CPA so that,

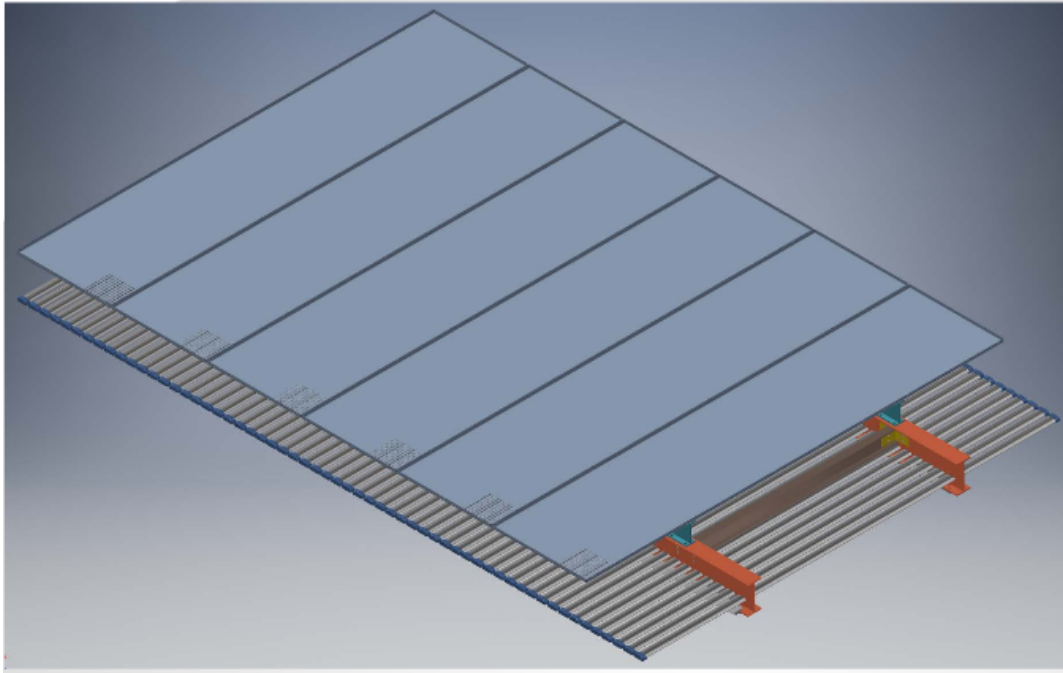


Figure 4.20: 3D model of one fully assembled FC+GP module, for the top of the field cage.

`fig:fc_f`

once in position, they should cover the CPA frame. Their dimension is still to be defined, depending on the final design of the CPA hanging scheme. Such pieces should also be connected to the modules covering the opposite drift region, when in final position;

- a further set of small panels should be installed on the outer modules of the FC, to extend the GP over the vertical FC walls, to further constrain the electric field in these regions. A FEA (Figure 4.21) shows that the optimized overhang distance is 20 cm, provided LAr is at 40 mm above the GP bottom. The maximal residual field in this configuration is of the order of 13 kV/cm, with less than 1 kV/cm field in the gas phase.

### 4.3.7 Designs of the Field Cage Modules

#### Top and bottom modules

#### End wall modules

### 4.3.8 Interfaces to Other TPC Components

#### Field cage to CPA

- On the top and bottom of the TPC, each field cage module is connected to two CPA columns through hinges. This design allows the field cage modules to be pre-attached to the CPAs during

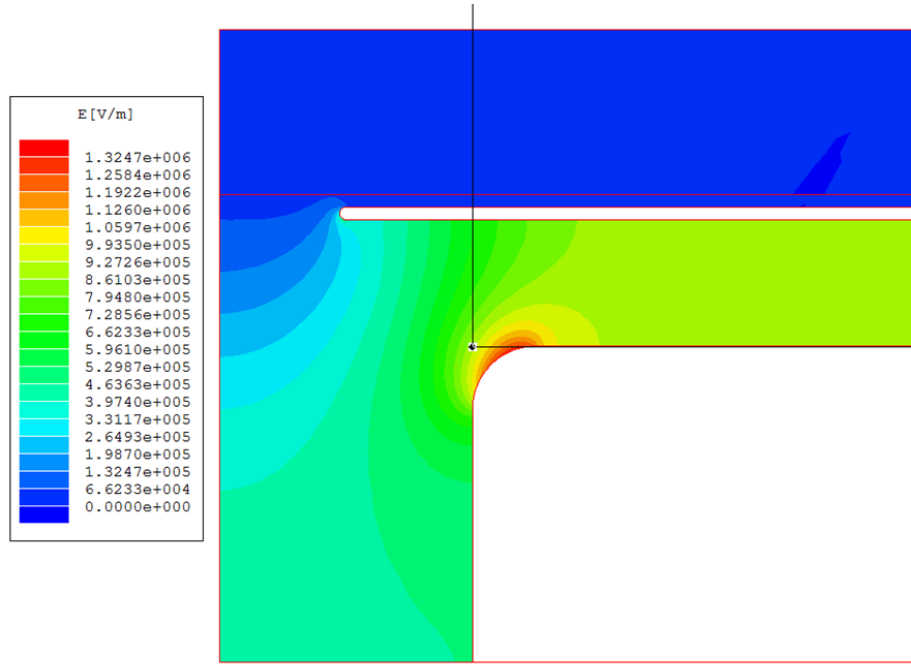


Figure 4.21: 2D FEA showing the field profile in liquid with a 200 mm overhang, gas-liquid interface 40 mm above the GP bottom. Highest field in the liquid phase is of the order of 13 kV/cm.

`fig:fea_`

- <sup>1</sup> installation, and prevent accidental damage to the APA wire plane when raising the field cage
- <sup>2</sup> module to link to the APA.
  
- <sup>3</sup> The end wall field cage modules are hung from the CPAs and APAs support rails. They do not have
- <sup>4</sup> strong mechanical coupling to the CPAs and APAs. However, there are at least 4 resistive divider
- <sup>5</sup> chains that must be connected to the CPA's HV bus.

## <sup>6</sup> Field cage to APA

- <sup>7</sup> The I-beams of the top/bottom field cage modules are designed to be latched onto the mating
- <sup>8</sup> brackets on the APAs. The design details are being developed at this moment. In addition to the
- <sup>9</sup> mechanical connection, the ground side of the divider chain must be connected to the APA's frame
- <sup>10</sup> ground as well.

## <sup>11</sup> Field cage to beam plug

- <sup>12</sup> Detail description of the connection between the beam plug and the field cage is described in the
- <sup>13</sup> beam window section.

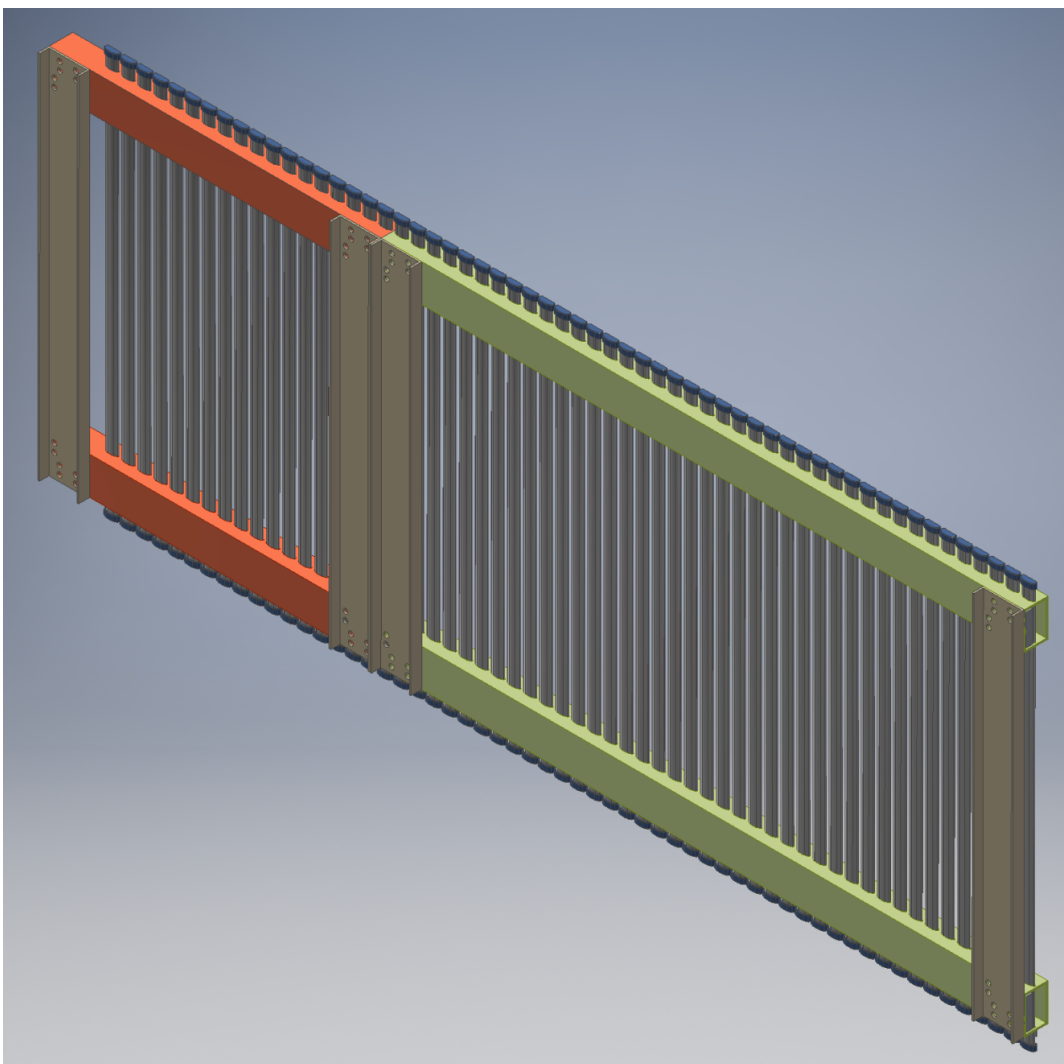


Figure 4.22: A view of a end wall field cage module

fig:fc-e

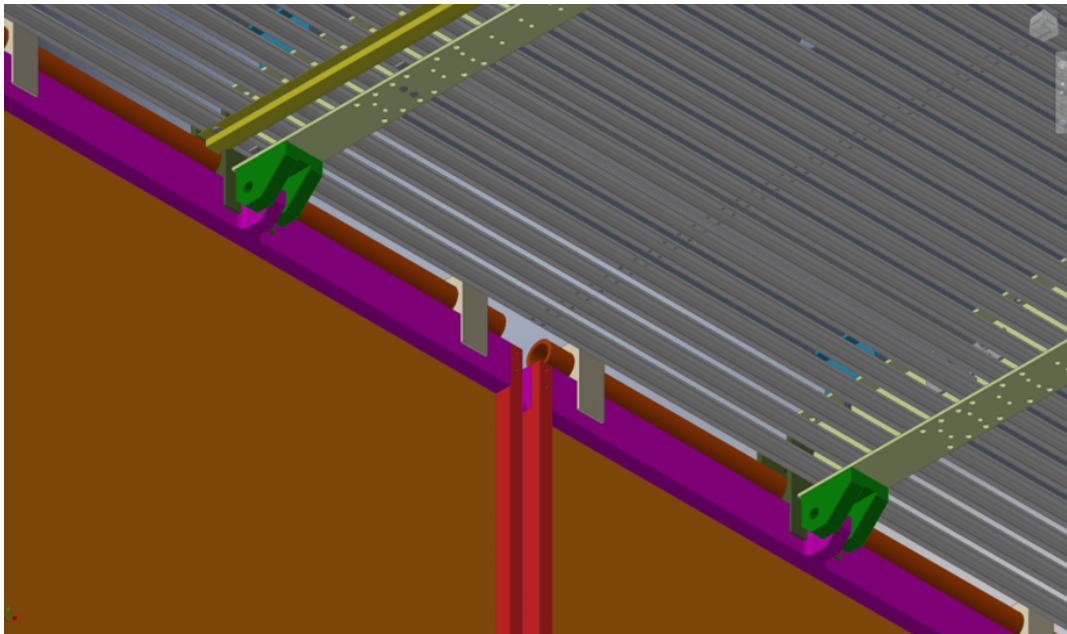


Figure 4.23: A top field cage module connected to 2 CPA modules

fig:cpa-

**1 Field cage to calibration lasers**

- 2 Four calibration laser windows need to be implemented on the downstream end wall field cage  
3 modules. The windows are planned to be at the mid-height of the TPC, therefore at the boundary  
4 of two end wall field cage modules. The opening for each laser beam is about 15cm square. The  
5 plan is to shorten 3 profiles by 7.5cm from the each edge of the field cage modules.

**6 4.3.9 Assembly Sequence and QC Procedures**

**7 4.3.10 Installation Sequence**

8 Do we have an installation section?

**9 4.4 HV components**

- 10 The TPC high voltage components include the HV power supply, cables, filter circuit, feedthrough,  
11 attachment to the resistive cathode plane arrays, the HV bus providing low-resistance connections  
12 between CPAs, connections to the field cage, and devices for monitoring steady state and transient  
13 conditions of current and voltage.

14 A schematic of the complete TPC HV circuit is shown in Fig. 4.24. [fig:TPCHVcircuit](#)

(Proto)DUNE FD TPC HV System Schematic Diagram

Version: 2016-06-01

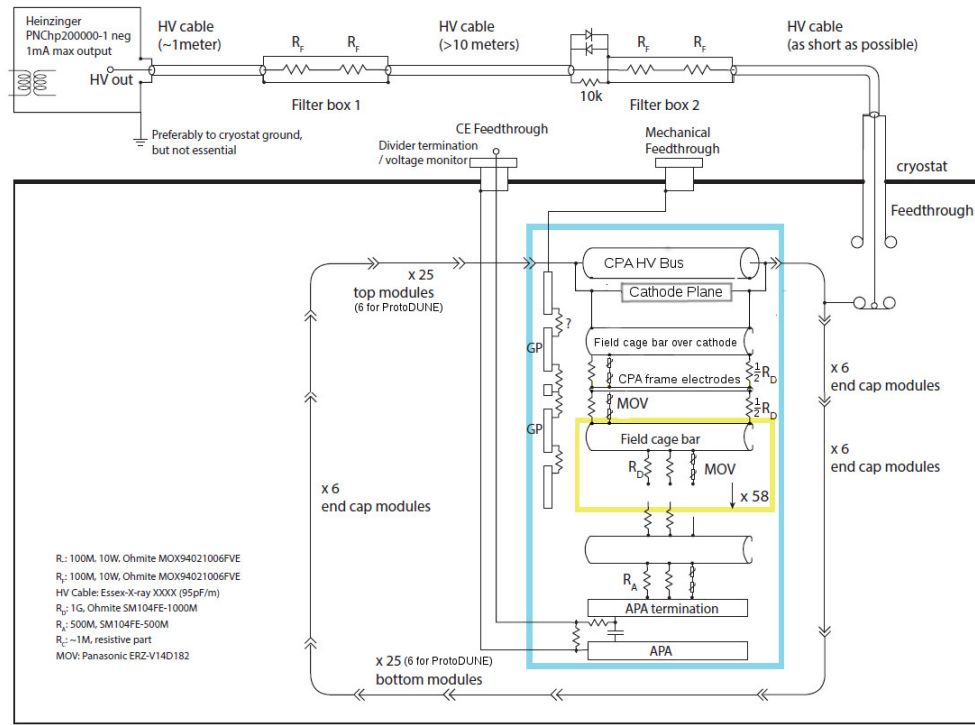


Figure 4.24: A schematic of the TPC high voltage circuit.

fig:TPCHV

- 1 The cathode plane will be biased at  $-180\text{ kV}$  to provide the required  $500\text{ V/cm}$  drift field. It will  
 2 be powered by a dedicated HV power supply through an RC filter and feedthrough. The power  
 3 supply for the cathode plane must be able to provide  $-200\text{ kV}$ . The output voltage ripple must  
 4 not introduce more than 10%

5     (?) check ripple requirement

- 6 of the equivalent thermal noise from the front-end electronics. The power supply must be pro-  
 7 grammable to shut down its output at a certain current limit. During power on and off, including  
 8 output loss (for any reason), the voltage ramp rate at the feedthrough must be controllable to pre-  
 9 vent damage to the in-vessel electronics from excess charge injection. The high-voltage feedthrough  
 10 must be able to withstand  $-250\text{ kV}$  at their center conductors in a 1 atm argon gas environment  
 11 when terminated in liquid argon.

12 **4.4.1 HV feedthrough design, Power supply, cabling**

- 13 In the present baseline option, the design of the HV feedthrough, the procurement of the Power  
 14 supply and HV cables and possibly the HV filtering scheme, will take advantage of the strong  
 15 synergies between Single phase and Double phase prototypes.

- The Heinzinger 300 kV power supply (residual ripple less than  $10^{-5}$ ) and the related HV cable foreseen for the DP detector are also well suited for the SP although used at lower voltage.
- The present DP HV feedthrough design is easily adapted to the SP without any major modification in the dimensions or in the mechanical features.
- The filtering scheme and the monitoring system is probably more demanding on the SP detector, due to the more sensitive front-end electronics, however a common development with the DP could be advantageous, allowing to get the same HV distribution chain for both the SP and the DP protoDUNE detectors.
- Common spare components are also envisaged.

The present design of the 300 kV feedthrough is based on the very successful construction technique adopted for the ICARUS HV feedthrough, which was operated at 75 kV uninterruptedly of more than three years without any failure. The feed through was also successfully operated for several days at 150 kV. A coaxial geometry is adopted: the design is based on an inner conductor (HV) and an outer conductor (ground) insulated by UHMW PE as shown in Figure 4.25. The outer conductor, made of a stainless-steel tube, surrounds the insulator extending inside the cryostat up to the LAr level. By such a geometry the electric field is always confined in regions occupied by high dielectric strength media (UHMW PE and LAr). The inner conductor is made of a thin wall stainless-steel tube, in order to minimize the heat input and to avoid the creation of argon gas bubbles around the HV lower end. A contact, welded at the upper end for the connection to the HV cable and a round-shaped elastic contact for the connection to the cathode, screwed at the lower end, completes the inner electrode. Special care has been taken in the assembling to ensure the complete filling with the PE dielectric of the space between the inner and the outer conductors and to guarantee leak tightness at ultra-high-vacuum level.

The design of the full HV chain foreseen for the DP detector, will be finalised after a series of tests on a prototype feed through and on the Heinzinger 300 kV Power Supply, which are presently ongoing at ETHZ and CERN. An alternative but similar design for the HV feedthrough is also under development at UCLA. Final decision on the design options will be based on max reachable HV, reliability /stability at design HV, residual noise performance.

Despite of the ripple spec of  $10^{-5}$  from the Heinzinger power supply, the ripple amplitude is still too large for the TPC. At 2.5m drift distance (the short drift configuration), the capacitive coupling between the cathode and the grid plane, assuming a simple parallel plate capacitor, is about 73 pF. About 20% of this coupling goes to the first induction plane (U). There are 800 U wires per APA, each wire faces the CPA with half of its length. So the capacitance between a U wire and the CPA is about 18 fF. To inject 100e noise into a U channel, it only needs about 0.9 mV of ripple on the cathode. While the power supply at 180 kV will generate ripple voltage of 1.8 V. Obviously for the SP TPC, further filtering of the HV output with attenuation factor of > 2000 is needed.

Additional filtering of the voltage ripples is done through the intrinsic HV cable capacitance and series resistors installed inside the filter box. Established techniques and practices will be implemented to eliminate micro-discharges and minimize unwanted energy transfer in case of an HV

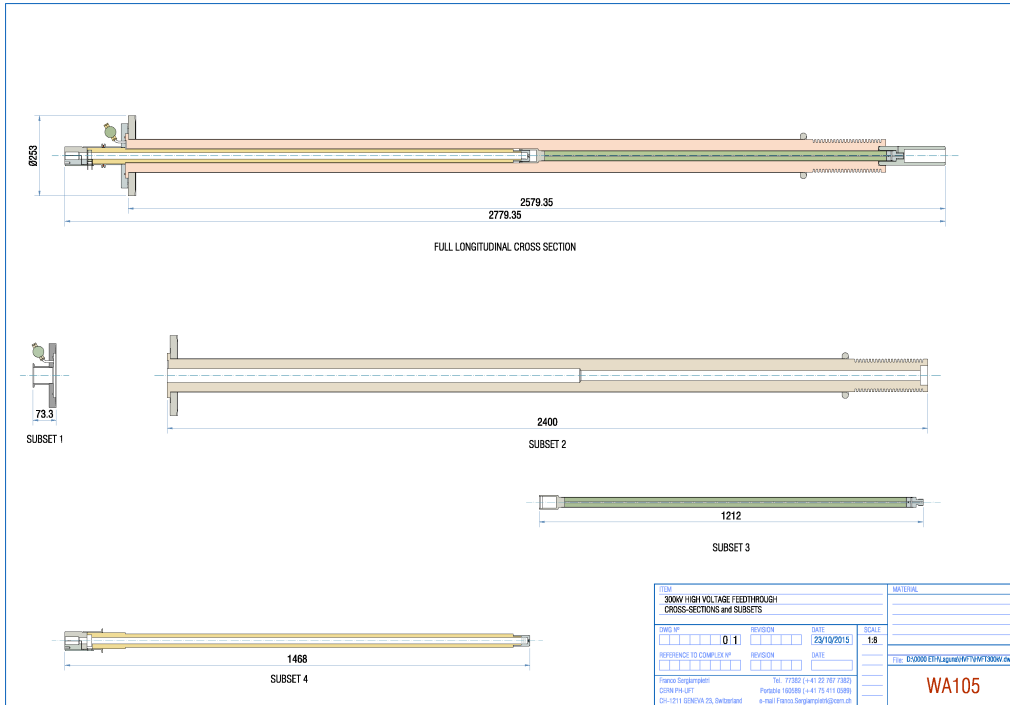


Figure 4.25: Preliminary design of the DP HV feed-through.

fig: hv-f

<sup>1</sup> breakdown.

## <sup>2</sup> 4.4.2 HV Bus

<sup>3</sup> As described in the CPA section above, the cathode planes will be resistive, with electrical connec-  
<sup>4</sup> tions at the corners, in order to control the energy delivered in any discharges. A low resistance  
<sup>5</sup> “high voltage bus” will provide the high voltage to the field cage circuit and cathodes with voltage  
<sup>6</sup> drop much less than 0.1% of the cathode voltage. Field-shaping electrodes on the faces of the CPA  
<sup>7</sup> frames will be part of the field cage circuit, described in the field cage section above. Field cage  
<sup>8</sup> electrodes on the outer edges of the CPA frames will be held at the cathode potential to provide  
<sup>9</sup> field uniformity and to protect the HV bus from discharge. The feedthrough will connect to a  
<sup>10</sup> high voltage cup on one side of a CPA at one end of the cathode plane. Interconnection of the  
<sup>11</sup> bus between CPAs will be through HV cables passed through the CPA frames. See Fig. 4.26 for  
<sup>12</sup> drawings of the high voltage bus and its interfaces.

Fig. HVBUS

## <sup>13</sup> 4.4.3 HV monitoring

<sup>14</sup> HV circuit monitoring devices include a toroid transformer to detect spikes and noise in the current  
<sup>15</sup> draw and a monitoring point at the end of the field cage resistor chain, which also provides a means  
<sup>16</sup> to control field shaping around the edge of the APA.

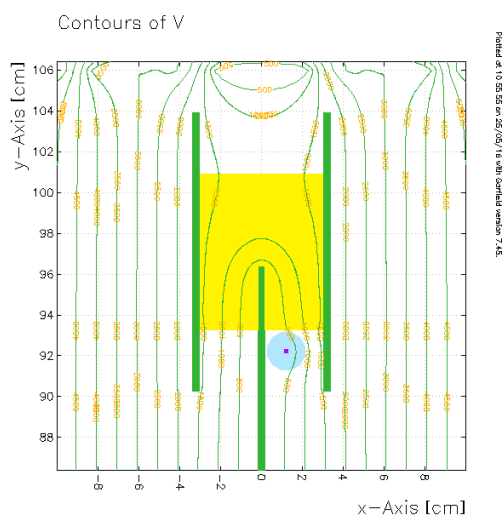
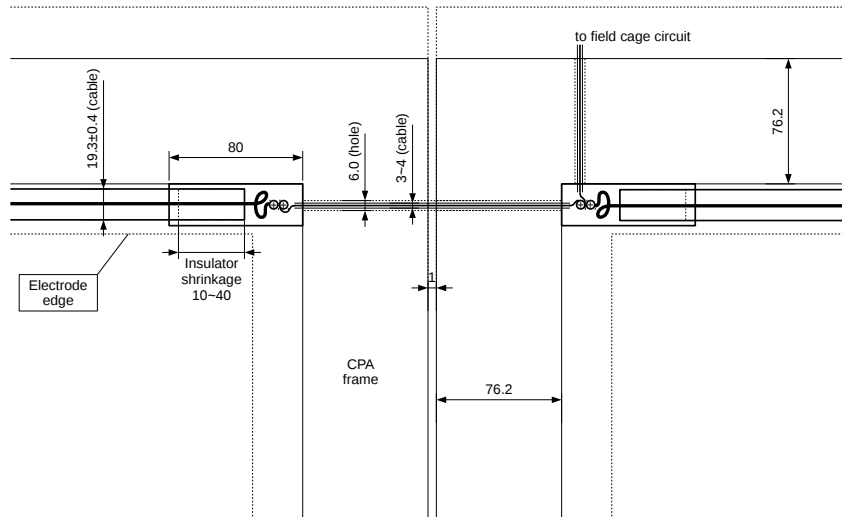
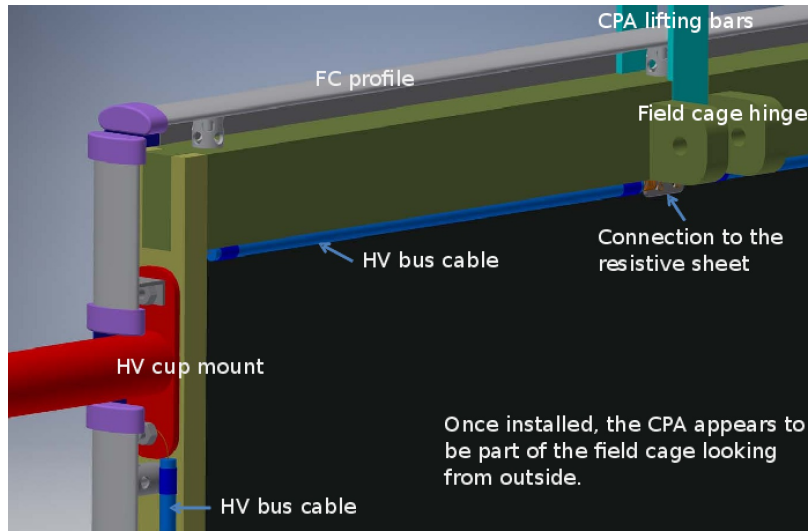


Figure 4.26: Top: A perspective view of CPA frame showing the location of the HV bus cable and attachments to the HV cup and resistive cathode, with CPA frame electrodes omitted to make HV bus visible. Middle: A sketch showing interconnection between two CPAs. Bottom: A transverse cross-section with equipotential lines around the HV bus and CPA frame.

fig:HVbu

#### <sup>1</sup> 4.4.4 HV testing

<sup>2</sup> To ensure safe and reliable operation, the HV components will be tested at a much higher voltage  
<sup>3</sup> than expected in routine operation ( $\sim 250$  kV) in LAr. Among these tests will be a planned “full  
<sup>4</sup> scale” high voltage test at Fermilab in which all components are subjected to the full voltage and  
<sup>5</sup> field in liquid argon in the 35-ton cryostat.

### <sup>6</sup> 4.5 Photon detection system

<sup>7</sup> Intro Exists? Retrieve from Norm and update as needed –Leon The scope of the photon detector  
<sup>8</sup> (PD) system for the DUNE far detector reference design includes design, procurement, fabrication,  
<sup>9</sup> testing, delivery and installation of the following components:

- <sup>10</sup> • light collection system including wavelength shifter and light guides,
- <sup>11</sup> • silicon photo-multipliers (SiPMs),
- <sup>12</sup> • readout electronics,
- <sup>13</sup> • calibration system, and
- <sup>14</sup> • related infrastructure (frames, mounting boards, etc.).

<sup>15</sup> LAr is an excellent scintillating medium and the photon detection system will exploit this property  
<sup>16</sup> in the far detector. With an average energy of 19.5 eV needed to produce a photon (at zero field), a  
<sup>17</sup> typical particle depositing 1 MeV in LAr will generate 40,000 photons with wavelength of 128 nm.  
<sup>18</sup> At higher fields this will be reduced, but at 500 V/cm the yield is still  $\sim 20,000$  photons per MeV.  
<sup>19</sup> Roughly 1/4 of the photons are promptly emitted with a lifetime of about 6 ns while the rest have  
<sup>20</sup> a lifetime of 1100–1600 ns. Prompt and delayed photons are detected in precisely the same way  
<sup>21</sup> by the photon detection system. LAr is highly transparent to the 128-nm VUV photons with a  
<sup>22</sup> Rayleigh scattering length of  $(66 \pm 3)$  cm [?] and absorption length of  $> 200$  cm; this attenuation  
<sup>23</sup> length requires a LN<sub>2</sub> content of less than 20 ppm. The relatively large light yield makes the  
<sup>24</sup> scintillation process an excellent candidate for determination of  $t_0$  for non-beam related events.  
<sup>25</sup> Detection of the scintillation light may also be helpful in background rejection and triggering on  
<sup>26</sup> non-beam events.

<sup>27</sup> The photon detection system reference design described in this section meets the required performance  
<sup>28</sup> for light collection for the DUNE far detector. This includes detection of light from proton  
<sup>29</sup> decay candidates (as well as beam neutrino events) with high efficiency to enable 3D spatial lo-  
<sup>30</sup> calization of candidate events. The TPC will provide supernova neutrino detection. The photon  
<sup>31</sup> system will provide the  $t_0$  timing of events relative to TPC timing with a resolution better than  
<sup>32</sup> 1  $\mu$ s (providing position resolution along drift direction of a couple of mm).

<sup>1</sup> **4.5.1 Packaging/mounting design**

- <sup>2</sup> – CSU – Dave Mechanical Design Mounting Mechanical Design Cabling Mechanical Design SiPM
- <sup>3</sup> mounting board QA/QC tracking for components

<sup>4</sup> **4.5.2 Light Guides and Radiators**

<sup>5</sup> **Rel Light yield of alternatives**

- <sup>6</sup> -IU Tallbo – Denver/Stuart Results of testing Fit to Determine Light Yield Fit/Ratio vs. Distance
- <sup>7</sup> to determine atten length

<sup>8</sup> **Absolute light yield**

- <sup>9</sup> Connection to Absolute – Tallbo-35T – Denver Tallbo, Celio, Jonathan, Alex –35T (This could get
- <sup>10</sup> dropped, or altered depending on status of 35T) Light yield by paddle Comparison to Simulation
- <sup>11</sup> pe's / MeV

<sup>12</sup> **4.5.3 Radiator/guide lifetime**

- <sup>13</sup> IU Tallbo and SDSM and T – IU design SDSM and T testing CSU QA/QC Design/Mfr Radiator
- <sup>14</sup> and guide Design/Mfr dipped guide – Toups Testing - cryogenic cycling rad guide dipped guide
- <sup>15</sup> QA/QC tracking and testing plan

<sup>16</sup> **4.5.4 Sensors**

<sup>17</sup> **SiPM performance and testing**

- <sup>18</sup> – NIU? Caltech? Testing plan for assembled SiPM boards QA/QC tracking for boards

<sup>19</sup> **SiPM Lifetime**

- <sup>20</sup> – IU HU Caltech NIU CSU Long term testing – IU light/dark tests (maybe not needed for proto-
- <sup>21</sup> DUNE TDR, but will for CD-3)

## <sup>1</sup> 4.5.5 Readout

### <sup>2</sup> Cables

- <sup>3</sup> ANL/CSU – performance/design Ganged SiPM studies - NIU Cable specification/testing ANL
- <sup>4</sup> QA/QC Cable labels and testing

### <sup>5</sup> Electronics SSP

- <sup>6</sup> – ANL Manual reference -> Summarize Leon? Performance results – IU/Denver and/or manual

### <sup>7</sup> DAQ interface

- <sup>8</sup> – ANL Manual -> English interface definition as in 35T – Alex or ??

## <sup>9</sup> 4.5.6 Calibration

- <sup>10</sup> – ANL – Zelimir Mechanical design – Zelimir interface with Bob Sands?

## <sup>11</sup> 4.5.7 Run Plan

- <sup>12</sup> Run/Measurement plan – Toups ? Light yield vs. field timing studies, beam off trigger

## <sup>13</sup> 4.6 TPC front-end electronics and DAQ

ch:ce

### <sup>14</sup> 4.6.1 Introduction

- <sup>15</sup> The TPC read-out electronics are referred to as the “Cold Electronics” (CE) because they will reside in LAr, mounted directly on the APA front-end (Figure 4.27). This will minimize channel capacitance and noise by keeping the length of the connection between an anode wire and its corresponding electronics input to an absolute minimum. The CE will be implemented as ASIC chips using CMOS technology, which performs well at cryogenic temperatures, and will provide amplification, shaping, digitization, buffering and multiplexing (Mux) of the signals. Because it is not possible to form a trigger for some important measurements, such as proton decay and supernova bursts, the CE will be continuously read out, with a digitized ADC sample from each

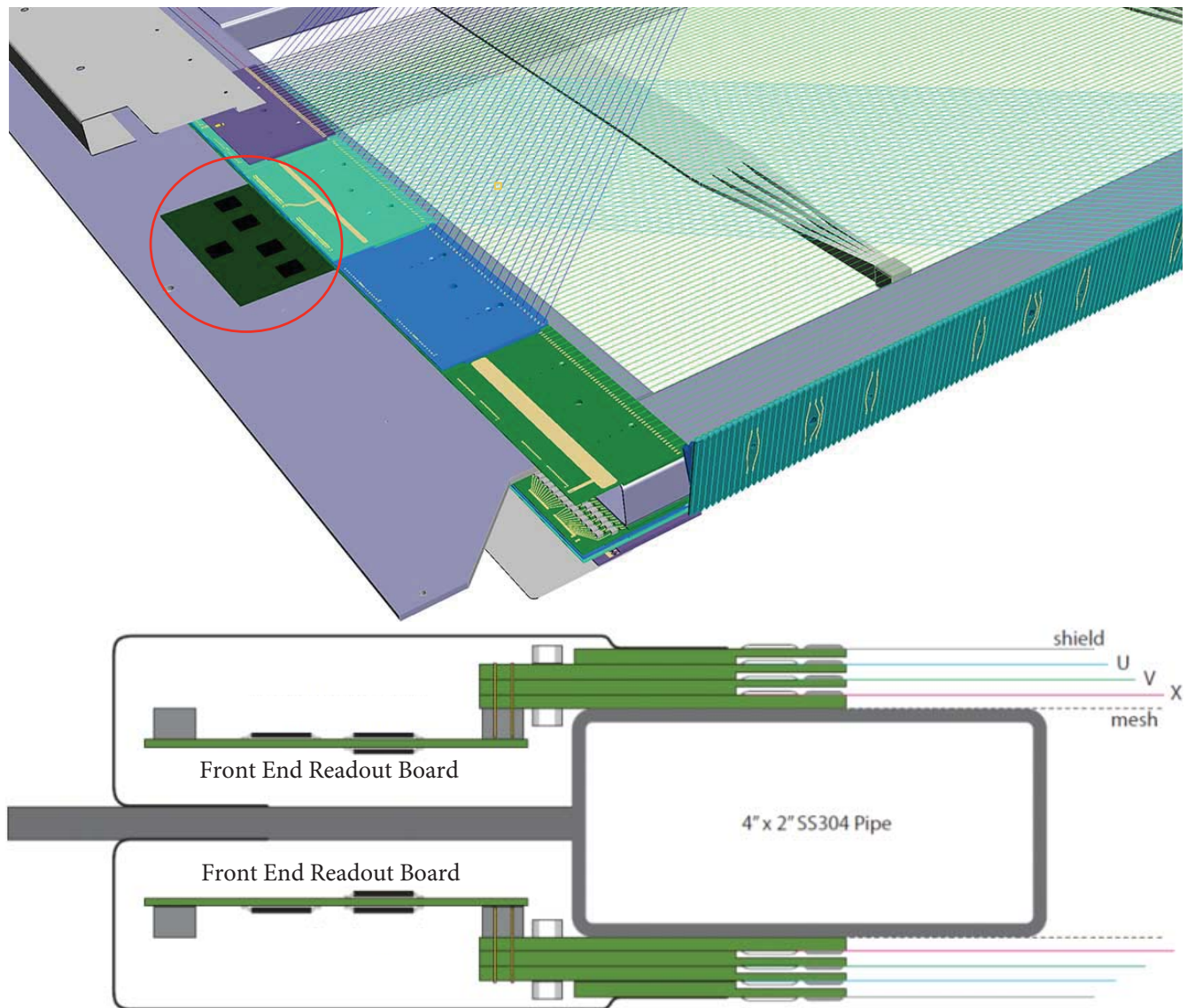


Figure 4.27: The front end electronics as mounted on an APA. **Top:** The front end electronics is shown in the red circle. **Bottom:** Cross section view.

fig:tpcc

<sup>1</sup> APA channel (wire) every 500 ns. For each of the six APAs in the protoDUNE cryostat, one cable  
<sup>2</sup> bundle will connect to the outside of the cryostat through a feedthrough, with one feedthrough  
<sup>3</sup> servicing two APAs.

<sup>4</sup> Or is this two feedthroughs for three APAs?

<sup>5</sup> Each of these cable bundles consists of wires for low-voltage power, TPC wire-bias voltages, data-  
<sup>6</sup> out, clock-in and digital-control IOs.

<sup>7</sup> The scope of the CE subsystem includes the design, procurement, fabrication, testing, delivery  
<sup>8</sup> and installation of the CE, the components of which are:

- <sup>9</sup> • Front-end cards installed on the APAs
- <sup>10</sup> • All electronics on those cards
- <sup>11</sup> • Feedthroughs (a single type, henceforth “signal feedthroughs”) which handle the signal, low-  
<sup>12</sup> voltage power, TPC bias voltage and control lines
- <sup>13</sup> • External interface crates containing the Warm Interface Boards (WIB)
- <sup>14</sup> • Power supplies, including low-voltage supplies for the CE and bias-voltage supplies for the  
<sup>15</sup> TPCs
- <sup>16</sup> • Signal, control and power cabling between the front-end cards and the feedthroughs, and  
<sup>17</sup> between the feedthroughs and external power supplies and interface crates

#### <sup>18</sup> 4.6.2 Design Considerations

<sup>19</sup> This contains an old reference to lar-fd-req, which is no longer in the bibliography.

<sup>20</sup> The requirements for the CE can be found in the requirements documentation <sup>lar-fd-req</sup> [?]. The most  
<sup>21</sup> significant ones are listed here. The CE shall:

- <sup>22</sup> • Provide the means to read out the TPCs and transmit their data in a useful format to the  
<sup>23</sup> Data Acquisition System (DAQ).
- <sup>24</sup> • Operate for the life of the facility without significant loss of function.
- <sup>25</sup> • Record the channel waveforms continuously without dead time.
- <sup>26</sup> • Use only materials that are compatible with high-purity liquid argon.
- <sup>27</sup> • Provide sufficient precision and range in the digitization to:

- 1     – Discriminate electrons from photon conversions;
- 2     – Optimize for high- and low-energy tracks from accelerator-neutrino interactions;
- 3     – Distinguish a Minimum Ionizing Particle (MIP) from noise with a signal-to-noise ratio  
4         $> 9:1$ ;
- 5     – Measure the ionization up to 15 times that of a MIP particle, so that stopping kaons  
6        from proton decay can be identified.
- 7     ● Ensure that all power supplies have:
  - 8        – Local monitoring and control
  - 9        – Remote monitoring and control through DAQ
  - 10      – Over-current and over-voltage protection circuits
- 11    ● Ensure that the low-voltage (signal) feedthroughs are able to withstand twice their nominal  
12        operating voltages with a maximum specified leakage current in 1-atm argon gas.
- 13    The responsibility and authority for the design, installation and use of the detector quiet-power  
14        distribution and detector-grounding system is held by the subproject electrical engineer. This  
15        engineer has oversight responsibility for all electrical and electronics design and installation tasks,  
16        including all attachments to the detector that create an electrical connection.

### :fe\_arch<sup>17</sup> 4.6.3 Architecture

- 18 The CE architecture is manifested in the Front End Mother Board assembly (FEMB), which  
19 consists of an analog mother board with a digital ASIC mezzanine (Figure 4.28). Each APA is  
20 instrumented with 20 FEMBs, for a total of 2,560 channels per APA.
- 21 The analog mother board is instrumented as a 128-channel board which uses eight 16-channel FE  
22 ASICs, eight 16-channel ADC ASICs, low-voltage regulators, and input-signal protection. The 16-  
23 channel FE ASIC provides amplification and pulse shaping. The 16-channel ADC ASIC comprises  
24 a 12-bit digitizer, local buffering, and an 8:1 Mux stage with two pairs of serial readout lines in  
25 parallel. This has already been prototyped and tested, using a commercial FPGA to perform the  
26 role of the digital ASIC (Figure 4.29).
- 27 The Cold Digital Data (COLDATA) ASIC and its voltage regulators are mounted on the digital  
28 ASIC mezzanine. The COLDATA ASIC provides:
- 29 ● The communication protocol with the data acquisition system (DAQ)
  - 30 ● The control required to program and read out the FE and ADC ASICs

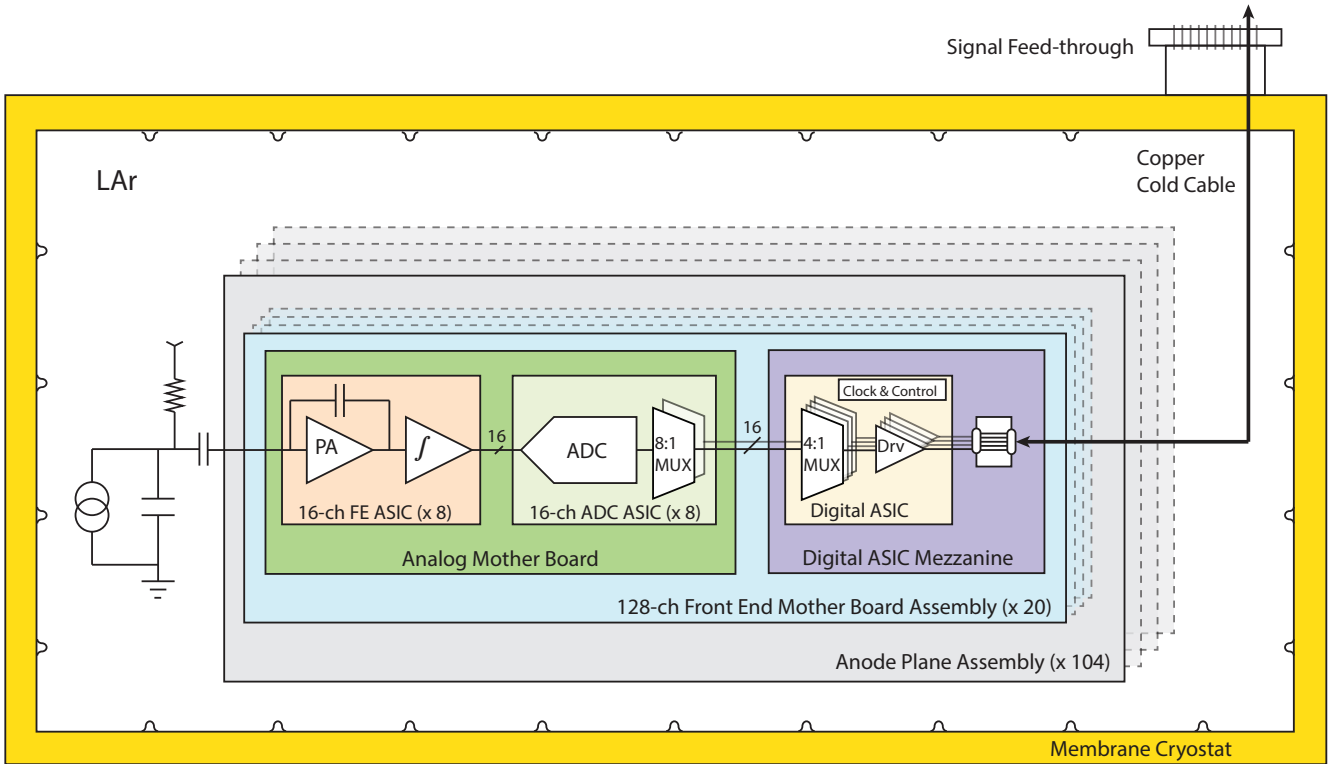


Figure 4.28: The CE Architecture. The basic unit is the 128-channel FEMB

fig:tpc

- <sup>1</sup> • The system clock interface
- <sup>2</sup> • Four 4:1 Muxs that combine 16 serial lines from the ADCs of eight channels each into four serial lines of 32 channels each
- <sup>3</sup>
- <sup>4</sup> • Four 1-Gbps serial drivers that form the data link to DAQ

<sup>5</sup> Have we decided on the 4:1 Mux? Is the 8:1 still an option?

<sup>6</sup> If it is demonstrated that the COLDATA ASIC can achieve 2 Gbps, then the 4:1 Mux will be increased to 8:1 and only two serial drivers will be implemented, with a subsequent reduction in cabling, etc. In either case, the data rates will not be high enough to require the use of optical fibers in the cold, nor is there a need for zero suppression or data compression. This greatly reduces the complexity of the COLDATA ASIC, with a corresponding decrease in overall risk, including risk of failure-to-implement (within a fixed schedule and budget) and risk of device failure during long-term operation. Data will be driven to DAQ through copper cable utilizing low-voltage differential signaling (LVDS). Output data cables will go to a signal feedthrough and from there to an external crate mounted nearby. Under DAQ scope, further data processing is done in the external crate and data is transmitted via optical fiber to front-end computers.

<sup>16</sup> The analog FE ASIC has 16 channels.

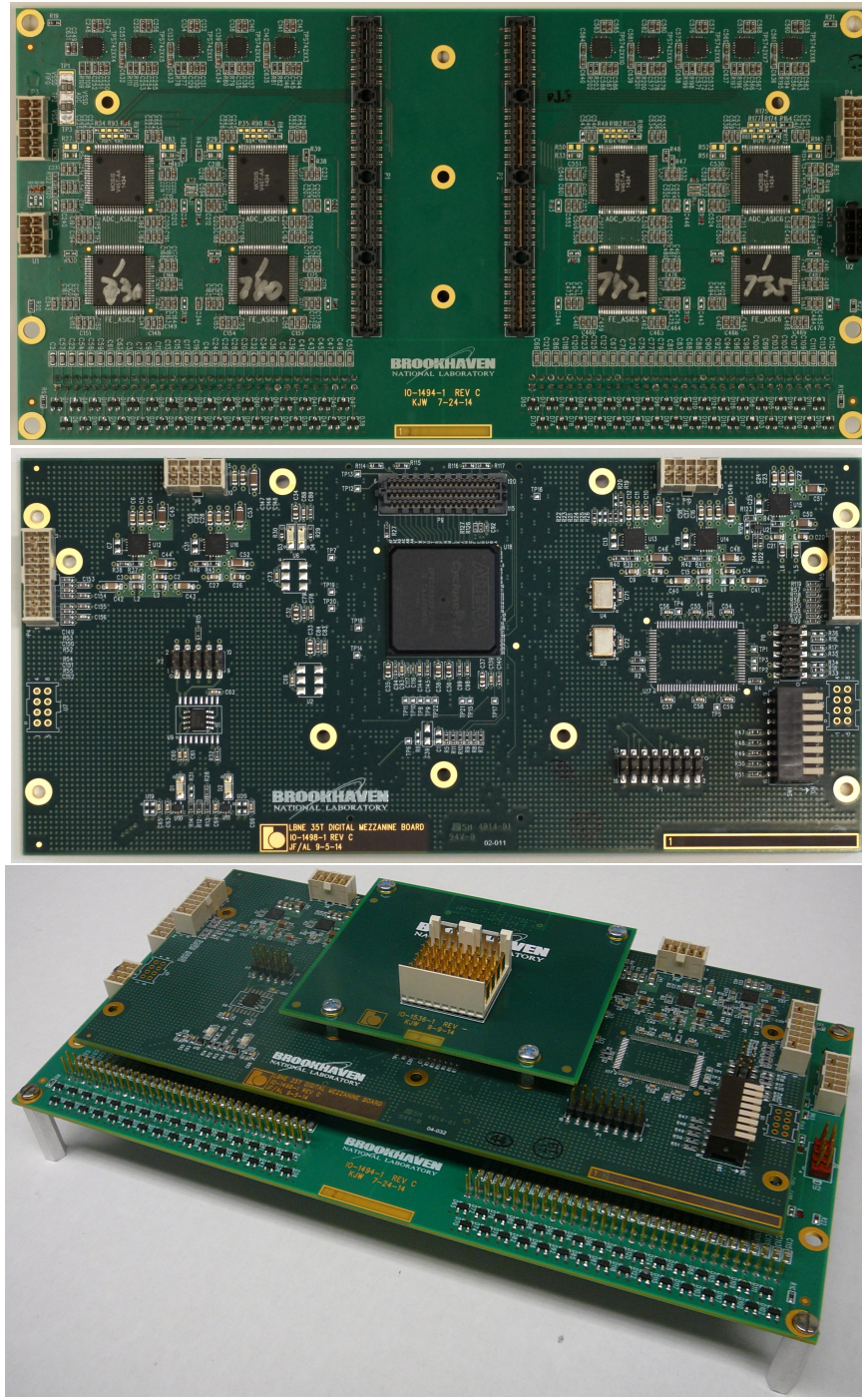


Figure 4.29: The Front End Mother Board (FEMB), as used in the early set of tests. **Top:** The analog mother board, showing four ADC ASICS and four FE ASICS surface mounted. The other side of the board has another four ADC and FE ASICS. Except for anticipated small modifications, this board is essentially the final version. **Middle:** The FPGA mezzanine, used in place of the digital ASIC mezzanine for the early set of tests. **Bottom:** The complete FEMB assembly as used in the early set of tests. The uppermost mezzanine board is the cable connection.

fig:tpc

1 Are these gains and time constants still correct?

2 Each channel includes a charge amplifier with a gain selectable from one of 4.7, 7.8, 14 and  
3 25 mV/fC (full scale charge of 55, 100, 180 and 300 fC), a high-order anti-aliasing filter with  
4 adjustable time constant (peaking time 0.5, 1, 2, and 3  $\mu$ s), an option to enable AC coupling,  
5 and a baseline adjustment for operation with either the collecting or the non-collecting wires.  
6 The 16-channel FE ASICs then transmit the shaped pulse to a 16-channel 12-bit 2 MS/s ADC  
7 ASIC. Shared among the 16 channels in the FE ASIC are the bias circuits, programming registers,  
8 a temperature monitor, an analog buffer for signal monitoring, and the digital interface. The  
9 estimated power dissipation of FE ASIC is about 6 mW per channel at 1.8 V supply. Shared  
10 among the 16 channels in the ADC ASIC are the bias circuits, programming registers, an 8:1 Mux,  
11 and the digital interface. The estimated power dissipation of FE ASIC is below 5 mW per channel  
12 at 1.8 V supply.

13 **4.6.4 CMOS Circuit Design**

14 Compared to the situation at 300 K, charge-carrier mobility in silicon increases at 89 K while  
15 thermal fluctuations decrease with  $kT/e$ . These effects result in a higher gain (transconductance/current ratio =  $g_m/i$ ), higher speed, and lower noise at 89 K than at 300 K. For a given  
16 drain-current density, the same degree of impact ionization (measured by the transistor substrate  
17 current) occurs at a somewhat lower drain-source voltage at 89 K than at 300 K. The charge  
18 trapped in the gate oxide and its interface with the channel causes degradation in the transcon-  
19 ductance (gain) of the transistor and a threshold shift. The former is of major consequence as it  
20 limits the effective lifetime of the device (defined in industry and the literature as 10% degra-  
21 dation in transconductance). Thus, an MOS transistor has equal lifetime due to impact ionization  
22 at 89 K and at 300 K, but at different drain-source voltages  $V_{DS}$ , as illustrated in Figure 4.30.  
23 This property can be exploited to stress the transistor with both increased current and increased  
24 voltage while monitoring the substrate current and the change in  $g_m$  due to impact ionization.  
25 Under these conditions, the lifetime can be reduced arbitrarily by many orders of magnitude, and  
26 the limiting operating conditions for a lifetime in excess of  $\sim 20$  years can be determined. With  
27 this foundation, more conservative design rules (lower current densities and voltages) can be de-  
28 rived and applied in the ASIC design. With this accelerated testing the expected lifetimes can  
29 be verified for the several widely available CMOS technologies under consideration (TSMC, IBM,  
30 AMS). It should be noted that this is a standard test method used by the semiconductor industry;  
31 it is used to qualify electronics for deep space NASA missions as well as commercial PCs.

32 To successfully design CMOS circuits that will operate at cryogenic temperatures, two critical issues  
33 must be addressed and resolved. The first issue is the need for realistic models at the operating  
34 temperature of all active and passive components in order to reliably predict operating points,  
35 signal response and noise during the design process. The second issue is that the design must ensure  
36 a long operational lifetime, since once the TPC is filled with LAr the far detector must operate  
37 for about 15 years without any access to the electronics for repair or replacement. Concerning the  
38 availability of realistic models, our preliminary results from the cryogenic characterization (down  
39 to 40 K) of a complete

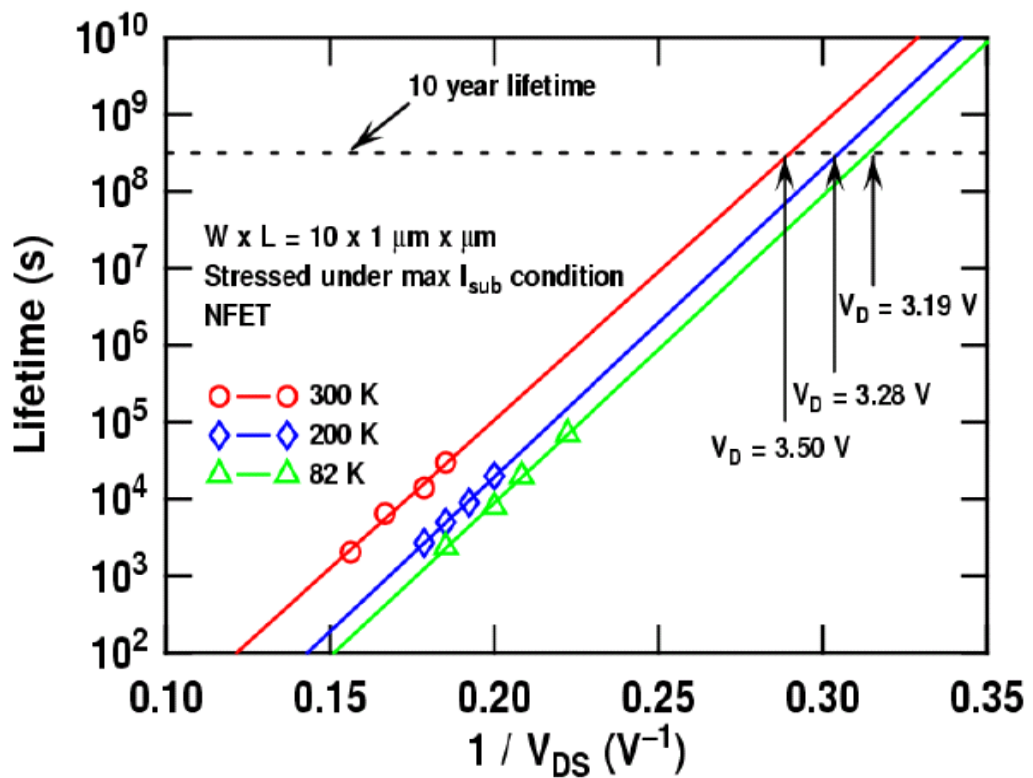


Figure 4.30: Lifetime at different temperatures vs  $V_{DS}$

fig:tpcc

1 This contains an old reference to CMOS-Compton, which is no longer in the bibliography.

2 mixed-signal ASIC [?] in a commercial CMOS  $0.25\text{ }\mu\text{m}$  technology, originally developed for room-  
3 temperature applications, indicates that the models are useful to first order. To refine these models,  
4 several single-transistor test structures were fabricated on the first prototype of the  $0.18\text{ }\mu\text{m}$  device.  
5 Measurements of the properties of these structures at cryogenic temperatures have been used to  
6 refine the device models at 89 K.

7 The lifetime of CMOS circuits is limited by several mechanisms which degrade the performance  
8 over time, eventually causing the circuit to fail to perform as specified.

9 This contains old references to CMOS-lifetime and PMOS-model, which are no longer in the  
bibliography.

10 The rates of most degradation mechanisms in CMOS, such as electro-migration (EM), stress mi-  
11 gration (SM), time-dependent dielectric breakdown (TDDB), thermal cycling (TC), and negative  
12 bias-temperature instability (NBTI), all scale with temperature such that cryogenic operation is  
13 favored [?][?]. The only mechanism that could affect the lifetime at cryogenic temperature is the  
14 degradation due to impact ionization, which causes charge trapping in the MOSFET gate oxide  
15 at large drain-current densities (the “Hot Carrier” effect).

16 This contains an old reference to CMOS-reliability, which is no longer in the bibliography.

17 Results from a CMOS reliability study [?] provide general design guidelines (for device geometry,  
18 bias and current density) that should guarantee a lifetime well in excess of 15 years for continuous  
19 cryogenic operation. These design guidelines also provide information for designing test conditions  
20 to observe the deterioration mechanism and to extrapolate from accelerated deterioration rates,  
21 measured under stressed conditions within practical times, to the ultimate lifetime under normal  
22 operation.

23 A monitor of the impact ionization is the bulk current, which reaches a maximum at  $V_{DS} = V_{DD}$   
24 and at  $V_{GS} = 0.5V_{DD}$ . When operating constantly in this condition at room temperature, a  
25 properly designed device will typically have a lifetime (defined as a 10% degradation in  $g_m$ ) of  
26 about 10 years.

27 This contains an old reference to CMOS-reliability (the 2nd one), which is no longer in the  
bibliography.

28 The bulk current (i.e., the impact ionization) increases by roughly a factor of four from 300 K to  
29 77 K [?] and a circuit designed for operation at room temperature would have a proportionately  
30 shorter useful life at cryogenic temperature. As stated above, in order to guarantee the required  
31 lifetime at cryogenic temperatures, design guidelines must be modified for both analog and digital  
32 circuits. For analog circuits, this is done by operating the devices at moderate-to-low drain current  
33 densities, where impact ionization becomes negligible. For digital circuits, operating the devices

1 with reduced  $V_{DD}$  (about 20%) and using non-minimum channel length L is easily accommodated  
2 since at cryogenic temperature the speed of the digital circuit increases, compensating for the  
3 increased L. These guidelines will be verified with accelerated aging tests, at increasing values of  
4  $V_{DD}$ , on dedicated structures. Such tests also will be conducted on prototype samples throughout  
5 the development process to verify the long-term reliability of the final ASICs.

## 6 Cold Analog ASICs

7 The development of the readout ASIC began by designing and fabricating in a commercial CMOS  
8 process ( $0.18 \mu\text{m}$  and 1.8V) a 16-channel ASIC implementing the complete analog front-end section.  
9 The FE ASIC layout is shown in Figure 4.31. This process is expected to be available for at least  
10 another 10 years. The charge amplifier input MOSFET is a p-channel biased at 2 mA with a L/W  
11 (channel length/width) ratio of  $0.27 \mu\text{m} / 10 \mu\text{m}$ , followed by dual cascade stages. The charge  
12 amplification and shaping filter have digitally programmable gain and peaking time (as listed in  
13 Section 4.6.3).

14 This contains an old reference to microboone-[url](#), which is no longer in the bibliography.

15 Each channel also implements a high-performance output driver, which is used to drive a long  
16 cable when it is used in a standalone mode, as it is in MicroBooNE.[\[?\]](#) The buffer can be disabled  
17 when it is interfaced to an ADC ASIC to reduce the power consumption. The ASIC integrates a  
18 band-gap reference (BGR) to generate all the internal bias voltages and currents. This guarantees  
19 a high stability of the operating point over a wide range of temperatures, including cryogenic. The  
20 ASIC is packaged in a commercial, fully encapsulated plastic QFP 80 package.

21 Is "five cycles" correct? Or is it six?

22 This ASIC has now been through five design/fabrication/testing revision cycles. Prototypes from  
23 each cycle have been evaluated and characterized at room (300 K) and liquid nitrogen (77 K)  
24 temperatures. During these tests the circuits have been cycled multiple times between the two  
25 temperatures and operated without any change in performance. Figure 4.32 shows the measured  
26 pulse response, along with details on the adjustability of the gain, peaking time and baseline.  
27 These results are in close agreement with the simulations and indicate that both the analog and  
28 the digital circuits and interface operate as expected in a cryogenic environment. Also reported  
29 in Figure 4.32 are the outputs of the BGR and temperature sensor, which are in close agreement  
30 with the simulations as well.

31 Are these noise values the latest? Should we include anything from the 35t test?

32 Figure 4.33 shows the measured ENC versus filter-time constant (peaking time). At  $1 \mu\text{s}$  about  
33  $650 \text{ e}^-$  was measured, to be compared to the simulated value of  $500 \text{ e}^-$ . The difference is mainly  
34 due to the thermal noise from a  $\sim 11\text{-ohm}$  parasitic resistance of the input line (shown in the detail  
35 of Figure 4.33), which contributes about 350 electrons at 77 K. The width of the line has been

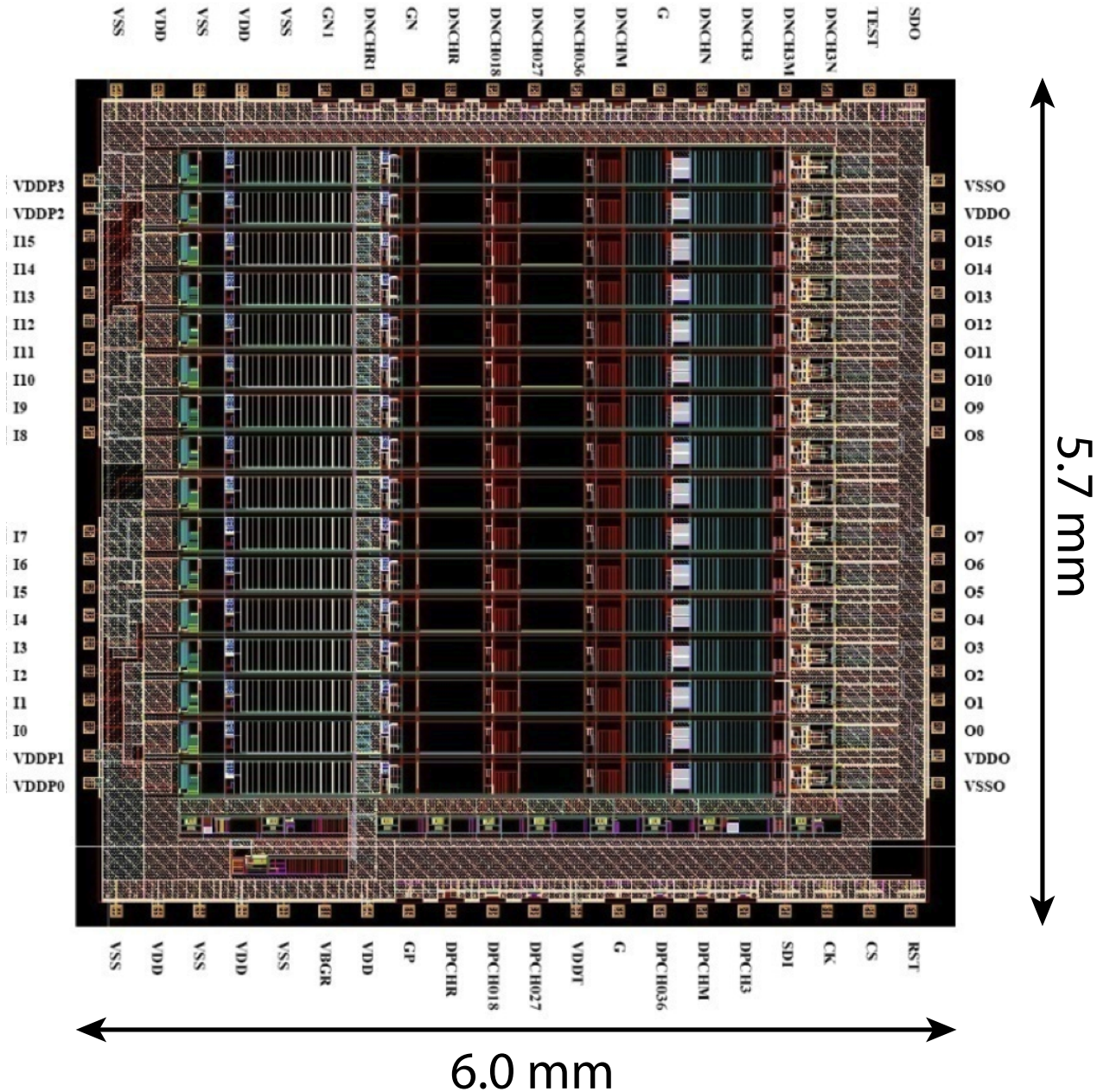


Figure 4.31: The layout of the 16-channel analog FE ASIC

fig:tpcc

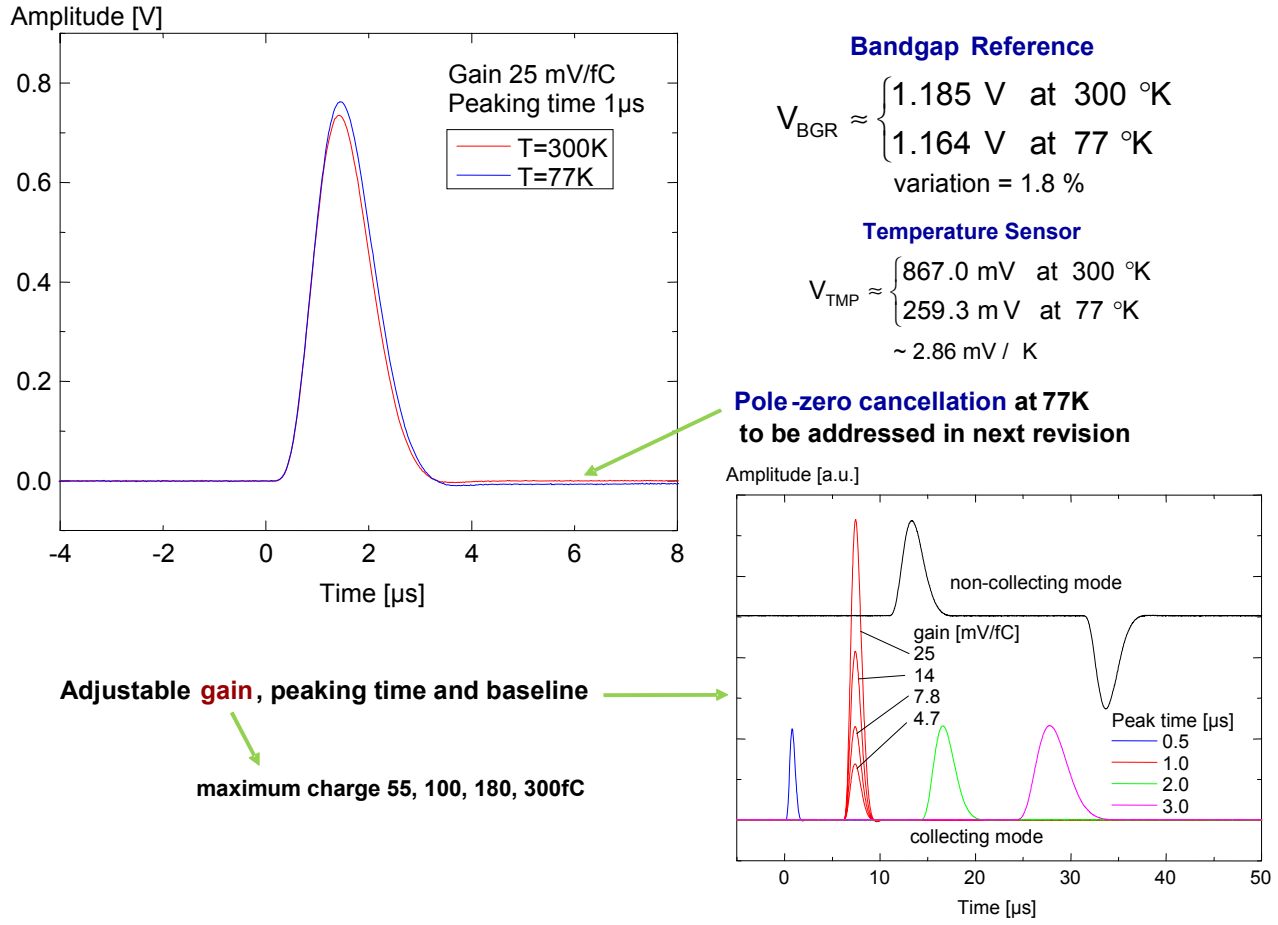


Figure 4.32: Measured pulse response with details on gain, peaking time and baseline adjustments

fig:tpcc

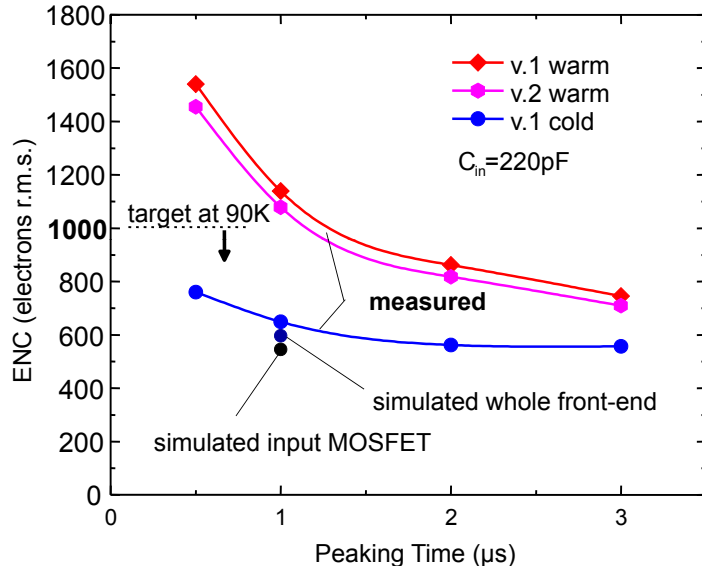


Figure 4.33: Measured ENC vs filter time constant from the first two versions of the analog front end ASICs

fig:tpcc

1 increased in a revision in order to make this contribution negligible. A second contribution, on  
 2 the order of  $100 e^-$ , was due to the dielectric loss from the capacitor ( $220 \text{ pF}$ ) used to simulate  
 3 the wire (the cases of MICA and NPO ceramic were compared). This contribution would not be  
 4 present with the input connected to a sense wire in the TPC.

5 Each channel is equipped with an injection capacitor which can be used for test and calibration  
 6 and can be enabled or disabled through a dedicated register. The injection capacitance has been  
 7 measured using a calibrated external capacitor. The measurements show that the calibration  
 8 capacitance is extremely stable, changing from  $184 \text{ fF}$  at room temperature to  $183 \text{ fF}$  at  $77 \text{ K}$ .  
 9 This result and the measured stability of the peaking time demonstrate the high stability of  
 10 the passive components with the temperature. Channel-to-channel and chip-to-chip variation in  
 11 the calibration capacitor are typically less than 1%. Measurements are being carried out on the  
 12 individual test structures fabricated on this ASIC to confirm device models and design guidelines.

13 The development of the ADC ASIC is also using the CMOS process ( $0.18 \mu\text{m}$  and  $1.8\text{V}$ ). A  
 14 16-channel ASIC has been prototyped and tested. The layout of the ADC ASIC is shown in  
 15 Figure 4.34. The ADC ASIC has 12-bit resolution,  $2 \text{ MS/s}$  sampling rate, built in FIFO, two 8:1  
 16 multiplexing and two pairs of serialized output.

17 I believe the number of transistors has increased. What is the latest count?

18 The ADC is a complex design, which has more than 300,000 transistors. All of the transistor  
 19 design has been done following the rules for long cryo-lifetime.

20 The ADC ASIC has an input buffer with offset compensation to match the output of the FE ASIC.  
 21 The input buffer first samples the input signal (with a range of  $0.2 \text{ V}$  to  $1.6 \text{ V}$ ), then provides a

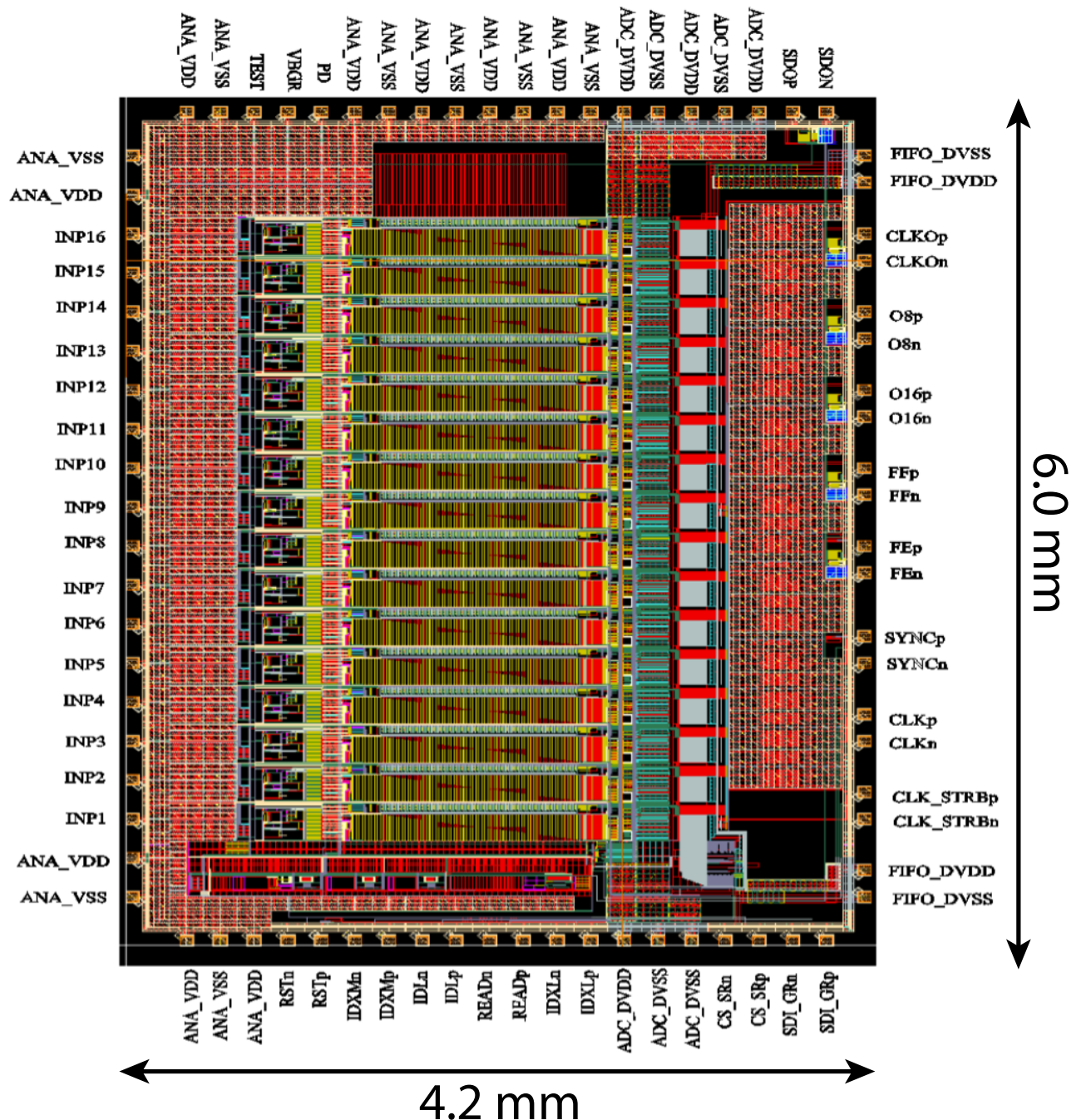


Figure 4.34: The layout of the 16-channel ADC ASIC

fig:tpcc

1 current output after compensating for offset voltage error. This current output is then supplied to  
2 the ADC which converts the input to digital in two phases. The MSB (Most Significant Bit) 6 bits  
3 are first determined followed by the LSB (Least Significant Bit) 6 bits. After the conversion the  
4 thermometer code is converted to binary and latched. The output of ADC 16 can be monitored  
5 externally. The data from the 16 ADCs is transferred in parallel to the FIFO block. The built-in  
6 FIFO is 32 bits wide and 192 bits long, it has the full and empty indicator flags to make it easy to  
7 interface to FPGA or digital ASIC. The ADC along with the input buffers are biased internally  
8 using a bias generator and a bandgap voltage reference. The bandgap voltage (VBGR) can be  
9 monitored and/or controlled externally. It can be put in the low-power sleep mode, and woken up  
10 in less than 1  $\mu$ s.

11 Is "five cycles" correct? Or is it six?

12 The ADC ASIC has now been through five design/fabrication/testing revision cycles. Prototypes  
13 from each cycle have been evaluated and characterized at room (300 K) and liquid nitrogen (77 K)  
14 temperatures. During these tests the circuits have been cycled multiple times. The effective  
15 resolution with reference to the input referred noise is  $\sim$ 11.6 bits at both 300 K and 77 K. The  
16 differential non-linearity (DNL) is less than 4 LSBs for 99% of ADC bins at both 300 K and 77 K.  
17 The performance of the ADC meets the far detector requirements.

18 This contains an old reference to microboone-[url](#) (the 2nd one), which is no longer in the bibliography.

19 An analog front-end ASIC was adopted by the MicroBooNE experiment in 2010.[\[?\]](#) The fabrication  
20 and installation was successfully completed in early 2014, and now a total of 8,256 channels (516  
21 FE ASICs) instrument the MicroBooNE TPC. A total of 2,048 channels (on 128 FE ASICs and  
22 128 ADC ASICs) are used to instrument the 35-ton LArTPC. The FEMBs have been produced  
23 and tested at 300 K and are currently being tested at 77 K before final installation.

## 24 Cold Digital Data ASICs

digital

25 The development of the Cold Digital Data (COLDATA) ASIC will follow the same general guidelines  
26 developed for the cold analog ASICs, but will differ from the analog design in a couple of  
27 aspects. It is anticipated that the digital ASIC will make use of a 65-nm CMOS technology and  
28 require a digital library with accurate cold timing models allowing for high-level language design  
29 and automated place-and-route for design blocks using extensive digital logic.

30 A block diagram of the COLDATA ASIC is presented in Figure 4.35. The major components of  
31 the COLDATA ASIC include a downlink which is required to receive the system clock and the  
32 control/download information transmitted from the DAQ. The download data must be transmitted  
33 to the FE and ADC ASICs on the FEMB. The system clock will provide a frequency reference  
34 to a crystal-based Phase Lock Loop (PLL) which will generate a low-jitter stable clock to the  
35 high-speed serializer.

[fig:tpcce\\_COLDATA](#)

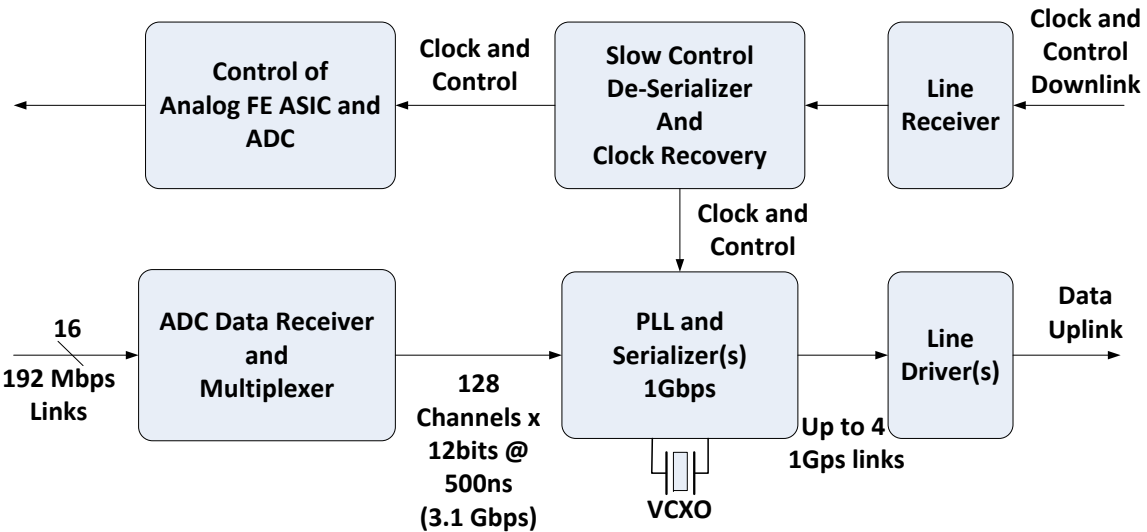


Figure 4.35: Functional Block Diagram of the Cold Digital Data (COLDATA) ASIC

fig:tpcc

- 1 A single COLDATA ASIC on each FEMB will also be receiving the data from each of the eight
- 2 ADCs on a board. Each ADC will transmit two streams of data at 192 Mbps for a total data input
- 3 of 3.072 Gbps. All data will be transmitted off-board to DAQ. Twelve bits of ADC data per APA
- 4 channel every 500 ns yields a single-channel bit rate of 0.024 Gbps. With 8B10B encoding, for
- 5 example, this increases to 0.03 Gbps, plus some overhead for frame data to indicate event blocks.
- 6 Assuming a conservative serial-link transmission speed of 1 Gbps, a single link can therefore handle
- 7 32 channels. Thus, it is planned to drive four 1 Gbps links from each COLDATA ASIC. A line
- 8 driver will be designed that is capable of driving a copper link for the approximate 20 m required
- 9 to exit the LAr environment. If a speed of 2 Gbps can be achieved, which is possible but not yet
- 10 demonstrated, the number of serial links for data transmission will be cut in half.

## 11 4.6.5 Signal Feedthroughs, Cabling, and Power

- 12 A single type of feedthrough, henceforth “signal feedthrough”, will handle the signals, supply volt-
- 13 ages and control lines. The TPC data rate per APA, using the full event-buffer scheme described
- 14 earlier, is sufficiently low that it is within the capability of a single LVDS channel on copper, with
- 15 an overall 32:1 Mux and 80 LVDS channels per APA. There is, therefore, no need for high-speed
- 16 optical links inside the cryostat, so all cables inside the cryostat will be copper. This has the
- 17 significant benefit of avoiding a major R&D effort which would be required to demonstrate both
- 18 functionality and adequate lifetime of optical converters in LAr. In addition to the high-speed
- 19 data-output channels, LVDS connections will be made to each APA to distribute a clock signal
- 20 and control information. These data can be transmitted at a lower bit rate. Optical fiber will be
- 21 employed externally to the cryostat, under DAQ scope.

## <sup>1</sup> Signal Feedthroughs

<sup>2</sup> The design for the signal feedthroughs is complete except for some small adjustments, which  
<sup>3</sup> are expected to be complete by June 2016. We have been working in tandem with the SBND  
<sup>4</sup> group because of our very similar feedthrough needs. Some views from the current design of a  
<sup>5</sup> signal feedthrough is shown in Fig. 4.36. Based on a standard 14-in conflat flange, each of these  
<sup>6</sup> feedthroughs would serve the bias/power/digital IO needs of two APAs.

<sup>7</sup> All cables inside the cryostat will be attached to their corresponding feedthroughs distributed  
<sup>8</sup> throughout the cryostat roof. The other ends of the cables will be connected to the matching  
<sup>9</sup> connectors on the APAs in the cryostat. The cables for the lower APAs must be carefully threaded  
<sup>10</sup> through the hollow frames of the APA stacks; these cables will be strain-relieved on the mounting  
<sup>11</sup> rails above the APAs.

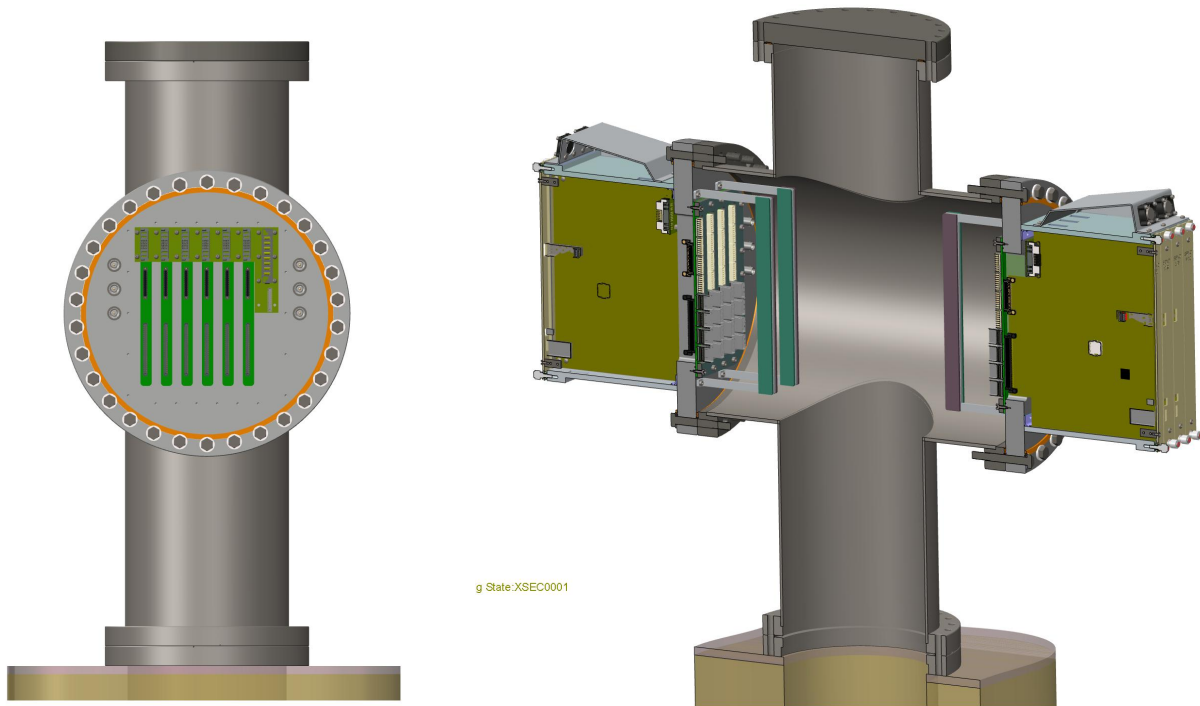


Figure 4.36: The signal/power feedthrough

<sup>12</sup> For the protoDUNE detector APA there will be 20 electronics boards. While the electrical connec-  
<sup>13</sup> tion requirements are straightforward, the reliable gas tightness of the flange with an embedded  
<sup>14</sup> circuit board has been fully verified. Also the planned method of reducing contamination from  
<sup>15</sup> the cable plant in the ullage (the warmer gas phase at the top of the cryostat) continues to be  
<sup>16</sup> carefully studied.

This contains an old section reference to "sec:mts", formerly defined in lbne-fd-closeout/chapter-r-and-d.tex:

<sup>1</sup> Measurements in the Materials Test Stand at Fermilab (described in Section ??) have shown that  
<sup>2</sup> impurities (principally O<sub>2</sub> and H<sub>2</sub>O) embedded in objects submerged in the liquid argon do not  
<sup>3</sup> result in a decrease in electron-drift lifetime, whereas impurities in objects located in the ullage  
<sup>4</sup> do. This indicates the importance of minimizing the amount of material in the ullage.

[sec:mts]

## <sup>5</sup> Cabling for the Cold Electronics

<sup>6</sup> Five basic types of cables will be required to penetrate the cryostat and service the Cold Electronics.  
<sup>7</sup> We will require low-voltage cables to power the FE boards, wire bias cables to provide the reference  
<sup>8</sup> voltages for the wire planes, moderate-speed cables for a communication downlink to the FE  
<sup>9</sup> boards, high-speed cables to carry the data out of the cryostat and signal cables to carry the  
<sup>10</sup> photon detection out. All of these cables will pass through the feedthrough port provided for each  
<sup>11</sup> pair of stacked APAs.

<sup>12</sup> Have the connectors been selected?

<sup>13</sup> The cables — and connectors — will be selected to have a low outgas and provide minimal  
<sup>14</sup> contamination to the LAr environment. Connectors will also need to be tested for usage in LAr  
<sup>15</sup> to make sure that a low ohmic contact is maintained in the cryogenic environment.

<sup>16</sup> We are looking into several types of cables and connectors. The low-voltage cabling will be chosen  
<sup>17</sup> based on power needs and whether we decide to go with a higher-voltage/lower-current feed using  
<sup>18</sup> DC/DC convertors or a low-voltage/higher-current feed used by low-voltage regulators. Studies  
<sup>19</sup> will take place to decide the most efficient and practical usage.

<sup>20</sup> The wire-bias cables must deliver voltages up to two or three thousand volts with less than a  
<sup>21</sup> couple of millamps. We anticipate using a coaxial cable and connectors which have been tested  
<sup>22</sup> and found sufficient to provide this load.

<sup>23</sup> The cables for the moderate speed downlink could utilize LVDS signaling and low-skew pairs.  
<sup>24</sup> Again, testing will be required to select the final cable and connectors.

<sup>25</sup> For the high-speed data links, we anticipate using a low-skew copper twinax cable. We have  
<sup>26</sup> prototyped such a cable and found that we can drive data at 2 Gbps for a 20 m length.

<sup>27</sup> Finally, the photon detector cables currently make use of shielded twisted pair cables which carry  
<sup>28</sup> both the DC bias voltage as well as the signals.

<sup>29</sup> Should we add a requirement about the connectors being keyed?

<sup>30</sup> It will be important that all cables and connectors be somewhat rugged, locking and able to  
<sup>31</sup> withstand a minimum of several tens of mating cycles. This is in addition to concerns about  
<sup>32</sup> material compatibility and the fact they must work in the cryogenic environment.

## <sup>1</sup> Warm Interface Board

<sup>2</sup> This section needs more meat, and some fact-checking (i.e., two FEMBs per WIB?).

<sup>3</sup> The warm interface boards (WIB) reside on the warm side of the feedthroughs. Each WIB connects  
<sup>4</sup> to two FEMBs, and acts as a flexible, optical interface to DAQ. While the FPGA on the FEMB  
<sup>5</sup> in the cold would in principle be able to provide any required flexibility, all flexibility is lost  
<sup>6</sup> once the FPGA is replaced with the COLDATA chip, which represents a hard compilation in  
<sup>7</sup> permanent silicon of a particular instance of FPGA code. The right panel of Fig. ?? shows the  
<sup>8</sup> WIBs installed on a feedthrough. The WIB is nearly identical to that for SBND; we are therefore  
<sup>9</sup> working in tandem with SBND on this.

## <sup>10</sup> Power for the Cold Electronics

<sup>11</sup> Haven't we made some changes here, regarding DC/DC converters?

<sup>12</sup> The power-per-channel for the FE electronics is designed be about 25 mW and the total low-voltage  
<sup>13</sup> power requirement for each APA is expected to be about 64 W. Power will be supplied to the  
<sup>14</sup> electronics on each APA separately by low-noise power supplies outside the cryostat, either directly  
<sup>15</sup> by low-voltage (1.8 V), high-current (36 A) conductors or by high-voltage (48 V) low-current (2 A)  
<sup>16</sup> conductors to DC-DC converters placed locally in the LAr. The use of DC-DC converters requires  
<sup>17</sup> conductors with smaller cross section, minimizing heat input to the cryostat (and ice formation  
<sup>18</sup> on the feedthroughs). However, the power dissipated by the (somewhat inefficient) converters in  
<sup>19</sup> the LAr will create boiling which may introduce contamination directly into the high-purity LAr,  
<sup>20</sup> and if enough LAr is vaporized, may also produce strong mixing of the ullage gas, driving more  
<sup>21</sup> impurities into the liquid. These effects of boiling LAr, unless they can be demonstrated to be  
<sup>22</sup> harmless, will drive a preference for eliminating DC-DC converters, and directly powering the  
<sup>23</sup> front-end readout boards.

<sup>24</sup> Heat conduction through the high-current feedthroughs and the self-heating ( $I \cdot R$ ) of the wires  
<sup>25</sup> are the factors contributing to additional heat load on the cryogenic system. The sum of the these  
<sup>26</sup> two factors as a function of the wire gauge, however, has a minimum due to the two opposing  
<sup>27</sup> dependencies on the copper-wire cross section. An optimum wire gauge can be chosen to minimize  
<sup>28</sup> heat input to the cryostat.

## <sup>29</sup> Wire-Bias Voltages

<sup>30</sup> Each anode plane assembly requires three bias voltage connections at +820V, -370V, and -665V.  
<sup>31</sup> The current on each of these supplies is expected to be zero at normal operation. However the  
<sup>32</sup> ripple voltage on the supply must be carefully controlled to avoid noise injection into the front-end  
<sup>33</sup> electronics.

<sup>1</sup> The power supplies for the wire bias will be similar to those used for conventional multi-wire  
<sup>2</sup> proportional chambers. Additional filtering networks will be needed to further reduce voltage  
<sup>3</sup> ripples. The default feedthroughs are the commercial SHV type. However, other, higher-density  
<sup>4</sup> multi-channel feedthroughs capable of withstanding the maximum voltage are under investigation.

## <sup>5</sup> 4.6.6 CE Installation

<sup>6</sup> Cold electronics will be mounted on the TPC and installed inside the cryostat. Because access to  
<sup>7</sup> the cold electronics is not possible after the cryostat is sealed, a full complement of tests will be  
<sup>8</sup> performed during the development stage and before the final installation (Figure 4.27).  
<sup>fig:cece\_CMBonAPA</sup>

## <sup>9</sup> Prototype Testing

<sup>10</sup> Do we want to keep some or all of this here? Or, should this migrate to the QA/QC section?

<sup>11</sup> Dedicated test boards for the FE ASIC and ADC ASIC, were used to characterize the performance  
<sup>12</sup> of prototype ASICs at both 300 K and 77 K, and taking them through multiple thermal cycles.  
<sup>13</sup> An automated test board was built for the FE ASIC to evaluate large numbers of FE ASICs at  
<sup>14</sup> room temperature, and another such board is currently being designed for the ADC ASIC.

<sup>15</sup> The development of the FE and ADC ASICs has proceeded through a series of prototype designs.  
<sup>16</sup> A 128-channel prototype analog mother board has been developed and tested in the lab. Together  
<sup>17</sup> with an FPGA mezzanine in place of the digital ASIC mezzanine, they form a FEMB for use in the  
<sup>18</sup> protodUNE TPC, since the COLDATA work is unlikely to be advanced enough to provide more  
<sup>19</sup> than a fraction of the electronics needed for the aggressive protodUNE schedule. A test stand  
<sup>20</sup> has been developed to test the FEMB using a commercial FPGA evaluation board as a mini-DAQ  
<sup>21</sup> system. All evaluation test data are stored on a desktop PC and analyzed to determine whether  
<sup>22</sup> the board is ready to be installed on the detector.

<sup>23</sup> During the prototype testing, a procedure has been developed for the production test of the cold  
<sup>24</sup> electronics boards. This includes key parameters (gain, noise, non-linearity, etc.) that should be  
<sup>25</sup> tested, detailed steps of the test to collect data and extract these parameters, and also the work  
<sup>26</sup> flows to perform the test at both 300 K and 77 K.

<sup>27</sup> Prototype cold electronics has been tested with prototype TPC and DAQ system, to evaluate the  
<sup>28</sup> performance of the APA assembly, and help the development of the DAQ software. A vertical  
<sup>29</sup> slice test has been used as the test bed for the integration test. It is an important step to identify  
<sup>30</sup> potential issues, check out system integration and performance before the installation into the  
<sup>31</sup> cryostat.

## <sup>1</sup> Assembly Testing

- <sup>2</sup> The front-end readout boards will be thoroughly tested. A testing program has been identified:
- <sup>3</sup> • A small number of the ASICs will undergo a complete suite of tests, including thermal cycling to determine the batch yield.
  - <sup>5</sup> • If the yield is high (> 95%), all ASICs will be mounted on the front-end boards. Tests will be performed on each board and bad chips replaced as needed.
  - <sup>7</sup> • If the yield is not high, an automated test fixture will be fabricated to validate every ASIC chip before mounting on the readout boards. Board-level tests after mounting the ASICs will be conducted. However, previous experience indicates that this scenario is very unlikely.
  - <sup>10</sup> • The fully assembled front-end boards will be thermally cycled multiple times while connected to a simple DAQ system to ensure reliable operation.
  - <sup>12</sup> • After the front-end electronics boards have been installed on an APA, an initial calibration of all electronic channels will be performed. The electronic gains and noise levels of all channels will be recorded in a database.
  - <sup>15</sup> • Electronic calibration on all channels will be performed while the APA is cold and again after it is warmed up. Significant differences in the cold and warm calibration results will be investigated and remediated.

## <sup>18</sup> Commissioning

- <sup>19</sup> During installation, the DAQ system will be running continuously. As soon as each stack of APAs is connected to the pre-routed cables, a suite of calibration runs will be performed to validate that all connections have been made properly. Repair or replacement at this stage will still be straightforward.
- <sup>23</sup> Following the installation of the APAs and the sealing of the cryostat, another complete test will be performed to verify the integrity of the cold electronics before the filling with argon. After the cryostat is filled with LAr and the detector is cooled down, an electronics calibration test will be performed to evaluate the detector performance prior to data taking.

<sup>27</sup> Space-permitting, it seems to me that more details on commissioning would be in order.

## <sup>1</sup> 4.7 PDS front-end electronics and DAQ

## <sup>2</sup> 4.8 Cryostat and feedthroughs

- <sup>3</sup> The cryostat consists of a steel warm structure, layers of insulation and an inner cold membrane.  
<sup>4</sup> The steel warm structure represents the mechanical support of the inner membrane cold cryostat  
<sup>5</sup> and its insulation. It consists of vertical beams alternated with a web of metal frames, capable  
<sup>6</sup> to withstand the hydrostatic pressure of the liquid argon, the pressure of the gas volumes and all  
<sup>7</sup> possible external constraints. The steel warm structure for NP04 is shown in Figure 4.37

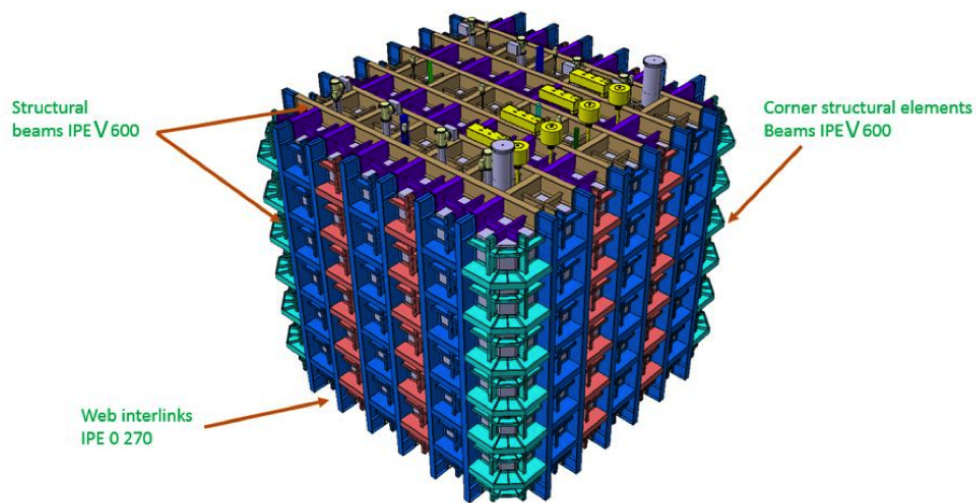


Figure 4.37: IWarm vessel layout showing the various major components

- <sup>8</sup> The main requirement is that this mechanical structure is constructed in EHN1 without any  
<sup>9</sup> mechanical attachment to the floor or the building side walls. Inside the steel structure, a 10 mm  
<sup>10</sup> skin of stainless steel plates are welded to provide a gas barrier to the outside.
- <sup>11</sup> The top of the cryostat will be accessible for installation of the detectors, the electrical/signal  
<sup>12</sup> feed-through, the detector supports and other cryogenics services. In Figure 4.38 you can see a  
<sup>13</sup> drawing of the structure. The dimensions requirements are dictated by the need to provide a  
<sup>14</sup> sufficient active volume of LAr to the detector. This means a transversal internal dimension of the  
<sup>15</sup> liquid volume of width = 8548 mm, length = 8548 mm and height = 7900 mm. The dimensions  
<sup>16</sup> have been adapted in order to ensure that all crossing penetrations are arranged as requested and  
<sup>17</sup> that there is enough space for maintenance.
- <sup>18</sup> Section view B in Figure 4.38 shows the warm structure on the outside, 10 mm SS skin, 800  
<sup>19</sup> mm of insulation and the inner cold vessel. The secondary membrane that is located within  
<sup>20</sup> the insulation layer is not shown in this view. The cold vessel is based on the GTT membrane  
<sup>21</sup> technology. The initial thermal requirements call for an insulation thickness of 800 mm, including  
<sup>22</sup> the primary and secondary membrane. These two membranes will provide a first and second  
<sup>23</sup> level of containment. There is no requirement at this point to have an additional containment

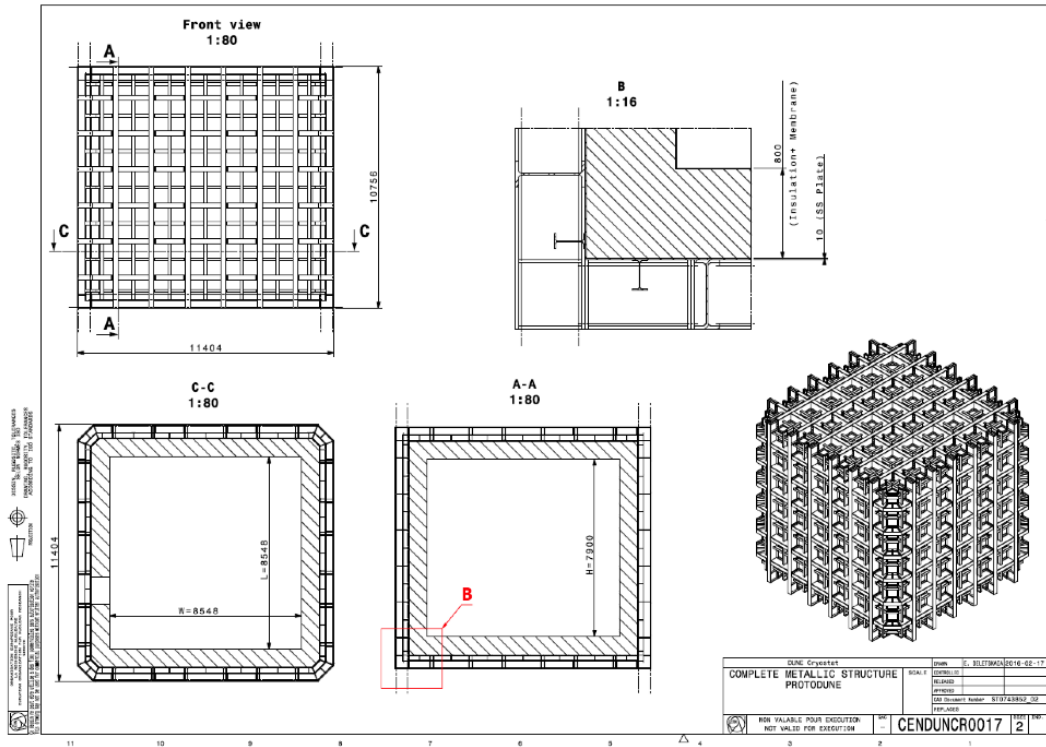


Figure 4.38: 2D drawing of the structure

fig:cryo

- 1 at the level of the warm steel structure. The SS skin of 10mm thickness between the warm
- 2 structure and insulation will provide an effective gas enclosure, which will allow controlling the
- 3 Argon atmosphere inside the insulation volume. All necessary information can be found in <https://edms.cern.ch/document/1531438/3>

5 make it a citation

- 6 The 3D detailed cad model is visible in <https://edms.cern.ch/document/1531439/3>

7 make it a citation

- 8 Prior to installation of the GTT insulation and cold liquid membranes, the gas tightness of the
- 9 SS 10mm membrane will be qualified by CERN using dye penetrant analysis, local vacuum bags
- 10 techniques and He leaks sniffing detection at the level of the natural He present in the atmosphere
- 11 ( $\sim 2 - 3 \times 10^{-6} \text{ mbar/l/sec}$ ) and a report will be presented to GTT.

## 12 4.8.1 Storage characteristics

- 13 The expected function of the cryostat is to store LAr in liquid form at atmospheric pressure or just
- 14 above. The cryostat will be placed inside an existing CERN experimental hall at CERN (EHN1
- 15 building). The cryostat is required to store the LAr at a temperature between 86.7 K and 87.7 K

1 with a pressure inside the tank of  $950 < P < 1100$  mbar. A special emphasis has been made on  
2 the thermal fluxes. They must be controlled and kept under  $5 \text{ W/m}^2$  on the walls/floor in contact  
3 with liquid to prevent boiling of the LAr.

- 4 1. The inner dimensions are  $7900\text{mm} \times 8548\text{mm} \times 8548\text{mm}$  (*height*  $\times$  *length*  $\times$  *width*). This  
5 corresponds to a total volume of  $580 \text{ m}^3$ .
- 6 2. Tank liquid capacity (assuming a 4% ullage):  $\sim 557\text{m}^3$
- 7 3. Residual Heat Input (RHI): 5-6  $\text{W/m}^2$
- 8 4. Insulation weight: 90 kg/m<sup>3</sup>
- 9 5. Insulation thickness (all included): 0.8 m
- 10 6. Design pressure: Max 1350 mBar / Min 950 mBar. The 1350 mBar is for an accidental  
11 condition during the cryogenics operation.
- 12 7. Operating temperature: 86K-89K

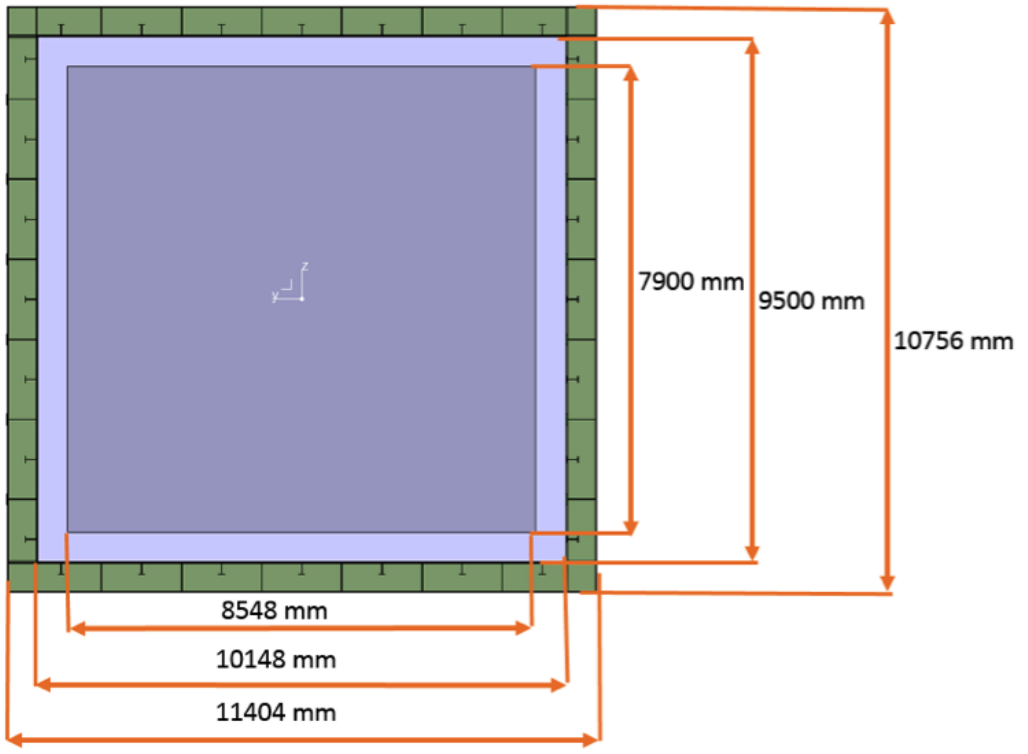
13   
Figure 4.39 shows the inner dimensions of the cryostat, dimensions of the 10 mm SS skin and the  
14 overall outer dimensions of the warm structure.

Figure 4.39: Overall dimensions

fig:cryo-overall-dim

## <sup>1</sup> 4.8.2 Fe warm cryostat design

- <sup>2</sup> The design and structural analysis of the warm support structure including the 10 mm SS gas
- <sup>3</sup> containment membrane is not a part of this study and has to be treated as a CERN deliverable.
  
- <sup>4</sup> The structural beams are the main elements of the floor, roof and side walls of the warm structure
- <sup>5</sup> and the corner structural elements can be found only at the corners where the side wall is connected
- <sup>6</sup> with the other side wall. The structural beams are the principal load bearing elements of the
- <sup>7</sup> structure. Their purpose is to withstand the hydrostatic pressure from the LAr, as well as to
- <sup>8</sup> support the roof load. They consist of IPE V 600 standard profile.

<sup>9</sup> add and reference figures Figure 4.40 and Figure 4.41

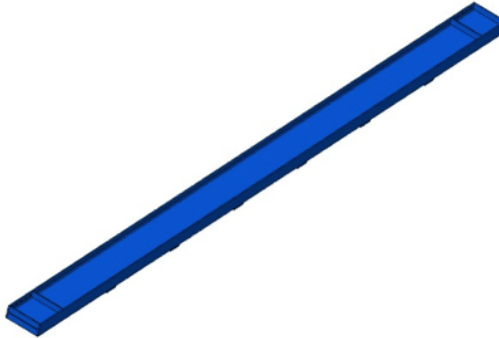


Figure 4.40: Structural beam detail

fig:struc

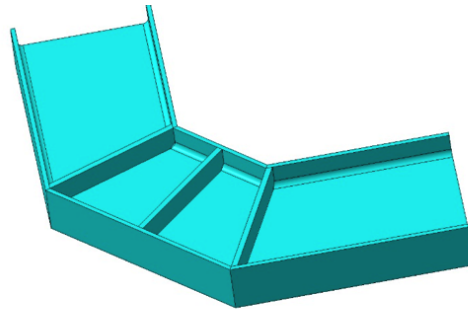


Figure 4.41: Corner structural element detail

fig:corr

## <sup>10</sup> 4.8.3 The web interlink structure

- <sup>11</sup> The web interlink structure purpose is to provide an adequate support of the polyurethane insu-
- <sup>12</sup> lation of the membrane. They consist of IPE O 270 profiles.

<sup>13</sup> Reference Figure 4.42

fig:web-interlinks-detail

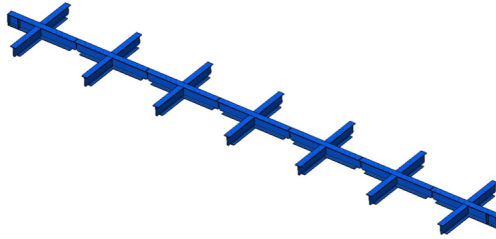


Figure 4.42: Web interlinks detail

fig:web-

- 1 Additional 10 mm stainless steel plates are welded to the web interlink structure to create a gas  
2 containment barrier to the inside, as well as to ensure even better support for the membrane  
3 insulation. The web interlink structure is also used for the floor, in-between the corner beams, as  
4 well as for the roof structure.
- 5 A very detailed technical report is available at <https://edms.cern.ch/document/1531442/1>

6 make it a citation

- 7 . In this report the following items are discussed:

- 8 • all of the various load conditions including boundary conditions and the safety factors,  
9 • buckling analysis,  
10 • design and stress calculations for all of the bolted connections,  
11 • finite element analysis calculations for the 10 mm skin and structure, and  
12 • the compliance with the required codes.

#### 13 4.8.4 Cold GTT Vessel

14 Inside the warm support structure, which includes the stainless steel gas enclosure membrane, the  
15 GTT cold vessel will be installed. It consists of a thermal insulation, a primary corrugated stainless  
16 steel membrane, as well as a secondary thin membrane, to provide primary and secondary liquid  
17 containment. A cross sectional view of this is shown in Figure 4.43. fig:xsec-insulation-layers

18 The primary membrane is made of corrugated stainless steel 304 L and is 1.2 mm in thickness.  
19 The standard size of the sheets is 3 m x 1 m. The secondary membrane is made of Triplex. This  
20 is a composite laminated material of a thin sheet of aluminium between two layers of glass cloth  
21 and resin. It is positioned inside the prefabricated insulation panels between two of the insulation  
22 layers. Details of the two membranes are shown in Figure 4.44. The insulation is made from  
23 reinforced polyurethane foam. The insulation panels are bonded to the inner 10 mm skin using fig:prim-2nd-membranes

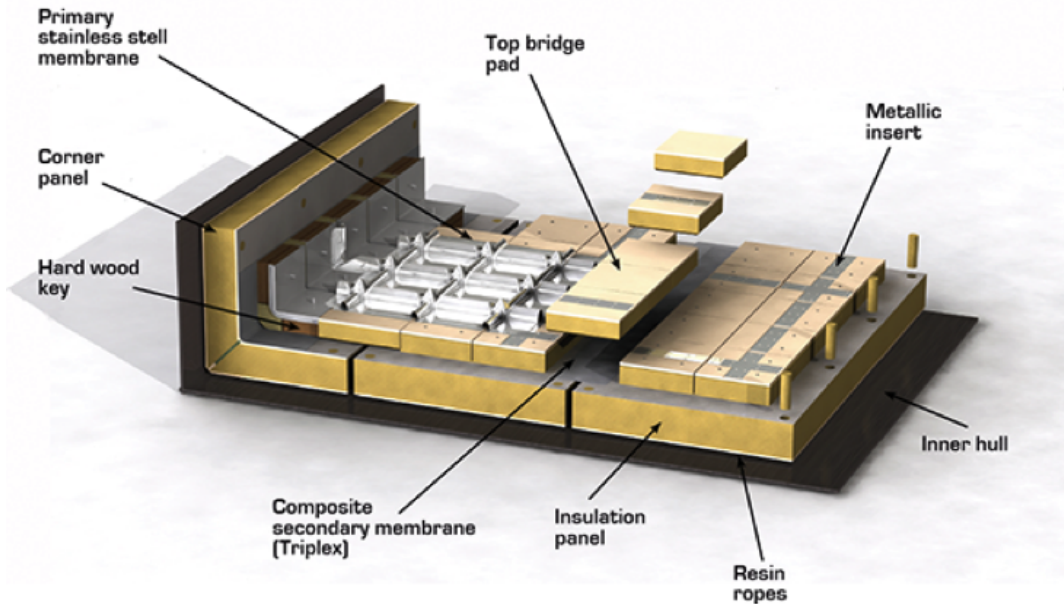


Figure 4.43: Cross section of insulation layers on membranes

fig:xsec

- 1 resin ropes. The insulation layers will be instrumented with gas inlets, outlets, temperature and
- 2 pressure sensors.

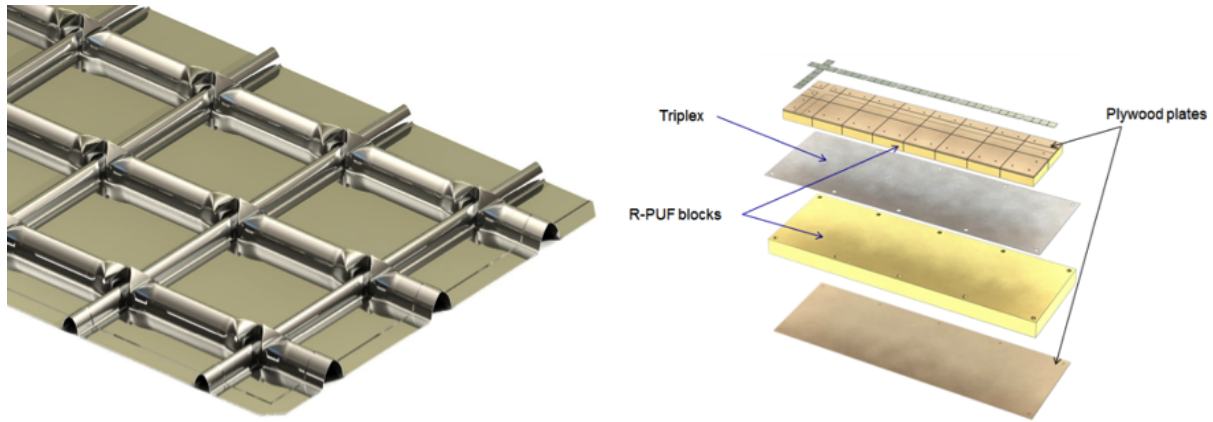


Figure 4.44: Left shows the primary stainless steel corrugated membrane and right shows the prefabricated panels of insulation and the secondary membrane

fig:prim

### 3 4.8.5 TCO (Temporary Construction Opening)

- 4 A dedicated access window will be necessary to install the NP04 detector. This is referred to as
- 5 the TCO. This means that no insulation or membrane can be installed at the beginning in this
- 6 location. Once the detector installation has progressed as far as possible and all of the large TPC
- 7 components are inside the cryostat, the TCO will be closed. The 10 mm SS skin, insulation and
- 8 cold membranes will be installed and welded in place.

1

`fig:front-tco-np04`  
reference Figure 4.45

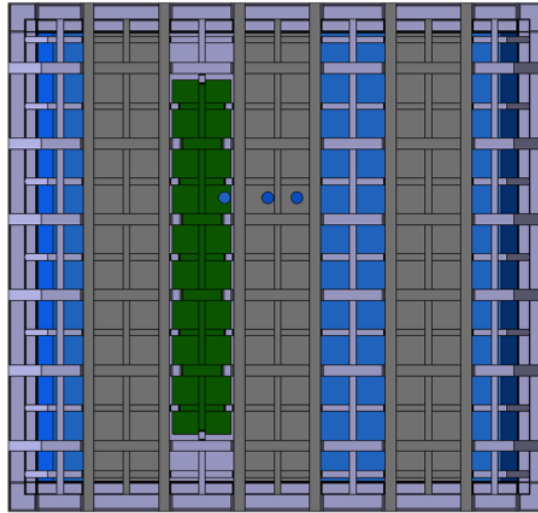


Figure 4.45: Front view of the TCO for the NP04 cryostat

`fig:front-tco-np04`

## 2 4.8.6 LAr pump penetration

3 On one side wall, as low as possible, a special penetration has to be foreseen to connect the  
 4 extraction liquid argon pumps that will allow the liquid recirculation to an external filtering system.  
 5 For both solutions the penetration will be the same but placed in different locations (see section  
 6 8.2). To keep the high level of purity required, an external pump is connected on the one side to  
 7 the bottom of the liquid, through a dedicated system of safety valves. This penetration requires a  
 8 local modification of the insulation panels and the SS primary membrane, and will be a crossing  
 9 tube with diameter of 168 mm for the insulation and the membrane and a larger diameter hole at  
 10 the stainless steel plate.

## 11 4.8.7 Beam window penetration

12 Once constructed, the NP04 detector will be exposed to the charged particle beams from the SPS  
 13 accelerator. To minimize energy loss and multiple scattering of the beam particles in the dead  
 14 material of the cryostat and its insulation, a beam window will be inserted which will remove  
 15 a large fraction of this unnecessary material. The beam window dimension is about 220 mm in  
 16 diameter. This beam window will be placed upstream of the primary membrane and therefore the  
 17 primary membrane will remain intact. The details of the beam window system design is described  
 18 in 4.13.

`sec:beamwindow`

## <sup>1</sup> 4.8.8 Roof signal, services and supports penetrations

<sup>2</sup> The penetrations through the cryostat have been arranged by positions and diameters (see Section  
<sup>3</sup> 8). Most of the penetrations are placed on the ceiling of the cryostat. They have been differentiated  
<sup>4</sup> into two main groups according to their function and the thermal stresses they will be submitted  
<sup>5</sup> to: whether they can be used to support the weight of the detector or not. The penetrations  
<sup>6</sup> on the roof of the cryostat for the NP04 cryostat details are shown below. A 3D cad model to  
<sup>7</sup> identify all position can be found at: <https://edms.cern.ch/document/1543241/3> and drawing  
<sup>8</sup> CENDUNCR0016.

<sup>9</sup> make them citations

<sup>10</sup> *tab:roofpenetrations*  
add reference to Table 4.2

Table 4.2: Detector penetrations, roof

Component	Header Column 2??	Quantity	Value
West TPC translation suspension:	N.3	crossing tube diameter	200 mm
Center TPC translation suspension:	N.3	crossing tube diameter	200 mm
East TPC translation suspension:	N.3	crossing tube diameter	200 mm
Signal cable chimney FTs:	N.8	crossing tube diameter	250 mm
Spare on Signal cable row FTs:	N.2	crossing tube diameter	250 mm
Laser FTs:	N.1	crossing tube diameter	160 mm
Calibration Fiber CPA FT:	N.1	crossing tube diameter	250 mm
Spare on CPA line FTs:	N.2	crossing tube diameter	150 mm
HV FT:	N.1	crossing tube diameter	250 mm
Manhole:		crossing tube diameter	710 mm
Angled beam windows – west side:		crossing tube diameter	250 mm
		Vertical: 11.342°	
		Horizontal: 11.844°	
TCO - side:		1200mm × 7300mm	
Cryogenic pipes - roof:			
	N.4	crossing tube diameter	250 mm
	N.1	crossing tube diameter	304 mm
	N.5	crossing tube diameter	152 mm
	N.1	crossing tube diameter	125 mm
	N.3	crossing tube diameter	250 mm
Cryogenic pipes – north side:	N.1	crossing tube diameter	168 mm

## <sup>11</sup> 4.8.9 Mechanical mounts and supports

- <sup>12</sup> • Introduction

- <sup>1</sup> • Layout and general design
- <sup>2</sup> • Technical information and specifications
- <sup>3</sup> • Interface with cryostat and warm structure
- <sup>4</sup> • Interface with TPC including electrical/grounding
- <sup>5</sup> • Structural analysis and factors of safety

## <sup>6</sup> 4.9 Installation

### <sup>7</sup> 4.9.1 Anode Plane Assemblies (APAs)

### <sup>8</sup> 4.9.2 Cathode Plane Assemblies (CPAs)

### <sup>9</sup> 4.9.3 Field Cage (FC)

### <sup>10</sup> 4.9.4 Photon Detection System (PDS)

### <sup>11</sup> 4.9.5 Cold Electronics (CE)

## <sup>12</sup> 4.10 Cryogenics and LAr purification systems

### <sup>13</sup> 4.10.1 Overview, Overall planning and ES&H

<sup>14</sup> The scope of the ProtoDUNE Cryogenics includes the design, procurement, fabrication, testing,  
<sup>15</sup> delivery, installation oversight and acceptance tests of a comprehensive cryogenic system that  
<sup>16</sup> meets the performance requirements for purging, cooling down and filling the cryostat, acquiring  
<sup>17</sup> and maintaining the LAr temperature within  $\pm 1$  K around nominal temperature (88.3 K), purifying  
<sup>18</sup> the Liquid Argon (LAr) outside the cryostats, and re-condensing and purifying the boil-off Gaseous  
<sup>19</sup> Argon (GAr). The reference-design for the ProtoDUNE cryogenics infrastructure includes the  
<sup>20</sup> External, Proximity and Internal Cryogenics.

<sup>21</sup> The External Cryogenics includes the systems used for the storage and eventual production of the  
<sup>22</sup> cryogens needed for the operation of the cryogenic system (LN<sub>2</sub> for cooling, LAr for the cryostat)  
<sup>23</sup> and GAr generated from the cryogenic storage tanks. In particular, it encompasses:

- The receiving facilities for LAr and Liquid Nitrogen (LN<sub>2</sub>) tanker trucks.
  - The cryogenics transfer lines to deliver LAr and LN<sub>2</sub> to the Proximity Cryogenics (in the vicinity of the cryostat).
  - The ambient vaporizer and transfer lines to deliver GAr to the cryostat for the piston purge and the GAr make-up.
- The Proximity Cryogenics takes the cryogens from the External Cryogenics and delivers them to the Internal Cryogenics under the required pressure, temperature, purity and mass flow rate. It encompasses:
- The condenser (with heat exchanger) to re-condense the boil-off GAr.
  - The LAr purification system with inline purity monitor.
  - The LAr recirculation pumps.
  - The LAr Phase separator to feed the cryostat.
  - The LN<sub>2</sub> Phase separator to feed the condenser.
  - The GAr purification system.
  - The cryostat-purge equipment.
- The Internal Cryogenics includes all the cryogenic equipment located inside the cryostat. It encompasses:
- The cryostat/detector cool down manifolds
  - The LAr distribution manifold
  - The GAr purge distribution manifold.
- The equipment described in this chapter will be used for the cool-down, filling, operation, purification, emptying and warm-up of the ProtoDUNE Single Phase cryostat. These operations are described in greater detail in Section 4.10.3.
- The development of the ProtoDUNE cryogenics is part of a common effort between CERN and Fermilab that include the cryogenics for the ProtoDUNE Single Phase and Dual Phase detectors at CERN, and the Short Baseline Neutrino Near Detector (SBND) and Far Detector (SBN-FD) at Fermilab.
- The cryogenic systems for all four projects are developed jointly with a standard approach to minimize the duplication of work, benefit of existing knowledge (at Fermilab and CERN), and also prototype for the Long Baseline Neutrino Facility (LBNF)/Deep Underground Neutrino Experi-

<sup>1</sup> ment (DUNE) project. The systems build on the successful experience of the Liquid Argon Purity  
<sup>2</sup> Demonstrator (LAPD), 35 ton prototype, and MicroBooNE at Fermilab, and the development of  
<sup>3</sup> the WA105 1x1x3 Dual Phase prototype at CERN.

<sup>4</sup> The conceptual design for these cryogenic systems has been completed and a tender has recently  
<sup>5</sup> been issued for the completion of the design, the fabrication, the delivery, the installation and the  
<sup>6</sup> testing of all four systems, including the ProtoDUNE Single Phase detector. Replies to the tender  
<sup>7</sup> are expected at the beginning of July, with the goal to award a potential contract after the CERN  
<sup>8</sup> Finance Committee scheduled in September.

<sup>9</sup> [DM question: is this part ok in this document??]

<sup>10</sup> During all phases, CERN codes and standards will guide the design, procurement and installa-  
<sup>11</sup> tion phases of the ProtoDUNE Single Phase cryogenics. The planned work process will provide  
<sup>12</sup> for reviews throughout all phases of the project to guarantee stringent adherence to the safety  
<sup>13</sup> requirements.

<sup>14</sup> [Will this be written in another section?? If not, we can leave it here]DM

<sup>15</sup> The project requirements for the ProtoDUNE cryogenic system are identical to those of the DUNE  
<sup>16</sup> Far Detector cryogenics. The current list is available on DocDB n. 112

<sup>17</sup> Add citation

<sup>18</sup> .

<sup>19</sup> A selection of relevant ones is presented here:

- <sup>20</sup> • Cryo-se-4: The system shall allow recirculation and purification of the liquid argon inventory  
<sup>21</sup> to achieve the needed LAr purity to meet the scientific requirement (less than 10 day/volume  
<sup>22</sup> change based on ICARUS experience).
- <sup>23</sup> • Cryo-se-6: The purification system shall be capable of removing contaminants form the LAr  
<sup>24</sup> prior to filling and shall maintain purity during operation.
- <sup>25</sup> • LArFD-L2-se-44: Electron lifetime greater than 3 ms.
- <sup>26</sup> • Cryo-se-5: The system shall provide an argon gas boil off and reliquefaction system.
- <sup>27</sup> • Cryo-se-16: There shall be no sources of argon gas reliquefaction inside the cryostat, e.g.  
<sup>28</sup> uninsulated pipes carrying liquid argon.
- <sup>29</sup> • Cryo-se-25: The cryostat and cryogenic systems shall be designed for using the piston-purge  
<sup>30</sup> technique (introducing heavy gas at the bottom and taking out exhaust from the top) for  
<sup>31</sup> removing initial electronegative impurities.

- Cryo-se-8: The cryogenics system shall be designed so as not to introduce unwanted noise into the electronics.
- Cryo-se-10: The detector cryostat shall provide a stable liquid argon environment for the detector.
- Cryo-se-28: The cryostat and cryogenic system shall be designed to maintain a single phase in the entire liquid argon volume at as table temperature. The chose temperature is 88.3 K +/- 1 K.

## 4.10.2 Cryogenics Layout

The Process Flow Diagram (PFD) of the ProtoDUNE cryogenic system is shown in Figure 4.46. The External Cryogenics located outside of the EHN1 building, is shared with the Dual Phase prototype, which is located in the same experimental hall, few tens of meters away.

Figure 4.46: Process Flow Diagram

Waiting for orig diagram for process flow from DM

The system has the following functions:

- It provides the GAr for the piston purge phase and the GAr make-up.
- It provides the LAr to the cryostat.
- It provides the LN2 to the condenser.
- It provides the cooling power by means of evaporation of liquid nitrogen and condensation of GAr, to the liquid argon cryostat, for its cool-down, normal operation and warm-up phases.
- It provides the capability to purify the cryostat liquid argon volume to a level of parts per trillion (ppt) Oxygen equivalent contamination; the purification process uses mole-sieve and active copper.
- It provides the capability to purify the re-condensed boil off before reintroducing it inside the cryostat.
- It provides a mean to cool down the cryostat and the detector following the requirements.
- It distributes the LAr and GAr inside the cryostat to meet the requirements.

Figure 4.47 shows a 3D view of the cryogenic installation as currently designed. The red and green lines coming from the bottom of the view are the LN2 and LAr supply lines respectively from the

1 external cryogenics.

Figure 4.47: 3D view of the installation

fig:3d-v

2 Waiting for orig diagram for 3D view of the installation from DM; May be replaced with a  
more complete one with building also

3 Figure 4.48 shows a 3D view of a detail of the internal cryogenics: the cryostat and detector cool  
4 down manifolds at the top of the cryostat.

Figure 4.48: Detail of the internal cryogenics

fig:int-

5 Waiting for orig diagram for int-cryogenics-detail from DM

6 There is a common receiving facility for NP-02 and NP-04 located outside the building, from which  
7 Argon and Nitrogen lines take LAr, GAr, and LN2 to the respective installations.

8 A 50 m<sup>3</sup> (69 tons of LAr capacity) vertical dewar will allow for receipt of LAr deliveries for the  
9 initial filling period. This liquid argon dewar serves also as a buffer volume to accept liquid argon  
10 during the fill period. An analyzer rack with instruments to check water, nitrogen, and oxygen  
11 content of the trailers will also be located in the vicinity. A

12 XXX

13 kW vaporizer is used to vaporize the liquid argon from the storage dewar prior to the GAr delivery  
14 pipes.

15 The cryostat will have its own argon condenser (16 kW of cooling power), argon-purifying equip-  
16 ment and overpressure protection system. The full power of the argon condenser is used during  
17 the initial cool down phase only, which is expected to take two to three weeks.

18 A

19 50 m<sup>3</sup>

20 vertical dewar will allow for receipt of LN2 deliveries and storage of LN2 for cool down and normal  
21 operations. LN2 is flown into the heat exchanger of a condenser located in close proximity of the  
22 cryostat to recondense the boil-off GAr coming from the cryostat itself.

23 Two LAr recirculation pumps are placed outside of the membrane cryostat to circulate liquid from  
24 the bottom of the tank through the purifier and then back to the tank to ensure the needed LAr  
25 purity.

26 The purification filters are located in the vicinity of the cryostat. The filters contain dual media,  
27 a molecular sieve for removal of water and a copper coated catalyst media for oxygen removal.

<sup>1</sup> There is one gas filter that is used during the purge in closed loop phase and two liquid filters  
<sup>2</sup> used during the filling and normal operations to continuously purify the bulk of the LAr inside the  
<sup>3</sup> cryostat. Associated with the filters, there will be regeneration equipment such as heaters and a  
<sup>4</sup> Ar/H<sub>2</sub> mix.

<sup>5</sup> Before returning to the cryostat, the LAr flows into a phase separator: the liquid is taken from  
<sup>6</sup> the bottom and delivered to the cryostat, while the gas is returned to the condenser.

### <sup>7</sup> 4.10.3 Modes of operations

<sup>8</sup> The major functions of the cryogenics servicing the cryostat are: cryogens supply for cool down and  
<sup>9</sup> fill, gas filtration, argon condensing, liquid filtration and circulation, and argon-purity analysis.  
<sup>10</sup> The methods presented in this section are motivated by experience from the cryogenic systems of  
<sup>11</sup> other LAr Time Projection Chamber (TPC) experiments, such as ICARUS, LAPD, the 35 ton,  
<sup>12</sup> MicroBooNE.

#### <sup>13</sup> Cryostat piston purge

<sup>14</sup> After the cryostat construction and following the installation of all scientific equipment, the cryo-  
<sup>15</sup> stat will be cleaned and purged in preparation for cool down and filling. Construction procedures  
<sup>16</sup> leading up to this point will ensure that the completed cryostat does not contain debris and is free  
<sup>17</sup> of all loose material that may contaminate the LAr.

#### <sup>18</sup> Purge in open loop

<sup>19</sup> Argon piping will be isolated, evacuated to less than 0.1 mBar

<sup>20</sup> (lower??)

<sup>21</sup> absolute pressure and backfilled with high-purity argon gas. This cycle will be repeated several  
<sup>22</sup> times to reduce contamination levels in the piping to the ppm level. The reference-design choice  
<sup>23</sup> for removing air from the membrane cryostat will be to flow/piston-purge argon, introducing the  
<sup>24</sup> heavy argon gas at the bottom of the tank and removing the exhaust at the top. The exhaust will  
<sup>25</sup> be taken from the main GAr outlet, but also from all the side ports located on each penetration  
<sup>26</sup> through the roof to ensure that all volumes are properly purged.

<sup>27</sup> The flow velocity of the advancing GAr will be set to 1.2 m/hour. This is twice the diffusion rate  
<sup>28</sup> of the air downward into the advancing argon so that the advancing pure argon-gas wave front will  
<sup>29</sup> displace the air rather than just dilute it. A 2D ANSYS model of the purge process shows that  
<sup>30</sup> after about 13 hours of purge time and 2 volume changes, the air concentration will be reduced  
<sup>31</sup> to less than 1%. At 44 hours of elapsed time and seven volume changes, the purge process is

1 complete with residual air reduced to a few ppm. This simulation includes a representation of the  
2 perforated field cage at the top and bottom of the detector and heat sources due to the readout  
3 electronics. The cathode planes are modeled as non-porous plates although they will actually be  
4 constructed of stainless-steel mesh. Figure 4.49 shows a view of the 2D simulated model at the  
5 end of the purge in open loop phase.

Figure 4.49: 2D simulation of the purge in open loop process (end of the phase).

fig:2d-sim-purge

6 Waiting for orig diagram for 2D simulation of the purge in open loop process from DM; May  
be replaced with a more complete one with building also

7 The Computational Fluid Dynamics (CFD) model of the purge process has been verified in multiple  
8 arrangements so far: (1) in an instrumented 1 m-diameter by 2 m-tall cylinder, (2) in LAPD, a 3  
9 m-diameter by 3 m-tall cylindrical tank where gas-sampling measurements were at varying heights  
10 and times during the purge process, and (3) within the 35 ton membrane cryostat, a prototype  
11 vessel built for LBNE in 2013. The results of these tests are available here: .

12 xxx [add reference]

13 Once the residual air inside the tank is down to the ppm level, this step is completed and we  
14 continue the process in closed loop.

## 15 **Purge in closed loop**

16 Water and oxygen will continue to be removed from the system for several days following the initial  
17 purge. During this step the GAr is no longer exhausted but recirculated through the GAr purifier  
18 and sent back to the bottom of the cryostat to continue the process. The cryostat contains xxx tons  
19 of FR4 circuit-board material and a smaller inventory of plastic-jacketed power and signal cables.  
20 These somewhat porous materials may contain as much as 0.5% water by weight. Water-vapor  
21 outgassing from these materials will be entrained in the gas flow exiting the top of the cryostat  
22 and will be removed from the gas stream by filters. Adsorbed water will also be removed from the  
23 metallic inner surfaces of the cryostat and piping system. Water deep within porous materials will  
24 remain; this is not a problem since the water diffusion rate in FR4 at room temperature is already  
25 quite low ( $0.3 \mu\text{m}^2/\text{s}$ )

26 fix units

27 and the FR4 assemblies are relatively thick (1 cm).

28 This process reduces the oxygen and water contamination inside the cryostat to sub-ppm levels,  
29 at which point the cool down may commence.

<sup>1</sup> **Cool-Down**

<sup>2</sup> Purified LAr will be mixed with GAr and distributed by a set of dedicated sprayers near the  
<sup>3</sup> top of the cryostat and on the side of the TPC to cool down the cryostat and the detector in a  
<sup>4</sup> controlled way. The sprayers deliver a mix of LAr and GAr in atomized form that is moved inside  
<sup>5</sup> the cryostat by another set of sprayers flowing GAr only. The boil-off gas is re-condensed inside  
<sup>6</sup> the condenser and it then flows back as liquid to feed the LAr sprayers. Simulations have shown  
<sup>7</sup> that this cool-down method can maintain the cool down requirements of the detector, as listed in  
<sup>8</sup> Table 4.3<sup>tab:cryogen-install-params</sup>, and cryostat, which are less stringent. The required cooling rate is determined by the  
<sup>9</sup> maximum stress that detector components can tolerate. For example, the 150  $\mu\text{m}$  APA wires will  
<sup>10</sup> cool much more rapidly than the APA frames. A temperature-monitoring system will be used to  
<sup>11</sup> control the temperature difference across the cryostat and the detector.

<sup>12</sup> **Filling**

<sup>13</sup> Once the cryostat and the TPC are cold, LAr is introduced in the cryostat through the cryostat  
<sup>14</sup> filling pipework. Argon is transferred directly from the LAr storage tank after passing thorough  
<sup>15</sup> the LAr filtration system for purification. The filling process will take place over three to four  
<sup>16</sup> weeks.

<sup>17</sup> **Steady state operations**

<sup>18</sup> During steady state operations the following happens:

- <sup>19</sup> • LAr is continuously purified by means of an external LAr pump (two are installed for redundancy, but only one is in use).
- <sup>20</sup> • Boil-off GAr is re-condensed in a condenser situated outside the cryostat and purified before being reintroduced as LAr. The re-condensed LAr is sent to the LAr filtration system by means of a dedicated LAr pump and mixed in line with the bulk of the liquid coming from the cryostat. Alternatively, it is possible to send it to the inlet of the main LAr circulation pumps and from there as a single LAr stream to the filtration system.

<sup>26</sup> **Emptying**

<sup>27</sup> At the end of the operations (or if/when maintenance on the tank is needed) the tank is emptied  
<sup>28</sup> and the LAr removed. The LAr is returned to the storage tank outside the building and from  
<sup>29</sup> there unloaded back to LAr tankers.

## 1 Parameters

2 Table 4.3 presents a list of the relevant parameters for this installation. Note that the the filling  
3 flow rate of 18 l/min (0.42 kg/s) is an estimate. The actual value might be limited by the pressure  
4 inside the LAr storage dewar. We are also assuming that we are able to receive 2 trucks/day of  
5 LAr, which will need to be confirmed by the suppliers.

Table 4.3: List of engineering parameters for cryogenics installation

Mode	Parameter	Value	Notes
Piston purge	GAr flow rate	88 m3/hr	From 1.2 m/hr
Cooldown	Maximum cool-down rate TPC	40 K/hr 10 K/m 10 K/m	T sensors on the detector responsibility of detector
Cooldown	Maximum delta T between any two points in the detector	50K	T sensors on the detector responsibility of detector
Filling (*)	LAr filling flow rate	18 l/min (0.42 kg/s)	Assuming 2 trucks/day
Normal ops	Cryostat static heat leak	3.0 kW	GAr boil-off (18 g/s)
Normal ops	Other heat loads (estimate)	5.0 kW	Total estimate is ~8 kW
Normal ops	LAr circulation (5 days turnover)	72 l/min (1.67 kg/s)	72 l/min (1.67 kg/s)
Emptying	Max flow rate emptying (w both LAr pumps)	144 l/min (3.34 kg/s)	Limited by the size of tank/truck
All	Condenser size	16 kW	

### 6 4.10.4 Features

7 This section briefly describes the main features of the various parts of the cryogenic system.

### 8 External Cryogenics

9 The external cryogenics comprises the Liquid Argon and Liquid Nitrogen receiving facilities, the  
10 LAr/GAr and LN2 distribution systems, the Argon/Hydrogen mixture to regenerate the LAr/GAr  
11 purification filters and the mechanical filters on the LAr filling line.

12 The cryostat will hold an inventory of 760 ton of liquid argon. The standard grade specification  
13 for argon is a minimum purity of 99.995%, allowing a maximum concentration of 5.0 ppm for  
14 O<sub>2</sub> and 10.5 ppm for H<sub>2</sub>O. This is designated as Grade 4.5 in the gas-supply industry. Requiring  
15 higher-purity product might increase the cost and push out the schedule. Suppliers may also  
16 decide not to quote for such an amount of a higher purity fluid. Therefore, standard product will  
17 be procured.

18 Facilities are required for the offloading of LN2 and LAr road tankers. Vehicle access and hard-  
19 surfaced driving areas are being constructed adjacent to the LN2/LAr dewars and the LAr/LN2-

1 supply pipes. A LAr storage dewar will hold the contents of a road tanker in order to minimize  
2 off-loading time. Road tankers will connect to a manifold and will use their on-board pumps to  
3 transfer the LAr to the storage dewar. Each tanker will be tested to ensure that the LAr meets  
4 the purity specification. The LAr will be stored and transported as a liquid inside the cryostat  
5 during the filling process. The filling will be slower than the offloading, because we will not use a  
6 pump but only the available head height and some overpressure as driving force.

7 A battery of fourteen (14) 12-bottle racks containing 1.5% Hydrogen (by volume) and a balance  
8 of Argon will be stored outside the building as well. They will be used to regenerate the LAr and  
9 GAr purification filters as needed.

10 One 1-ppm mechanical filter is located on the LAr feed line. It prevents dirt and impurities from  
11 the LAr supply to enter the purification system and the cryostat.

## 12 Proximity Cryogenics

13 The Proximity Cryogenics comprises the argon condenser, the purification system for the LAr and  
14 GAr, the LAr circulation pumps, and the LAr/LN<sub>2</sub> phase separators.

## 15 Argon reliquefaction and pressure control

16 too many layers deep; AH

17 The high-purity liquid argon stored in the cryostat will continuously evaporate due to the un-  
18 avoidable heat ingress. The argon vapor (boil-off gas) will be recovered, chilled against a stream  
19 of liquid nitrogen, condensed and returned to the cryostat. A closed system is required in order  
20 to prevent the loss of the high-purity argon. The re-condensed boil-off can be returned to the  
21 cryostat in three ways:

22 • With a small LAr pump that sends it into the main LAr circulation stream (normal mode).

23 • Directly to the condenser (emergency mode, when we cannot go through the purification  
24 system).

25 • To the inlet of the main LAr circulation pumps (when the small LAr pump needs mainte-  
26 nance, to guarantee a continuous purification of the boil-off GAr).

27 During normal operation the expected heat ingress of approximately 8 kW to the argon system  
28 will result in an evaporation rate of 30 g/s and expanding in volume by a factor of 200 when it  
29 changes from the liquid to vapor phase. This increase in volume within a closed system will, in  
30 the absence of a pressure-control system, raise the internal pressure.

31 Argon vapor will also be removed from the top of the cryostat through the chimneys that contain

the cryogenic feedthroughs. As the vapor rises, it cools the cables and feedthrough, thereby minimizing the outgassing. The exiting gaseous argon will be directed to the same condenser as above, in which it is chilled against a stream of liquid nitrogen and condensed back to a liquid. As the argon vapor cools, its volume reduces and, in the absence of pressure control, further gas would be drawn into the heat exchanger, developing a thermal siphon. Therefore, a pressure-control valve on the boil-off gas lines will control the flow to the condenser to maintain the pressure within the cryostat at  $0.113 \text{ MPa} \pm 0.003 \text{ MPa}$ . The liquid nitrogen stream (that provides the coolant for the condenser) will be supplied from the LN2 phase separator, which is fed by the LN2 storage dewar located outside of the building. After the heat exchanger the returning N<sub>2</sub> vapor is exhausted outside the building. The estimated heat loads to the argon system are listed in Table 4.4.

tab:cryostat-est-heat

Table 4.4: Estimated heat loads within the cryostat

Item	Heat Load (kW)
Insulation Heat Loss	3.0
All other contributions (Recirculation pumps, pipes, filters, electronics, etc.)	5.0
Total	8.0

## 11 Argon purification

The cryostat is designed with one penetration below the liquid level for external pumps used to transfer LAr from it to the purification system. The pumps are inserted into a valve box that is an integral part of the proximity cryogenics. The pump suction must be located at a minimum distance (normally about 1.5 to 2.0 m) below the lowest liquid level at which they are to pump in order to prevent cavitation and vapor-entrapment. There are two pumps for continuous operation during maintenance, etc. but only one is expected to be in service at any moment in time.

The liquid-argon volume will turn over every 5.5 days, which corresponds to 1.63 kg/s (72 l/min) of flow rate. As a point of comparison, ICARUS T600 has a maximum turn-over rate of eight to ten days. In principle it is possible to operate both pumps at the same time and double the flow rate, should it be needed.

The multiple-pump arrangement provides a high level of redundancy, which will extend the maintenance-free operating period of the cryostat.

The liquid purification system, located nearby the cryostat, consists of two sets of three filter vessels containing molecular-sieve (1) and copper media (2) filters. They have been arranged in this configuration to reduce the size of the valve box containing them. Each molecular-sieve filter is 0.4 m in diameter by 0.9 m tall and contains 80 kg of media. Each copper filter is 0.6 m in diameter by 1.3 m tall and contains 298 kg of media. The filters are sized to provide effective media usage at low pressure drop over the expected range of flow rates. They are used during the filling and normal operations.

The gas purification system, located nearby the cryostat as well, is used to purify the GAr for the

32 purge in close loop process. It consists of one filter vessel containing molecular-sieve and copper  
1 media filters in the same vessel. The mol sieve part measures 0.3 m in diameter by 0.1 m tall and  
2 contains 5 kg of media. The copper part measures 0.3 m in diameter by 0.6 m tall and contains  
3 34 kg of media.

4 During the filling the LAr will flow through the liquid filtration, then the LAr phase separator and  
5 into the cryostat.

6 After the filling is completed, the cryostat liquid argon inventory is continuously circulated through  
7 one set of liquid purification filters to achieve and maintain the required purity. It then goes back  
8 to the cryostat via the LAr phase separator. The purification filter, containing molecular sieve  
9 media to remove water and copper media to remove oxygen, will become saturated. The nearly  
10 saturated purification filter is regenerated to vent the contaminants. The liquid argon flow is  
11 switched to the other purification filter for uninterrupted filtration.

12 A purity monitor after the purification filter will monitor the filter effectiveness. Purity monitors  
13 measuring electron lifetime will also be in the LAr bath and resident in the cryostat. It is a  
14 requirement that purity levels reach < 100 ppt oxygen equivalent to match the required electron  
15 lifetime of the detector.

16 The regeneration of a filter (either liquid or gas) is done in several steps. A saturated purification  
17 filter is first warmed with heated argon gas to an elevated temperature (500 K) driving the captured  
18 water into the gas. The regen mix (1.5% Hydrogen gas by volume with a balance of argon) is then  
19 introduced at high temperature (500 K). The Hydrogen reacts with the oxygen and makes water  
20 that is also released into the circulating argon gas. Argon gas is vented to purge water from the  
21 hot circulating gas.

22 The hot filter full of regenerated media is cooled by circulating chilled argon gas. The filter is now  
23 ready to be switched into service or held cold until needed.

## 24 Internal Cryogenics

25 Internal piping is positioned within the cryostat to support the purge and cool-down processes,  
26 but also the LAr distribution during filling and normal operations. Heavy argon gas is injected  
27 at the bottom of the cryostat and distributed through a set of pipes that pushes the air up and  
28 forces it out from the roof. The flow nozzles will be directed downward or to the side so that the  
29 injection velocity will not cause local vertical gas plumes or turbulent mixing but rather will spread  
30 across the bottom of the tank and produce a stable, upwardly advancing argon wave front. The  
31 vertical velocity of 1.2 m/hr for the gas purge includes a contingency for some level of turbulent  
32 mixing. In addition to the main vent, all nozzles and dead-end (stagnant) volumes located at the  
33 top of the cryostat will have gas-exhaust lines for the initial purge and for continuous sweep-purge  
34 of those volumes during normal operations. The sweep-purge during the initial stage of purging  
35 will be vented outside of the building, whereas the sweep-purge during normal operations will be  
36 re-condensed and recirculated as liquid.

<sup>37</sup> After all but trace amounts of air (less than 1 ppm) have been expelled, the gas returns will  
<sup>1</sup> be routed to the condenser before being returned to the cryostat. When cool-down to 120 K  
<sup>2</sup> is complete (and during steady state operations), the gas returns will be sent to the condenser  
<sup>3</sup> to be liquefied by heat exchange with a liquid nitrogen stream. The re-condensed liquid will be  
<sup>4</sup> filtered and sent back to the cryostat to complete the cool-down operation. All purge gas will be  
<sup>5</sup> contained and either vented outside of the building (purge in open loop), circulated in closed loop,  
<sup>6</sup> or condensed and reused (cool down and normal operations).

<sup>7</sup> The cool-down of the cryostat and detector is performed through a set of manifolds flowing LAr  
<sup>8</sup> (one) and GAr (two). The LAr manifold and a GAr manifold are joined together and terminate  
<sup>9</sup> with a set of sprayers that deliver a mist of LAr and GAr. This mist is circulated within the  
<sup>10</sup> cryostat by a jet of GAr coming from the other manifold, which also terminates with sprayers.  
<sup>11</sup> These manifolds are located on the Jura side and are off to the side of the TPC so as not to flow  
<sup>12</sup> LAr and GAr directly over the detector itself. The chosen sprayers guarantee a flat profile of the  
<sup>13</sup> fluid (LAr and GAr) coming out.

<sup>14</sup> The LAr-supply pipework distributes the LAr at the bottom of the cryostat, during filling and  
<sup>15</sup> normal operations. The outlets are at the end of the pipes, as far away as possible from the side  
<sup>16</sup> penetration from which the LAr is sent to the purification system.

#### <sup>17</sup> 4.10.5 Cryostat pressure control

<sup>18</sup> The pressure inside the cryostat is maintained within a very narrow range by a set of active  
<sup>19</sup> controls. There are pressure control valves controlling the pressure by venting GAr to atmosphere  
<sup>20</sup> and/or introducing clean GAr from the storage as needed, but also increasing or decreasing the  
<sup>21</sup> cooling power in the condenser by controlling the amount of LN<sub>2</sub> flowing to the heat exchanger  
<sup>22</sup> and being vented.

#### <sup>23</sup> Normal Operations

<sup>24</sup> The pressure-control valves are sized and set to control the internal cryostat pressure under normal  
<sup>25</sup> operating conditions to the nominal design pressure of 0.113 MPa. Fluctuations within the range  
<sup>26</sup> 0.105 MPa (50 mBarg) to 0.120 MPa (200 mBarg) will be allowed. Few percentages excursions  
<sup>27</sup> (values to be determined) above or below these levels will set off alarms to alert the operator  
<sup>28</sup> to intervene. Further excursion may result in automatic (executive) actions. These actions may  
<sup>29</sup> include stopping the LAr circulation pumps (to reduce the heat ingress to the cryostat), increasing  
<sup>30</sup> the argon flow rate through the condenser, increasing the LN<sub>2</sub> flow through the heat exchanger  
<sup>31</sup> inside the condenser, powering down heat sources within the cryostat (e.g., detector electronics),  
<sup>32</sup> venting some of the GAr to reduce the pressure in a controlled way. Eventually, if the pressure  
<sup>33</sup> continues to rise, it will trigger the Pressure Safety Valves (PSVs) to operate.

<sup>34</sup> If the pressure decreases, we can introduce fresh GAr in the cryostat through the GAr make-up  
<sup>35</sup> line, a dedicated GAr feed line that take argon directly from the outside vaporized for a quick

36 intervention. If the pressure continue to decline, it will trigger the Vacuum Safety Valves (VSVs)  
1 to operate.

2 reference table with label Table 4.5

tab:cryostat-norm-pressure

Table 4.5: Cryostat pressures during normal operations

Cryostat part	Pressure
Vessel ullage maximum operating pressure	0.121 MPa (200 mBarg)
Relief valve set pressure	0.135 MPa (350 mBarg)
Warm structure design working pressure	0.135 MPa (350 mBarg)

3 The ability of the control system to maintain a set pressure is dependent on the size of pressure  
4 upsets (due to changes in flow, heat load, temperature, atmospheric pressure, etc.) and the volume  
5 of gas in the system. The reference design has 0.4 m of gas at the top of the cryostat. This is  
6 5% of the total argon volume and is the typical vapor fraction used for cryogenic storage vessels.  
7 Reaction time to changes in the heat load is slow, on the order of an hour

8 (?? to be confirmed).

## 9 Overpressure control

10 In addition to the normal-operation pressure-control system, it is planned to provide a cryostat  
11 overpressure-protection system. This must be a high-integrity, automatic, failsafe system capable  
12 of preventing catastrophic structural failure of the cryostat in the case of excessive internal pressure.

13 The key active components of the planned system are Pressure Safety Valves (PSVs) located on  
14 the roof of the cryostat that will monitor the differential pressure between the inside and the  
15 outside of the cryostat and open rapidly when the differential pressure exceeds a preset value. A  
16 pressure-sensing line is used to trigger a pilot valve which in turn opens the PSV. The PSVs are  
17 self-contained devices provided specially for tank protection; they are not normally part of the  
18 control system.

19 The installation of the PSVs will ensure that each valve can periodically be isolated and tested  
20 for correct operation. The valves must be removable from service for maintenance or replacement  
21 without impacting the overall containment envelope of the cryostat or the integrity of the over-  
22 pressure protection system. This normally requires the inclusion of isolation valves upstream  
23 and downstream of the pressure-relief valves and at least one spare installed relief valve ( $n + 1$   
24 provision).

25 When the valves open, argon is released, the pressure within the cryostat falls and argon gas  
26 discharges into the argon vent riser. The valves are designed to close when the pressure returns  
27 below the preset level.

## <sup>1</sup> Vacuum-relief system

<sup>2</sup> The cryostat vacuum-relief system is a high-integrity, automatic, failsafe system designed to prevent  
<sup>3</sup> catastrophic structural failure of the cryostat due to low internal pressure. The vacuum-relief  
<sup>4</sup> system protects the primary membrane tank. Activation of this system is a non-routine operation  
<sup>5</sup> and is not anticipated to occur during the life of the cryostat.

<sup>6</sup> Potential causes of reduced pressure in the cryostat include operation of discharge pumps while the  
<sup>7</sup> liquid-return inlet valves are shut, gaseous argon condensing in the condenser (a thermo-siphon  
<sup>8</sup> effect) or a failure of the vent system when draining the cryostat. Vacuum-relief valves are provided  
<sup>9</sup> on LNG/LPG storage tanks to protect the structure from these types of events.

<sup>10</sup> The key active components of this additional protection system are Vacuum Safety Valves (VSVs)  
<sup>11</sup> located on the roof of the cryostat that will monitor the differential pressure between the inside  
<sup>12</sup> and the outside of the cryostat and open when the differential pressure exceeds a preset value,  
<sup>13</sup> allowing air to enter the cryostat to restore a safe pressure. A combo PSV-VSV may be used  
<sup>14</sup> instead of two separate devices, one for overpressure and one for vacuum.

## <sup>15</sup> 4.11 Detector monitoring and slow control

## <sup>16</sup> 4.12 Calibration Systems

<sup>17</sup> from Josh K

### <sup>18</sup> 4.12.1 Motivation

<sup>19</sup> The scientific program of protoDUNE is critical to the ultimate success of DUNE. protoDUNE  
<sup>20</sup> will be the DUNE Collaboration's only opportunity to measure the response of a DUNE-style  
<sup>21</sup> LAr-TPC to hadrons (as well as  $\gamma$ s,  $\mu$ s, and electrons), and to compare those measurements to a  
<sup>22</sup> model of the detector response. That model can then be used to predict the response for DUNE  
<sup>23</sup> itself. Precision measurements of response in testbeams are a common approach of long-baseline  
<sup>24</sup> neutrino experiments. As a recent example, NO $\nu$ A has found that some of their measurements  
<sup>25</sup> are limited by the lack of knowledge of this response, which a testbeam would have provided.

<sup>26</sup> By itself, however, protoDUNE does *not* provide a response measurement that can simply be  
<sup>27</sup> mapped onto DUNE. Rather, protoDUNE provides measurements of the part of the response that  
<sup>28</sup> depends on the interactions of various particle species in LAr. The remainder of the detector  
<sup>29</sup> response, which includes reconstruction resolutions and biases, the effects of noise, space charge  
<sup>30</sup> and how it impacts reconstruction, and the conversion from observed charge to energy, all must  
<sup>31</sup> be calibrated and ultimately removed from the physical hadron response. Misinterpreting, for

example, longitudinal diffusion as a fundamental part of shower development of  $\pi^+$ s means our understanding of  $\pi^-$ s will be wrong in DUNE—and there will be no test of that response in the DUNE FD, independent of neutrino events themselves. By building protoDUNE in a way that mimics the DUNE far detector, we anticipate that such errors will ‘cancel out’; in practice we cannot rely on such a cancellation without knowing how different the parameters governing the response may be.

Ultimately, what this means is that we must calibrate a model of the detector—likely a LArSoft model—and use it to predict the response to hadrons. If the detector model is accurate, differences between the predicted response to various hadrons and measurements allows a correction to the hadron response that can be used for the DUNE experiment.

The existing option for creating a calibrated detector model for protoDUNE is to presume that calculations of the electric field throughout the detector, including space charge effects and impurities, are accurate, and that with this as input the detector response is uniquely calculable throughout the volume and for all times, up to the details of the electronics transfer function (and of course the response to various particle species which is what is being measured by protoDUNE).

fig:35t Figure ?? shows the variations in electron lifetime within the 35 tonne prototype as a function of position, as measured by *in-situ* purity monitors. The clear differences top and bottom indicate that we cannot assume that measurements in just a few places represent the detector at a whole. In addition to these variations, changes with the ambient environment were also seen, indicating that measurements must be made with reasonable frequency as well. An idealized view of how an operating detector will behave would miss such variations.

The calibration program for DUNE has as its goal both the measurement of the parameters governing detector response and *tests* of the predicted response. Table 4.6 lists many of the critical

Table 4.6: Parameters to be calibrated for ProtoDUNE model

Parameter	Name	Ex-situ Calibration	Calibration	Test
$W$	Ionization Energy	Benchtop	None	Cosmics
$C$	ADC/Charge Map	Benchtop Pulsers	Front-End Pulsers	Cosmics
$f$	Energy Scale	Calculation	Stopped cosmics	Through-going cosmics
$R$	Electron recombination	Calculation	Laser	Cosmics
$\tau$	Electron lifetime	Purity Monitors	Laser	Cosmics
$\vec{E}(x, y, z)$	Electric Field map	Calculation	Laser	Cosmics
$v_d$	Drift Speed	Purity+temp+Calc.	Laser	Cosmics
$d$	Electron Diffusion	Calculation	Laser	Cosmics
$\rho_E$	Field response	Calculation	Photocathode	Cosmics

parameters that need to be measured. We assume in this note that there will be several auxiliary systems that already provide measurements or estimates of some of these parameters:

- Monitors of HV and current to the APAs

- Survey of wire positions
  - Temperature sensors *in situ* at several places in the volume
  - Purity monitors at several positions within the volume
  - Front-end electronics response calibration pulsers.
- These systems provide the initial input to the model for electric field, and for calculations of average drift velocity, electron lifetime, and electron diffusion. The goal of the calibration systems we describe in this note is first to measure the response parameters with granularity in time and position that cannot be accomplished by the above systems, and to test the resultant model with tracks of known positions, trajectories, and energy deposits.

## 4.12.2 Laser System

The primary goal of the laser system is to provide realtime measurements of the parameters that determine the detector response: electron diffusion, and position-dependent variations in electron lifetime and drift velocity. One way of viewing this is that the laser system provides a map of the electric field and impurities in the detector—in fact, it is really a generator of position-dependent corrections to the field and impurities. As a realtime device, it also provides measurements of how these things vary with time.

Given the high space charge that will build up due to the high cosmic flux on the surface, we expect the ProtoDUNE-SP detector to have large variations in electric field as a function of position. Simulation of an example uniformly distributed space charge in protoDUNE using the simulation package SpaCE [?] shows great variations in all three components of the electric field  $E_x$ ,  $E_y$  and  $E_z$  (up to 12%), leading to a 4.5 cm longitudinal and 20 cm transverse track distortion at the nominal electric field of 500 V/cm and protoDUNE nominal geometry with 3.6m drift length. Measuring the drift velocity from known laser trajectories allows a mapping of that field.

To accomplish this mapping, the laser system needs to be able to illuminate a large fraction of the TPC volume, and the trajectory of the laser needs to be measured by detecting the light on the far side of the active volume.

### Laser System Design

The design of the laser system follows that of a system built for the MiniCAPTAIN detector by the University of Hawaii. In the current ProtoDUNE-SP cryostat design includes four entry ports for laser periscopes, two in each of the two volumes between each of the anode planes and the single cathode plane. Two periscope entries are important to increase the volume of the TPC that will be illuminated and to ensure laser access even in a case of shortening the drift distance from 3.6 m to 2.5 m (or even 2.0m which is still under discussion). The final choice will depend on how

1 well the field distortions can be handled. Each periscopes will be placed behind the TPC cage and  
2 reflects the laser beam from a mirror at the bottom of the periscope into the TPC volume through  
3 the gap between anode assembly planes. Entire periscopes can rotate around their central axis for  
4 azimuthal coverage. The mirror at the bottom of a periscope can swivel in the vertical plane to  
5 send the beam at different polar angles.

6 Laser beam pulses will be generated by a pulsed Nd:Yag laser's fourth harmonic at 266 nm. The  
7 laser must deliver tens of mJ per pulse at 266 nm. The pulse frequency is typically 10 Hz and pulse  
8 duration around 5 ns. Important characteristic of the laser is small divergence of the beam. Two  
9 companies have been identifid: Quantel and Surelite that feature very low divergence beams at  
10 less than 0.5 mrad. This is important feature will ensure that the beam remains relatively tightly  
11 collimated over long distances, retaining high ux and producing a narrow ionization track inside  
12 the TPC. Laser beam will be directed through a set of mirrors to the mirror at the top of the  
13 cryostat oriented at 45° angle to the beam, that bends the beam at right angle into the periscope,  
14 hitting the mirror at the bottom of the periscope and delivering the beam into the TPC.

15 While the direction of the laser beam will be very well known based on the reading from a rotary  
16 position encoder and linear actuator that is part of the periscope assembly, there will still be some  
17 residual uncertainty or unpredictable shift in the pointing direction. Having in mind long length  
18 of the ionization track of more than 7 m, even a small offset in the pointing direction can lead to  
19 vastly different ionization track location, especially close to the end of the track. Such inaccuracies  
20 will directly impact the ability to precisely calibrate any variations in the electric drift field.

21 To mitigate this issue, each laser pulse will be localized by a laser positioning system (LPS) that  
22 will use groups of pin diodes. Five groups of these diodes are distributed in a cross-like pattern.  
23 One group is directly opposite the mirror when it is facing the front at 45° tilt mirror. Two groups  
24 are in the same vertical plane close to the top and bottom of the same vertical axis. The two  
25 final groups are to the left and to the right from the central group. The electronics used to collect  
26 signals from the LPS will be commercially made by CAEN.

### 27 **4.12.3 Cosmic Tracker**

28 While there may be motivations from a reconstruction standpoint for cosmic veto, from a calibra-  
29 tion standpoint what we are interested in a tracking system to provide known cosmic trajectories.  
30 The tracker may also be used for off-beam triggering on stopped muons, as well as detector trig-  
31 gering during times when there is no beam.

32 Counters for a cosmic tracker are available from spares made for the Double CHOOZ experiment  
33 by the Universit of Chicago. Light created in the counters is transmitted via fibers to a 64-anode  
34 PMT and readout via electronics that use a USB interface. The counter size is roughly 2.5 cm,  
35 but multiple layers of the counters could be used for finer granularity.

36 Although there are many possible configurations for deployment of the counters, a particularly  
37 interesting deployment would be fore-and-aft, therefore triggering on muons that had trajectories  
38 similar to beam events. In this configuration, the counters could also serve as a tagger for beam

1 halo events. By tagging such events, only those whose energy and position are reasonably well  
2 constrained will be part of the beam calibration.

3 While this deployment scheme works well for calibration plans, it provides little help on tagging  
4 cosmics that could cause difficulty for reconstruction algorithms, since the vast majority of those  
5 will be downward-going.

6 There are two primary goals for the cosmic tracker. The first is to use the parameters measured by  
7 the purity monitors and temperature sensors, and the measurements of electric field as a function of  
8 position and time provided by the laser system, to predict the precision and bias of reconstruction  
9 of straight tracks from cosmic muons. The reconstruction of the tracked cosmics can then be  
10 compared to the results of reconstructed simulated events. If the differences are within the  
11 uncertainties derived from the initial parameter measurements, then we have confidence that the  
12 Monte Carlo model is predictive with the precision needed to measure beam event responses.

13 The second goal is to provide a measurement of the detector's energy scale—essentially the global  
14 mapping of deposited energy to ADC counts. Such a measurement can use either the through-going  
15 cosmic rays that hit both the fore and aft counters, corrected for the expected energy spectrum  
16 (and calculated  $dE/dx$  for the primarily minimum-ionizing cosmics), to provide a MIP-based energy  
17 scale, or to trigger on stopped cosmics outside of the beam gate, and using the part of the muon  
18 trajectory that has a residual range anticipated to be in the minimum-ionizing regime (similar to  
19 what was done for MINOS).

## 20 4.13 Beam window systems

21 The main function of the beam window system is to allow charged particles from the H4 beam  
22 line to enter the TPC with minimal energy loss and multiple scattering. The system penetrates  
23 through the cryostat insulation layers, displaces approximately 45cm of passive LAr layer, and  
24 extends inside the active TPC region through an opening in the TPC field cage. To keep the  
25 primary stainless-steel membrane of the cryostat intact, the beam window is divided into two  
26 independent subsystems. The first system (system 1) is installed inside the cryostat insulation  
27 layer and ends at the primary cryostat membrane. The second system (system 2) is inside the LAr  
28 portion of the cryostat. For NP04, the H4 beam line is designed to be able to inject beam into the  
29 LAr cryostat at three different locations. Due to various engineering and safety constraints, only  
30 one of the beam injection points will have the full beam window system installed. The sketch of  
31 the beam window system is shown in Figure 4.50. The details of the design are described in the  
32 following sections.

### 33 4.13.1 System 1

34 A close-up view of the System 1 beam window is shown in Figure 4.51. The system 1 beam  
35 window is a cylindrical G10 (OD $\approx$ 22cm) tube with a nomex honeycomb core at each end. The

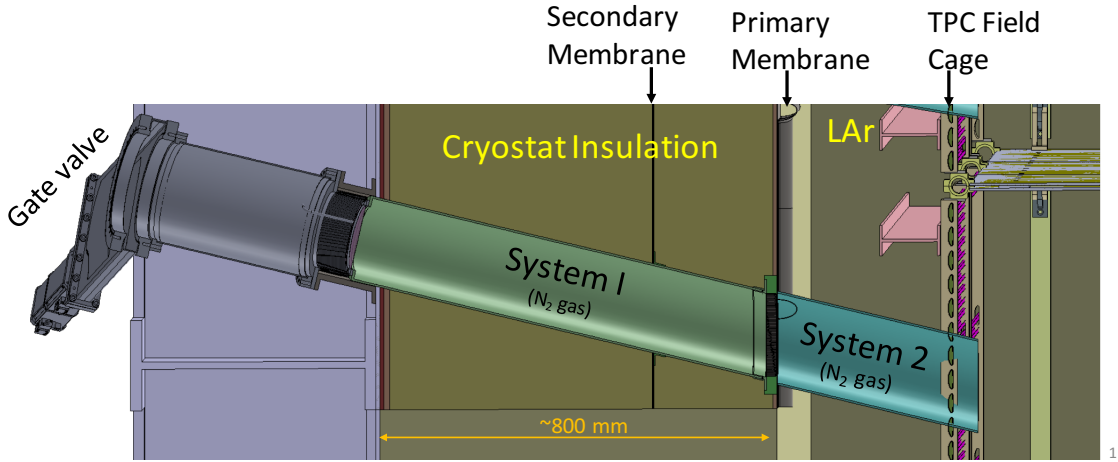


Figure 4.50: Beam window system 1 and 2.

fig:beamwindow

1 tube is filled with dry nitrogen gas and maintained at about 1 atm of pressure. It is designed  
 2 to provide thermal insulation with a heat load of less than  $5\text{W}/\text{m}^2$ . As shown in Figure 4.50,  
 3 system 1 beam window extends to the external steel support structure of the cryostat. The other  
 4 end of the beam window is in physical contact with the cryostat's primary membrane. When the  
 5 cryostat is filled with LAr, the nomex honeycomb core provides the structural support to prevent  
 6 the membrane from bulging outward. The honeycomb core on the other end of the tube, where the  
 7 bellow is located, provides thermal insulation to keep ice from building up on the outer surface.  
 8 The secondary membrane will be bonded onto a cylindrical disk attached to the G10 shell during  
 9 installation. The system 1 beam window is anchored to the outer steel structure of the cryostat  
 10 with a flange. As an additional safety measure, there is an option to install a gate valve on the  
 11 external end of the beam window.

## 12 4.13.2 System 2 (“beam plug”)

13 The system 2 beam window (a.k.a. beam plug) is designed to displace the passive LAr layer  
 14 between the TPC field cage and the inner cryostat membrane. As illustrated in Figure 4.52, it  
 15 is a cylindrical glass-fiber composite (type-V) pressure vessel about 50cm in length and 22cm in  
 16 diameter. It is filled with dry nitrogen gas to about 3 atm at room temperature. The beam plug  
 17 is secured to the field cage support structure (see Figure 4.53). The field cage support is designed  
 18 with sufficient strength to withstand the expected buoyancy force of about 200N when the beam  
 19 plug is immersed in LAr.

20 At nominal operation, the voltage difference across the beam plug could be as high as 160kV. To  
 21 minimize electrical discharges, the beam plug is divided into sections and each section is bonded  
 22 to a stainless-steel conductive grading rings. The grading rings are connected in series with two  
 23 parallel path of resistor chains. There are 7 grading rings. The ring that is closest to the field cage  
 24 is electrically connected to one of the aluminum field cage profiles. The last ring near the cryostat  
 25 wall is grounded to the stainless steel membrane. The type and value of the resistor is still under

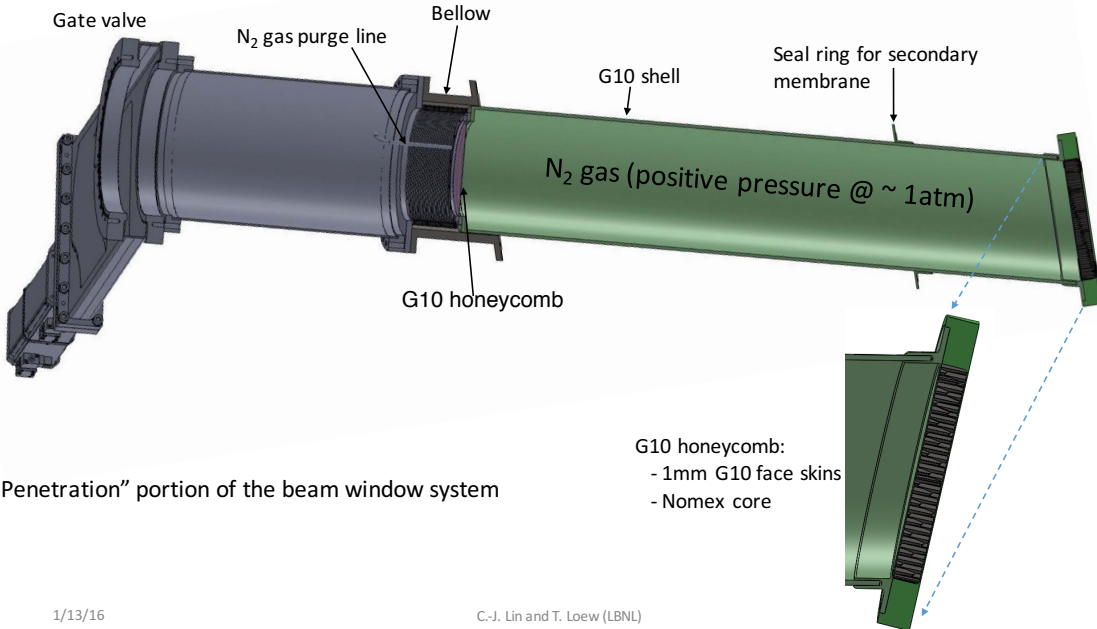


Figure 4.51: A detailed view of system 1 beam window.

fig:beam

- <sup>1</sup> evaluation. A likely candidate is the high voltage Super Mox 5GOhm resistor by OHMITE. The  
<sup>2</sup> maximum total power dissipated by the resistor chain is about 2W.

### <sup>3</sup> 4.13.3 Beam window system tests

<sup>4</sup> Do we want to discuss SLAC beam test and Field cage mockup test in PC4 in this TDR?



Figure 4.52: System 2 beam window. It is a type-V all composite pressure vessel filled with dry nitrogen gas to about 3 atm at room temperature. The vessel is about 50cm in length and about 22cm in diameter. The pressure vessel is divided into sections with each section bonded to a stainless-steel grading ring. The grading rings are connected by two parallel paths of resistor chain.

fig:beam

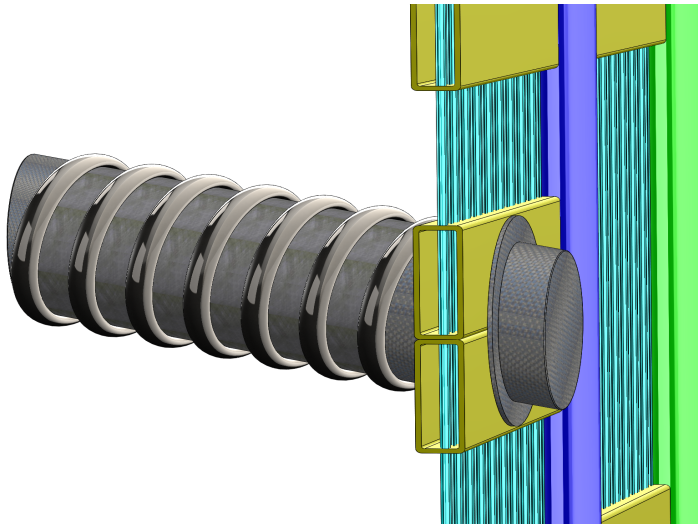


Figure 4.53: System 2 beam window mounting scheme (preliminary). The beam plug is mounted to the field cage support structure.

fig:beam

<sup>1</sup> Chapter 5

<sup>2</sup> ProtoDUNE computing and software  
<sup>3</sup> (Tom, Amir)[15 - 20 pages]

<sup>1</sup> Chapter 6

<sup>2</sup> Space and infrastructure requirements  
<sup>3</sup> (Maria)[10 pages]

# <sup>1</sup> Chapter 7

<sup>2</sup> Test beam specifications (**Paola,**  
<sup>3</sup> **Cheng-Ju)**[10 pages]

<sup>1</sup> Chapter 8

<sup>2</sup> Organization, cost estimate and schedule  
<sup>3</sup> (Maria, Jolie)[5-10 pages]

<sup>1</sup> Chapter 9

<sup>2</sup> Summary [2 pages]

<sup>1</sup> Appendix A

<sup>2</sup> LaTeX Writing Standards; Please Read!